HUNGARIAN UNIVERSITY OF AGRICULTURE AND LIFE SCIENCES

ANALYZING THE DRIVERS OF MULTI-SCENARIO URBAN VITALITY IN LUOHE CITY, CHINA: A LAND FUNCTION COUPLING PERSPECTIVE

DOI: 10.54598/006390

THE Ph.D. DISSERTATION

Xinyu Wang

Budapest

2025

The PhD School

Name:	**Hungarian University of Agriculture and Life Sciences** Landscape Architecture and Landscape Ecology
Discipline:	**Agricultural Engineering**
Head:	**Dr. László Bozó** University professor, DSc, MHAS MATE Institute of Horticultural Sciences Department of Water Management and Climate Adaptation
Supervisor(s):	**Dr. László Kollányi** Associate professor, Ph.D. MATE Institute of Landscape Architecture, Urban Planning and Garden Art Department of Landscape Planning and Regional Development

Approval of the Head of Doctoral School

Approval of the Supervisor(s)

LIST OF ACRONYMS

Land Factors & Functions Assessment		Vitality Assessment	
Abridge	**Full Name**	**Abridge**	**Full Name**
AI	Aggregation Index	AAAC	Atypical Activity Adjustment Coefficient
AS	Artificial Surfaces	AHP	Analytic Hierarchy Process
ASR	Artificial Surfaces Rate	AIC	Akaike Information Criterion
COHESION	Patch Cohesion Index	CCD	Coupling Coordination Degree
COP-DEM	Copernicus Digital Elevation Model	CRITIC	Criteria Importance Through Intercriteria Correlation
ED	Edge Density	DBI	Davies-Bouldin Index
FVC	Fractional Vegetation Cover	GLCM	Gray-Level Co-Occurrence Matrix
GI	Green Infrastructure	HMC	Human Mobility Consistency
GIR	Green Infrastructure Rate	HMI	Human Mobility Intensity
GPP	Gross Primary Productivity	HMV	Human Mobility Variability
LAI	Leaf Area Index	IQR	Interquartile Range
LERNCI	LST and EVI Regulated NTL City Index	LAR	Leisure Activity Ratio
LPI	Largest Patch Index	LEF	Land Ecological Function
LSI	Landscape Shape Index	LSF	Land Social Function
LST	Land Surface Temperature	MAD	Median Absolute Deviation
LULC	Land Use &Land Cover	MGWR	Multiscale Geographically Weighted Regression
MESH	Effective Mesh Size	OLS	Ordinary Least Squares
NDBI	Normalized Difference Built-up Index	OPGD	optimal parameters-based geographical detector
NDBSI	Normalized Difference Built-up and Soil Index	PCA	Principal Component Analysis
NDVI	Normalized Difference Vegetation Index	QE	Quantization Error
NTL	Nighttime Light	RF	Random Forest
OSM	OpenStreetMap	SOM	Self-Organizing Map
PD	Patch Density	TE	Topographic Error
POP	Population	UV	Urban Vitality
RSEI	Remote Sensing based Ecological Index	UVI	Urban Vitality Intensity
TOD	Transport-oriented Development	VIF	Variance Inflation Factor
VQ	Vegetation Quality	d-CCD	Distance-Considered Coupling Coordination Degree
WET	Wet		
WI	Weighted Integration		

TABLE OF CONTENTS

LIST OF FIGURES

LIST OF TABLES

1 INTRODUCTION

1.1 Background

Since the mid-20th century, human impact on ecosystems has been more profound than at any other time in history (World Health Organization, 2005). Evaluating urban vitality (UV) based on human activity intensity and analyzing the driving relationship between UV, land functions, and their coupling are critical for promoting regional sustainability, enhancing urban resilience, supporting compact growth, and optimizing the living environment and human well-being (Qiao & Huang, 2024).

1.1.1 Urbanization & human-land relationship

As Cai et al.(2021) highlighted, global urbanization is marked by two key features: the migration of populations from rural to urban areas and the rapid expansion of artificial surfaces. These human-land dynamics interact to reshape land-use patterns, creating growth cycles fueled by high population density and industrial concentration, which have emerged as primary drivers of urban development (X. Liu et al., 2020).

In 1979, Northam approximated the urban development process using an "S"-shaped empirical curve (Northam, 1979), which can be divided into three stages: an initial stage with low urbanization levels (<30%) and slow growth, an acceleration stage marked by rapid increases in urbanization levels, and a terminal stage where urbanization levels are high (>70%) and development stabilizes (Mulligan, 2006). As cities expand, numerous urban problems emerge, notably the unsustainable risks posed by the unrestrained expansion of construction land or the imbalance between urban development and population growth. Given the limitations of land carrying capacity, urbanization inevitably slows down, leading to over-concentration of populations in some areas and insufficient resource supply, resulting in phenomena such as "counter-urbanization" and "urban expansion" across regions (Liao & Liang, 2024). According to the 2022 World Cities Report, by 2070, urban land expansion is expected to occur primarily in low-income countries, and without effective planning, urban sprawl could become a widespread phenomenon.

As one of the fastest-urbanizing developing countries in the world, both domestic and

international scholars have conducted extensive theoretical and empirical research on key issues such as healthy urbanization, urban-rural integration, and land use efficiency (Bai et al., 2014; Li YuRui et al., 2015; Y. Liu et al., 2014; Qiao & Huang, 2024). There is a widespread consensus on issues such as China's inflated population urbanization rate and the disorderly, even uncontrolled, expansion of urbanized land. As urbanization deepens, the dynamics of human-land interactions are continually evolving. In March 2014, the Chinese government issued the National New-type Urbanization Plan (2014-2020), elevating the issue to a national strategic level and highlighting the urgent need to address the significant imbalance between the urbanization of land and population, as well as the inefficiency and expansion of construction land use. This plan underscores the transformative impact of urbanization on human-land relationships in China.

1.1.2 Urban and vitality development

A vibrant city can continuously expand with high efficiency (Montgomery, 1998). The New Urban Agenda emphasizes that residents are not only the ultimate beneficiaries of urban development but also key participants in the development process. This perspective has made the measurement of residents' activities/ vitality as a key research focus (Qiao & Huang, 2024).

As illustrated in Figure 1, research on UV has attracted widespread attention over the past 25 years. Notably, since 2010, the number of related articles has increased, with a sharper rise than the past decade, particularly after 2015. The English-language literature data was sourced from the Web of Science (WOS) database, particularly from the SCI core collection. The search query applied was: TS = (urban plan* OR city plan* OR landscape*) AND TS=vitality, covering the period from 2001 to 2024. After excluding irrelevant articles, a total of 340 English-language articles were selected. For Chinese literature, data was obtained from the SCI/CSSCI/EI/CSCD/Peking University Core Journals collection in the China National Knowledge Infrastructure (CNKI), spanning from 2001 to 2024. The search focused on themes such as "城市活力" (urban vitality), "景观活力" (landscape vitality), and "空间活力" (spatial vitality) (Nie et al., 2021). After removing irrelevant articles, a total of 399 Chinese-language articles were compiled.

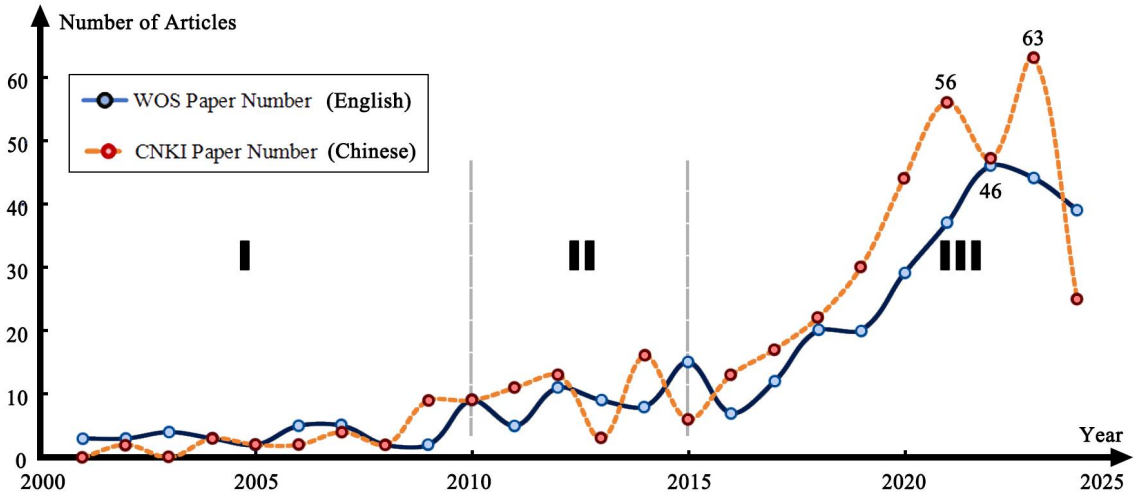

Figure 1 Temporal Distribution of the Number of Literature on UV in China & Abroad (2024-06).

By 2030, China's urbanization rate is expected to reach 73%, with cities continuing to expand and urban construction land further increasing (Desa, 2014). Synchronizing the building of urban vitality (UV) is important for achieving the United Nations' 2030 Agenda and Sustainable Development Goals (SDGs) (Cheng et al., 2022) at this year. In particular, understanding the response of vitality to land systems is essential for optimizing living environments, constructing productive and ecological spaces, and enhancing the management of human-land relations (Qiao & Huang, 2024). The China State Council's "Opinions on Further Strengthening Urban Planning, Construction, and Management" clearly states the need to "strive to build harmonious, livable, vibrant, and distinctive modern cities."

1.1.3 A new stage of urbanization in China

Since China implemented the Reform and Opening-up policy in 1978, urbanization has been a crucial driving force behind socio-economic development (Y. Long & Wu, 2016). In the initial stages, urbanization was primarily driven by the growth of urban populations and infrastructure development, leading to a rapid increase in the urbanization rate from 17.92% in 1978. After 1996, China’s urbanization rate surpassed 30%, entering an acceleration phase. By 2010, the rate had reached 49.95%, with an average annual increase of 1.37 percentage points during this period.

Currently, the urbanization rate has reached 66.16% (as of 2023), and the growth rate has gradually slowed (L. Li et al., 2022; T. Li, 2019). Overall, the urbanization process in China is expected to follow an S-shaped growth curve (Y. Long & Wu, 2016). In addition, compared to 2021, China's population decreased by 1.09 million in 2022. This marks not only the first decline

in decades but also indicates a trend of sustained negative growth projected for the subsequent three years (Figure.2). This suggests that China has entered a phase of negative population growth. In 2024, several cities renamed their Housing and Urban-Rural Development Bureaus to "Housing and Urban Renewal Bureaus."

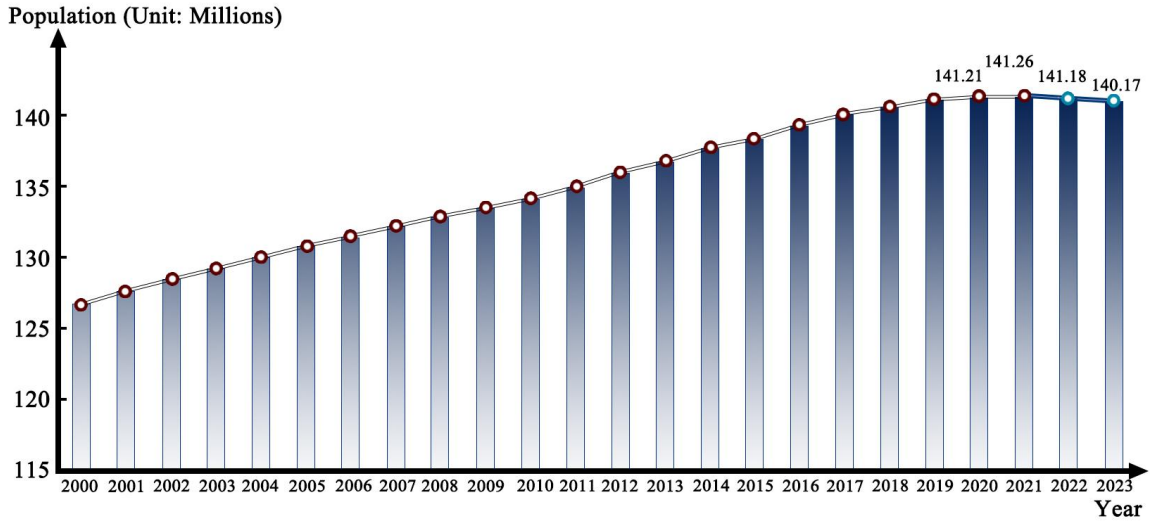

Figure 2 Changes in Chinese population (Source: China Statistical Yearbook).

In this new era, "Expanding cities, shrinking population" encapsulates the human-land relationship challenges that Chinese cities face (Kuang et al., 2016; Luo et al., 2018; Y. Zhang et al., 2024). Within this paradox lies the imbalance between land efficiency and the in spatial structure, which hinders high-quality urban development and manifests as a decline in UV. Despite the increasing modernization of the urban physical design, many functions are not perceived by the majority of the population, and human interaction with urban spaces is not effectively promoted. The inclusiveness of cities as habitats is diminished by factors such as textural damage, leading to a loss of urban vitality as a side effect of rapid urbanization. Urban decay or sprawl, such as “ghost cities” in China and “marginal villages” in Japan, is common, accompanied by imbalances in employment and housing, rising vacancy rates, population loss, and ecological degradation (Y. Long & Wu, 2016).

Currently, urban development in China faces tight constraints, and planning practices are gradually shifting from expansion-oriented to stock-oriented strategies, highlighting an urgent need to enhance the functionality of built-up areas and improve quality of life (Zhu et al., 2020). Developing a more comprehensive land function assessment framework will provide crucial guidance for balancing the potential adverse effects of dense construction, supporting future

urban planning and land resource management (X. Wang, Yao, et al., 2023).

1.2 Aims and questions

As outlined in the background, in the new phase of China's population growth and urbanization, enhancing urban vitality has become both a goal and a driving force for the development of major cities in this era. Land, as a fundamental resource for urban social development and a crucial carrier of human activities, requires a shift in its comprehensive utilization to meet the evolving demands of the era. Whether it is smart land development or compact development strategies to combat urban sprawl, or enhancing urban vitality through mixed-use and functional integration, it is essential in this new era to construct a comprehensive and rational framework for evaluating vitality and land use. And, it is necessary to explore the relationship between vitality and land based on new data (Artmann et al., 2019; De Roo, 2000).

1.2.1 Research questions

The core research question of this paper is: how to reasonably develop land functions to enhance urban vitality and achieve high-quality urban development. Based on the "Pattern-Mechanism-Response" framework, this question can be expanded into several specific areas for in-depth research.

1.2.1.1 “Pattern” research

Q1: Based on data characteristics, how can we construct a vitality framework incorporating a temporal dimension to quantitatively describe UV?

Over the past 60 years, research on "vitality" has gradually shifted from qualitative studies to quantitative analyses (Jacobs, 1961). Vitality, driven by residents' activities as a long-term process, requires consideration not only of activity intensity but also of temporal variations (Sulis et al., 2018). Therefore, this study hypothesizes the following: at the annual scale, vitality assessments should account for seasonal and climatic changes, using four seasons as a complete cycle; at the quarterly scale, urban vitality should distinguish between work and rest, using a week as a full cycle, with Monday to Friday as workday scenarios and Saturday to Sunday as weekend scenarios; at the daily scale, distinctions should be made between residents' active periods and sleep periods, with further attention to variability and stability at the hourly scale.

Q2: Based on the theory of land multifunctionality, how can we characterize land functions

in multiple dimensions, specifically, how can we quantitatively assess various land functions and their spatial patterns?

The current study adopts a "socio-ecological" land function assessment framework (X. Wang, Yao, et al., 2023). Land social function (LSF) includes traditional "social services," such as transportation networks and residential density as basic services, as well as "economic outputs," such as GDP per unit of land and the density of commercial establishments. Land ecological function (LEF) includes basic green infrastructure areas and broader vegetation conditions and ecological benefits. The basic assumption in the assessment is that LSF is primarily supported by "artificial surfaces" in land cover, while LEF is supported by "green infrastructure" in land cover. However, even the same type of land may exhibit varying intensities of comprehensive functions depending on its characteristics and the types and quantities of resources it supports.

1.2.1.2 “Mechanism” research

Q3: Based on the integration of vitality and land theories, what are the factors influencing urban vitality, and what are the specific mechanisms behind this influence? This question can be further divided into:

- **Q3.1:** What is the impact of land coupling on UV?
- **Q3.2:** What is the impact of land functions on UV?
- **Q3.3:** What is the impact of land factors on UV?

Land Coupling: Current research indicates that within built-up areas, or areas serving social functions, the mix of land uses—such as commercial, residential, and recreational functions—is positively correlated with UV (or UV at specific times) (S. Tang & Ta, 2022; A. Zhang et al., 2021). However, there is limited research on the relationship between the broader mix of socio-ecological functions and UV. In exploring the coupling and coordination of socio-ecological functions, the basic assumption is that the spatial distributions of these two sub-functions are not completely aligned. This spatial asynchrony allows for discussions on the spatial heterogeneity of the coupling coordination degree between the two systems.

Land Function: Previous studies indicate that UV has a higher dependency on the supply of urban social functions (Cen et al., 2024; L. Fan & Zhang, 2022). This is primarily determined by the inherent attributes of "urban" areas, as urbanization leads to the localized concentration of various production factors, including population. However, at different stages of development,

UV's demand for social and ecological services varies. Specifically, in the later stages of urbanization, residents' demand for ecosystem services increases significantly. Therefore, this issue involves not only qualitative comparisons but also aims to derive a quantitative correlation ratio. The basic assumption is that UV in the study area currently has a higher dependency on the supply of social functions but also has a certain demand for ecological functions.

Land Factors: The driving process of factor X on variable Y is not globally homogeneous, which is the fundamental assumption of geographically weighted regression (GWR). In this study, this assumption is further refined: Firstly, due to the complexity of geographical processes, driving factors typically do not act independently but rather in coordination (H. Wang et al., 2021). This means that when enhancing UV through the control of land factors, paired factors often achieve better results. Secondly, depending on the context, the same factors should exhibit different driving characteristics, such as driving coefficients or the homogeneity of impact (bandwidth), in different vitality scenarios (workdays/weekends).

1.2.1.3 “Response” research

Q4: How should land development policies be formulated to foster urban vitality? What are the corresponding planning responses?

Based on the preceding issues and the research findings on the driving relationships between land and UV, and considering the broader context of national spatial planning in the new era, multi-scale planning recommendations should be made for both spatial configurations and underlying mechanisms.

Response to Spatial Patterns Heterogeneity: At the macro and meso scales, planning recommendations should be proposed for enhancing vitality and land use patterns, thereby improving the spatial coordination of urban functions.

Response to Mechanism-Driven Factors: To enhance UV, policy recommendations at the macro scale should be guided by the land coupling coordination. At the meso scale, the optimization of land functions should be prioritized, with detailed planning tailored to specific functional areas. At the micro scale, planning should be based on land elements, focusing on refined land use and the allocation of elements to strengthen UV.

1.2.2 Research framework & aims

The theoretical framework of this study can be simplified into three key components (Figure.3): **1.** UV assessment**, 2.** Land function assessment, and **3.** Exploration of the relationship between UV and land functions.

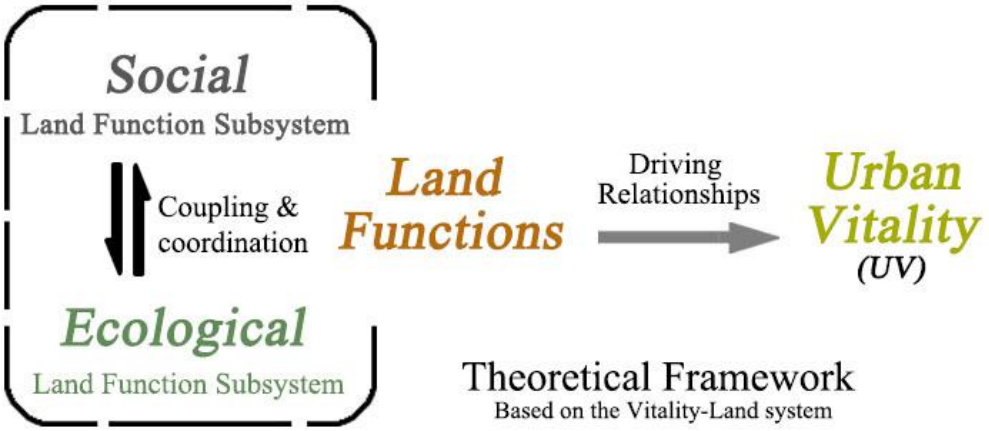

Figure 3 General Theoretical Framework.

This paper introduces a novel approach for evaluating UV using Baidu Map Human Mobility Data (Figure.4). Unlike traditional methods that directly rely on activity intensity, this method fully utilizes the temporal dimension of the data, employing self-calibration to achieve more accurate UV measurements. In this study, UV is differentiated based on residents' activity patterns across multiple scenarios, particularly in Weekend and Workday contexts.

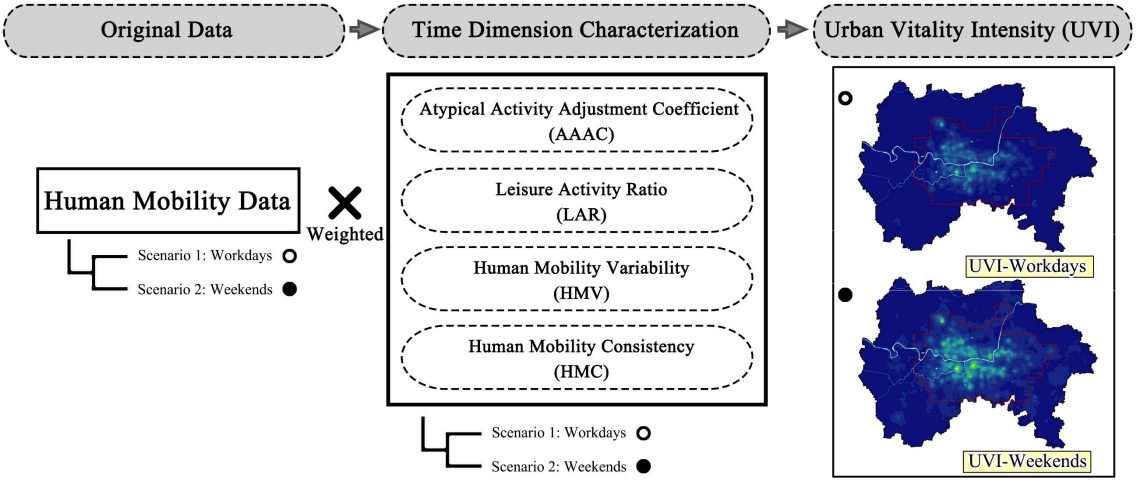

Figure 4 Urban Vitality Assessment Framework.

Second Section (Figure.5): The study assesses land functions using a variety of data sources. By applying a socio-ecological subsystem framework, we gained a comprehensive understanding of the spatial variability of land-use multifunctionality in terms of quantity, quality, and structure. Moreover, based on the intra-group Coupling Coordination Degree (CCD), we identified

communities formed by the spatial clustering of various functions. By calculating the inter-group CCD, we further integrated land functions, achieving a detailed and comprehensive understanding of land functionality.

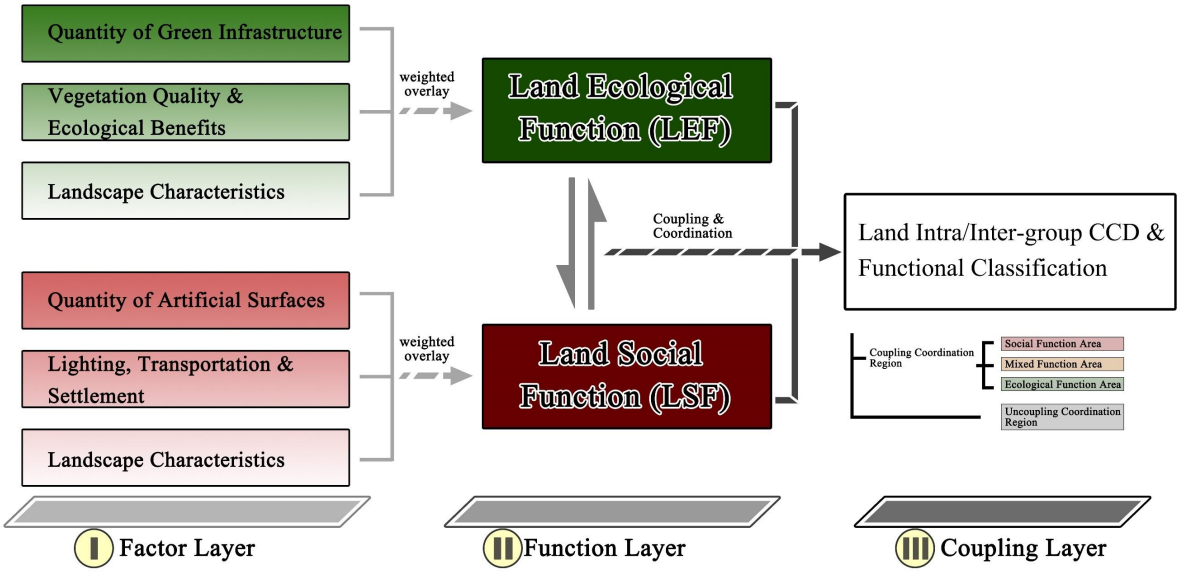

Figure 5 Land Functional Assessment and Coupled Coordination Framework.

Finally (Figure.6), we examined the relationship between vitality and land functions. Spatial correlation analysis demonstrated UV's dependence on socio-ecological land functions. Through Multi-Scale Geographically Weighted Regression (MGWR) and the Optimal Parameters-based Geographical Detector (OPGD), we deeply explored the interactive relationships between various land indicators and UV under different scenarios, as well as the driving forces and bandwidth changes related to UV. Lastly, using the CCD model, we validated the correlation between functional mixing and vitality, and further identified areas with poor CCD. By confirming the predominant functions within these areas, we provided planning recommendations to enhance UVI.

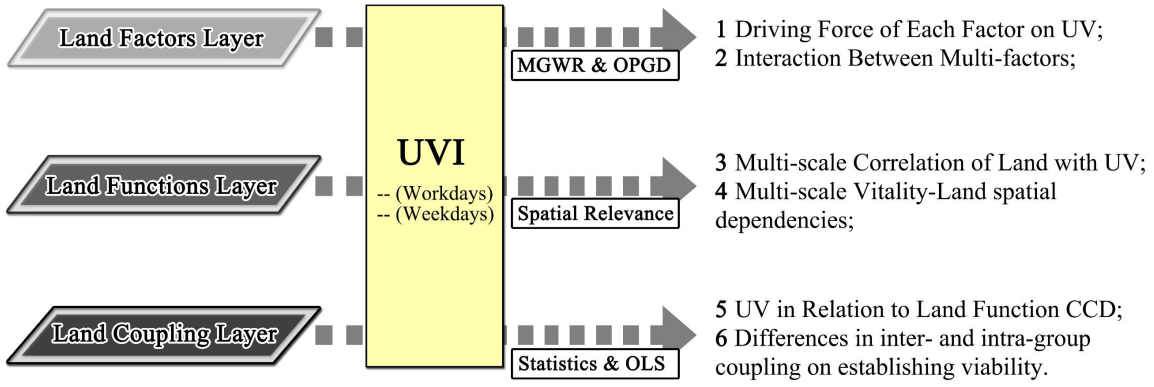

Figure 6 Vitality- Land Driving Relationship Framework.

1.2.3 Chapter contents

Chapter 1: This chapter introduces the fundamental background of the study, laying the groundwork for the thesis. It extracts specific research objectives and questions from the background information, emphasizing the significance and necessity of the research.

Chapter 2: This chapter delves into theoretical issues related to UV and land functions. It begins by clarifying key terms and defining concepts that lack clear definitions. The first section reviews the evolution of the concept of "urban vitality," discussing the changes in basic data sources and assessment methods as vitality evaluation has progressed over time, and examines factors influencing vitality. The second section explains the conceptual changes regarding land functions/multifunctionality and introduces commonly used land function assessment frameworks, such as the "socio-ecological" framework. The third section discusses the impact of land functions on UV, with particular emphasis on mainstream methods adopted domestically and internationally to enhance urban vitality.

Chapter 3: This chapter provides a detailed description of the study area, primary data sources, and research models. In introducing the study area, it not only provides basic locational information but also discusses the generality and uniqueness of the area selection concerning the background issues raised in Chapter 1. Finally, it outlines the specific methods employed to assess UV, land functions, and the relationships between them.

Chapter 4: This chapter presents the quantitative evaluation results of UV and land functions, followed by a further spatial pattern analysis. It stratifies the driving effects of different land evaluation factors on multi-scenario UV. At the system level, it analyzes the dependency and prioritization of UV on land ecological function (LEF) and social function (LSF). At the coupling coordination level, it illustrates how UV varies with the CCD, identifies the distribution of UV across different CCDs based on 2023 data. Finally, the effect of land factors on UV was the most important and the interaction between factors was further explored.

Chapter 5: This chapter introduces the new scientific contributions of this study, particularly how it addresses existing research gaps.

Chapter 6: This chapter summarizes the main findings of the study, reflects on the initially set

objectives and questions, and evaluates their broader implications. It also provides planning recommendations based on the research findings. Additionally, this chapter discusses the limitations of the study and suggests directions for future improvements (Figure.7).

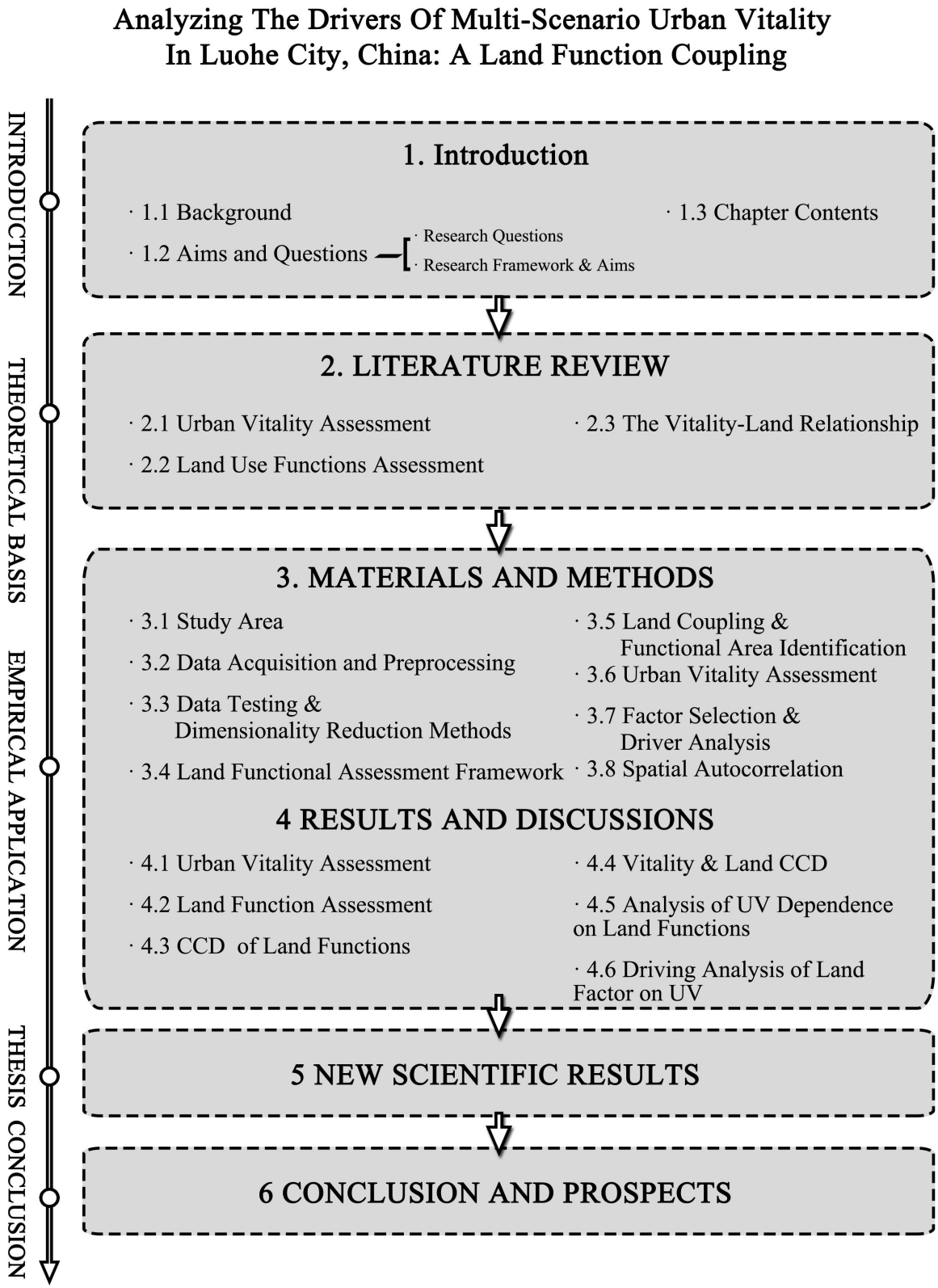

Figure 7 Contents of Individual Chapters.

2 LITERATURE REVIEW

2.1 Urban vitality assessment

Vitality is a crucial driver of sustainable urban development (Caprotti et al., 2017) and an essential indicator for evaluating the quality of urban environments (Paköz & Işık, 2022; S. Tang & Ta, 2022). Quantifying UV and understanding its interactions with various urban subsystems, particularly the land system, are crucial for the rational planning of human-land relationships.

2.1.1 Concept origins & development

Jane Jacobs (1961) was the first to introduce the concept of "vitality" in urban planning, associating it with street activity and diversity (Jacobs, 1961). She argued that the essence of UV lies in the continuous activity of people throughout the day and proposed four key conditions to promote and sustain urban diversity: (1) Neighborhoods should have at least two primary functions to attract and maintain diverse flows of people, thereby providing ample public amenities (mixed-use); (2) Blocks should be short to facilitate pedestrian movement and allow easy changes in direction (short streets); (3) Buildings should vary in age and condition to reflect economic diversity (building age); (4) The density of people should reach a specific level, encompassing both local residents and visitors (people density). These principles marked the qualitative phase of research on urban vitality.

Later, Alexander (1965) suggested that the inherent qualities of natural cities shape their vitality (Alexander, 1965) , while Kevin Lynch (1984) expanded this idea, stating that vitality reflects how well urban forms support essential functions, ecological needs, and human capabilities (Lynch, 1984). Maas (1984) characterized UV as a spatial quality emerging from diverse commercial opportunities and a varied, dense pedestrian population (Maas, 1984). Montgomery (1998) considered vitality a hallmark of successful urban areas, manifested through high levels of human and street activity (Montgomery, 1995, 2017). Chinese scholars, such as Jiang (2007) (Jiang, 2007), developed a framework grounded in social, economic, and cultural dimensions, positing that UV is the lifeblood of a city, reflecting its capacity to provide a humanized living environment for its residents.

UV lacks a precise definition in academic literature but generally includes two key aspects: (1)

the intensity and diversity of human activities. Common indicators used to measure the intensity of vitality include "activity," "aggregation," and "mobility" of residents (Montgomery, 1998; L. Tang et al., 2022; C. Wu et al., 2018). (2) The role of the city in sustaining human life, which emphasizes interactions between individuals and the urban environment. Drawing on complex systems theory, this concept of "vitality" describes cities as interconnected, dynamic, and organic entities composed of multiple systems (Portugali, 2016).

Building on the conceptual framework of urban vitality discussed earlier, Long and Zhou (Y. Long & Zhou, 2016) utilized big data to develop a framework for analyzing factors influencing vitality at the urban street level and employed regression analysis to examine how these factors affect various types of functional streets. Furthermore, scholars have long used multi-source data and methodologies such as correlation analysis and machine learning to explore the mechanisms influencing regional vitality. These studies not only reveal the impact of various forms and elements on urban vitality but also propose corresponding optimization strategies to further promote sustainable urban development (H. Guo et al., 2020; Z. Wang et al., 2024).

2.1.2 Vitality assessment datasets & methods

Early studies on UV primarily focused on constructing evaluation indicators, constrained by limitations in data acquisition. Traditional sources of survey data include government statistics and field research data. The former consists of macro socio-economic indicators (Huang et al., 1998), statistical yearbook data, employment rates (Harvey, 2001), and housing and land prices, typically used to assess UV at a macro scale from sociological and economic perspectives. Although this type of data is relatively comprehensive, it lacks specificity. Conversely, field research data includes attributes of the built environment, land use, human activity characteristics, and survey questionnaires. Such data requires extensive fieldwork and often lacks sufficient spatiotemporal precision (Biddulph, 2012; Gehl & Architects, 2004), making it challenging to capture the dynamic characteristics of UV. Consequently, these studies are often qualitative and present certain limitations.

With the advent of the information and digital age, new urban insights have emerged through the use of OpenStreetMap (OSM) GPS data, social media check-in data, and smart card data (Batty, 2018; Cats, 2024; Neuhaus & Neuhaus, 2015). These data not only reveal intrinsic influences on UV but also enable the identification of significant relationships between specific elements of the

built environment and UV, which can be translated into measures, such as using the number and diversity of small food and beverage establishments as indicators of vitality (Ye et al., 2018). Moreover, data from bike-sharing (Zeng et al., 2020) , GPS (J. Wu et al., 2018) , commuting surveys (Sung et al., 2015) , social media check-ins (Meng & Xing, 2019) , and street view image (Kang et al., 2021) have also been extensively utilized in UV research. However, due to spatial sampling biases, these datasets often require calibration with supplementary data, such as road accessibility (Sulis et al., 2018).

Building on the aforementioned single-indicator evaluations and explorations into the mechanisms of urban vitality, some scholars have begun to explore methods that integrate multi-source data and multiple indicators to assess UV from diverse perspectives. For instance, Ravenscroft (2000) developed a framework for monitoring and assessing the health of town centers, aiming to evaluate the vitality and vibrancy of city cores (Ravenscroft, 2000). Braun et al. (2015) developed a composite index of urban vitality based on factors such as compactness, density, regional and local connectivity, destination accessibility, land use mix, and social diversity, to assess the downtown vitality of 48 major U.S. cities (Braun & Malizia, 2015). Similarly, He et al. (2018) utilized geographic big data, including POI density, urban function mixed-use areas, check-in density, holidays, and population changes, to measure the vitality of newly developed areas in Chinese cities from 2005 to 2015 (He et al., 2018).

Given that many current studies tend to oversimplify data processing, often using only the quantity or intensity of crowd movement in sampled areas as the sole representation of UV without fully considering the temporal characteristics of the data (L. Fan & Zhang, 2022; Z. Fan et al., 2021), this study adopts the concept of multi-indicator vitality evaluation and innovatively proposes using temporal volatility as a self-correcting coefficient in the assessment method. Additionally, employing a single data source permits a deeper exploration of the driving mechanisms of urban vitality influenced by other multi-source data (primarily various land use functions), further enriching the understanding and analytical approaches of UV.

2.1.3 Vitality creation & drivers

Indeed, analyzing the factors that influence and drive UV is a crucial component in fostering UV. As part of the urban system, the spatial heterogeneity of UV is influenced by the functions of other city systems, including essential social services such as education, healthcare, and

transportation, as well as neighborhood landscape features and recreational services like green spaces and rivers.

Current research methods on urban vitality and its influencing factors and mechanisms can be broadly divided into three main categories: observational summary, subjective preference, and correlation analysis (GAO et al., 2023). **Observational Summary Method:** This approach relies on empirical observation and documentation to analyze the patterns between the spatial environment and spatial vitality. Early scholars, including Jane Jacobs, Jan Gehl, and Kevin Lynch, used this method to identify conditions and indicators of vitality. **Subjective Preference Method:** This method has been widely applied over an extended period and involves techniques such as semantic differential (SD) analysis, fuzzy evaluation, and analytic hierarchy process (AHP) to quantify the weights of various factors influencing specific groups. **Correlation Analysis Method:** This approach employs mathematical and statistical techniques, such as correlation and regression analysis, to investigate the relationship between spatial vitality and the built environment. It has been extensively used in recent years. For instance, Long and Zhou (2016) utilized big data to develop a framework for analyzing factors influencing vitality at the urban street level and examined how these factors affect various types of functional streets using regression analysis. Additionally, scholars have explored the mechanisms influencing regional vitality by employing multi-source data and methodologies like correlation analysis and machine learning. These analyses have elucidated the impact of various forms and elements, proposing corresponding optimization strategies (H. Guo et al., 2020; Z. Wang et al., 2024).

However, research on the driving mechanisms behind UV has predominantly focused on the driving coefficients of various factors or the spatial heterogeneity of vitality, with less emphasis on human-land interactions, scale dependence, and scenario comparisons (S. Liu et al., 2020; Z. Wang et al., 2024). Moreover, while current research has uncovered various mechanisms influencing urban vitality, there is still considerable scope for expanding studies on land functions. This paper aims to explore how land uses and spatial functions can synergistically enhance urban vitality and investigate how these functions can be effectively integrated into planning and design to achieve sustainable urban development goals.

Overall, research on UV has transitioned from qualitative theoretical exploration to quantitative, method-based measurement. The continuous refinement of data sampling's spatiotemporal

dimensions has driven a shift towards more diversified and human-centered research perspectives.

2.2 Land use functions assessment

2.2.1 Land use functions

Land serves as the physical foundation for human activities, and its use fundamentally represents the transformation of the Earth's surface through human intervention. According to urban ecology theory, land use directly affects ecological systems, economic performance, and social functions (Steffen et al., 2007). Activities such as production, infrastructure development, and housing are intrinsically tied to specific modes of land use (Bertrand et al., 2008).

"Land Use Functions" or "Land Functions" refer to the private and public goods and services that land provides through various utilization methods. This concept was introduced by the SENSOR project under the European Union's Sixth Framework Programme, titled "Sustainability Impact Assessment: Tools for Environmental, Social, and Effects of Multifunctional Land Use in European Regions" (Pérez-Soba et al., 2008). Land Functions are determined by the structure of various elements (subsystems) within the land use system (E. F. Moran et al., 2005). Humans use land to create a rational utilization structure, aiming to derive economic, social, and ecological benefits and values (J. Zhang et al., 2008), reflecting the capacity of land use systems to provide human welfare (Gaodi et al., 2010; Wiggering et al., 2006).

The state and performance of land use functions in a given area, including economic, social, and ecological functions, are often referred to as the "multi-functionality of land use." However, this concept is often used interchangeably with Land Functions (Pérez-Soba et al., 2008). The concept of land use multifunctionality originally arose from studies on agriculture, ecosystem services, and landscape functions. In 1994, the Uruguay Round Agreement on Agriculture (URAA) first introduced the concept of "Agricultural Multifunctionality" to WTO member states (Article 20 of URAA)(Bohman et al., 1999). The OECD further clarified "multifunctionality" in 2001 as the natural and objective characteristics of certain economic activities, noting that agriculture not only fulfills the function of food production but also contributes to environmental protection, landscape preservation, rural employment, and food security (Barthélemy & Nieddu, 2007; Wiggering et al., 2006). Vereijken and others expanded the concept of "Multifunctional

Agriculture" (MFA) to encompass "Multifunctional Land Use" (MLU), which has since evolved into a broader concept of multifunctional land use (Gadjiev et al., 2007).

2.2.2 Land assessment framework

In the late 1990s, following adjustments in global agricultural policies (such as those by the Food and Agriculture Organization, the Organization for Economic Co-operation and Development, and the World Trade Organization) and European policies (like the European Union's Common Agricultural Policy), scholars have increasingly recognized the universal guidance of multifunctionality (Hediger, 2006). This recognition has elevated 'multifunctionality' to an important scientific theme of sustainable development (Helming et al., 2008) and a key guiding principle in EU urban policies. A specific assessment framework for land use functions should include economic, environmental and social dimensions that are closely related to the regional context. This definition has been widely accepted in the international academic community (Pérez-Soba et al., 2008; Wiggering et al., 2006).

In China, land use functions are evaluated based on rational use, aiming to determine land value according to specific objectives by assessing attributes, efficiency, and output quality of land use (HUANG & YANG, 2008). A systematic understanding of the elements, implications, and dimensions of land use is fundamental for assessment, typically manifested in different frameworks such as single-objective and multi-objective evaluations (Cui et al., 2020).

Different stages of societal development require diverse land use strategies, resulting in the creation of various assessment frameworks. For instance, when a city is abstracted into a linear model, the direction of land function evaluation is determined by a single indicator, such as economic output (C. G. Liu et al., 2005) or physical output (Pendall, 2003). As the focus of assessments shifts from purely economic or fiscal outcomes to rational use and sustainable development, greater attention is given to ecological resources and social services (Batty, 2002; Lin et al., 2022).

The emergence of integrated frameworks reflects this shift in research paradigms. These include, among others, the classic socio-economic-environmental (SEE) framework mentioned earlier, which is widely used in sustainable development research (Jing & Wang, 2020; Weng et al., 2022). Researchers have merged, subdivided, or expanded subsystem frameworks depending on

specific regional contexts and objectives (Lin et al., 2022; J. Liu et al., 2020; Zhongping et al., 2011). In practice, considering the endogenous relationships between social and economic systems, these three elements are often further integrated into the Social-Ecological framework (also known as the Soc-Eco, SE framework) (Ji et al., 2024; Z. Zhang et al., 2023). This framework posits that socio-ecology factors dominate urban development and are characterized by complexity, non-linearity, and uncertainty (Levin et al., 2013; Z. Zhang et al., 2023) rather than unidirectional relationships (Dong et al., 2021; L. Li et al., 2022; Lin et al., 2022; Weng et al., 2022). This multidimensional analytical framework facilitates a better understanding of the interrelations between land use sub-functions and the dynamic interactions between human activities and land functions.

Overall, human understanding and utilization of land use functions have evolved from simple to complex, and from singular to multifaceted. The "Multi-functionality of Land Use" is a fundamental concept and methodological framework for evaluating the impact of land use changes on its functions. It helps assess the comprehensive benefits brought by diversified land use (Zhen et al., 2010) and gauges the human well-being derived from such diversification (W. Zhao & Fang, 2014). Furthermore, in the context of rapid urbanization, research on the multifunctionality of land use and multipurpose management strategies provides new perspectives for the efficient use of land resources, fostering urban vitality, and optimizing urban environments.

2.3 The vitality-land relationship

2.3.1 The impact of land on vitality

The source of urban vitality is intricately linked to both people and environment; therefore, research on creating and enhancing urban spatial vitality primarily focuses on residents and land use. The impact of urban land use on vitality has been expressed earlier in Howard's Garden City concept (Howard et al., 2013), which aimed to enhance urban vitality by optimizing land use distribution to improve living conditions. New Urbanism has introduced a new direction by advocating for the integration of urban spatial form and the built environment (Y. Long & Huang, 2019) to enhance urban vitality and sustainability. This concept offers a foundational theoretical basis for studying the roles of urban functions, attributes, and systems in promoting UV (Katz,

1994).

Internationally, scholars have examined how the built environment of neighborhoods attracts pedestrian activity by delineating pedestrian activity spaces (Jalaladdini & Oktay, 2012). These studies have confirmed the applicability of Jacobs' theories across different geographical contexts (Delclòs-Alió et al., 2019). A review of previous research, particularly studies on multi-indicator frameworks for vitality assessment, reveals that urban vitality is strongly associated with land use mix, accessibility to transportation and facilities, and urban functional activities. Alexander (1975) argued that the vitality of an urban environment depends on its continual repair and adaptation to maintain a healthy state.

The first Congress for the New Urbanism in 1993 established three levels of principles for New Urbanism based on scale of practice: (1) the region, metropolis, city, and town; (2) the neighborhood, district and corridor; and (3) the block, street, and building (Katz, 1994). The Seaside community in Florida, one of the earliest examples of New Urbanism, represents a classic model of traditional neighborhood development. Port's study on the Greater Boston area demonstrated that the principles of New Urbanism are feasible for infill development and effective in controlling urban sprawl (Port, 2004).

In recent years, as China's urbanization goals have shifted from quantity to quality, scholars have increasingly focused on urban vitality assessment to facilitate city transformation and create more vibrant urban spaces, conceptualizing the city as a "living organism." Modern urban planning pursues "organized complexity," akin to life sciences, viewing the city as a dynamic, organically connected whole composed of multiple systems (Portugali, 2016). For example, Ye et al. (2018) summarized the principles of fostering urban vitality, emphasizing that appropriate development intensity, a high degree of functional mix, and good street accessibility are critical factors for enhancing urban vitality (Ye et al., 2018). Mao et al. (2020) utilized coupling degree and geographically weighted regression (GWR) models to demonstrate that economic density, educational and research resources, infrastructure development level, and digital informatization are pivotal factors influencing urban vitality (MAO & ZHONG, 2020). Wang et al. (2023) applied gradient boosting decision tree-Shapley additive explanations (GBDT-SHAP) models to quantify the nonlinear impact of the built environment on urban vitality (Z. Wang et al., 2023).

2.3.2 Land mixed-use development

The Athens Charter (1933) introduced four fundamental functions of modern cities: living, working, recreation, and transportation, leading governments to segregate cities into distinct functional zones. However, rigid functional zoning weakened the organic structure of cities, leading to a decline in urban vitality. In response, theories of urban renewal and strategies to enhance urban vitality emerged in the 1960s, emphasizing the intrinsic relationship between urban vitality and land use patterns. Jane Jacobs (1961) introduced the concept of mixed primary uses, contending that functional segregation failed to capture the complex dynamics of urban operations. She suggested that organically mixing diverse functions could enhance the attractiveness and vitality of an area, fostering successful communities.

In the 1960s, land use control methods such as Planned Unit Developments (PUDs) and Overlay Zoning were promoted in the United States, emphasizing flexible development and mixed land use. The Urban Land Institute (1976) in the United States proposed principles for mixed-use development, including the spatial combination of various functions, the integration of physical and functional elements, and comprehensive planning control. These principles aim to guide the compatibility and integration of mixed land use. Subsequently, the Machu Picchu Charter (1977) criticized the Athens Charter's concept of single-use zoning, advocating for cities as integrated environments with multiple functions. Mixed-use theory has since become a cornerstone of spatial development strategies, promoting urban vitality and sustainability (Witherspoon et al., 1976).

Subsequently, urban mixed-development theories and models such as New Urbanism, Compact City, Smart Growth, and Community Building were gradually introduced. These approaches share common principles, including the development of public spaces, mixed-use development, compact growth, and a human-centered focus (D. Wang et al., 2019). As urban renewal and sustainable development movements gained momentum in the United States and Europe, mixed land use emerged as a crucial tool to counteract the decline of urban vitality and promote sustainable urban development, gradually becoming a fundamental paradigm in modern urban planning (Port, 2004) . It matured as an urban land policy through both research and practice(Arts et al., 2016; Grant, 2002; Rowley, 1998).

2.3.3 Coupling of land functions

Research on mixed land use in China started relatively late. It was introduced in the 1990s along with the rapid urbanization process following the reform and opening-up policy. Generally, it is believed that mixed land functions are the source of urban diversity and vitality, effectively responding to the diverse activities and needs of humans (Y. Huang, 2008) . These mixed-use zones have evolved in practice, with rich connotations, and should align with the intrinsic value of land use rather than merely serving as simple tools for land compatibility. However, current research on "mixed land use" in China focuses more on functional zoning in urban areas, primarily relying on data from Points of Interest (POI), nighttime lights, and reviews (Cen et al., 2024; G. Zhao & Song, 2022) , with a focus on the mixing of residential, commercial, and entertainment functions (S. Tang & Ta, 2022) , while discussions on broader functional mixing remain relatively scarce.

In terms of analytical methods, common approaches include using the Entropy Index or "land-use mixing" calculation models (C. Wu et al., 2023) , and measuring the degree of land-use mixing at a certain scale or landscape through the Shannon diversity index (G. Zhao & Song, 2022). However, the goal of mixed land use should be to create positive externalities, rather than simply resulting in "organic chaos" (Gu et al., 2019; D. Wang et al., 2019) . Therefore, the research direction is gradually shifting toward exploring the interaction and coordination of multiple systems, focusing on the development of the overall system (Liao & Liang, 2024; Wang et al., 2023).

The concept of coupling originates from physics, referring to the effects and synergies generated by the interaction between two or more systems. Geographers have borrowed and expanded this concept, applying it to the study of complex interdependencies and interactions between human, natural, and social systems(Morzillo et al., 2014; Qi et al., 2012) . This helps us gain a more comprehensive understanding of the complex relationship between land use and urban vitality during urbanization.

In practical applications, dual-system models (M. Huang et al., 2022) or multi-system models (H. Liu et al., 2019) , can effectively analyze complex coupling mechanisms and reveal the impact of urbanization and ecological interactions on the overall system. These models evaluate system

patterns, flows, drivers, and response mechanisms, uncovering the relationship between the self-organization of underlying elements and the emergent behavior of the system, and they have profound effects on urban development in spatial and temporal dimensions.

In conclusion, the role of mixed functions in promoting vitality is widely recognized. However, current research primarily focuses on the mixing of socio-economic functions or land use in built-up areas, with limited attention to the coupling and coordination of urban systems and their impact on urban vitality (D. Wang et al., 2019).

3 MATERIALS AND METHODS

3.1 Study area

3.1.1 Location & economic development

Luohe City (113°27′–114°16′ E, 33°24′–33°59′ N) is located in the south-central part of Henan Province, central China (Figure 8). The terrain is predominantly flat, and the Sha Li River bisects the urban area into three distinct zones. The southern zone, known as the old town, is characterized by historical and densely built-up areas. The northern zone, or the new town, has undergone significant urban expansion in recent years and now serves as a hub for administrative and commercial activities. The western peninsula area is focused on integrating green spaces and promoting residential development.

Luohe spans an area of 2,697.15 km² and, as of 2023, has a permanent population of 2.37 million, indicating moderate population density and growth. Economically, the city ranks at a medium development level within Henan Province, placing 15th out of 18 cities in GDP in 2022. However, it demonstrates notable economic dynamism, ranking 3rd in GDP growth rate among Henan's cities in the same year. This rapid growth is driven by emerging industries, particularly in food processing and logistics, bolstered by Luohe's strategic location along major transportation corridors, which enhances its role as a regional trade and logistics center. Additionally, the local government's efforts to improve infrastructure and attract investment have expanded the city's socio-economic functions.

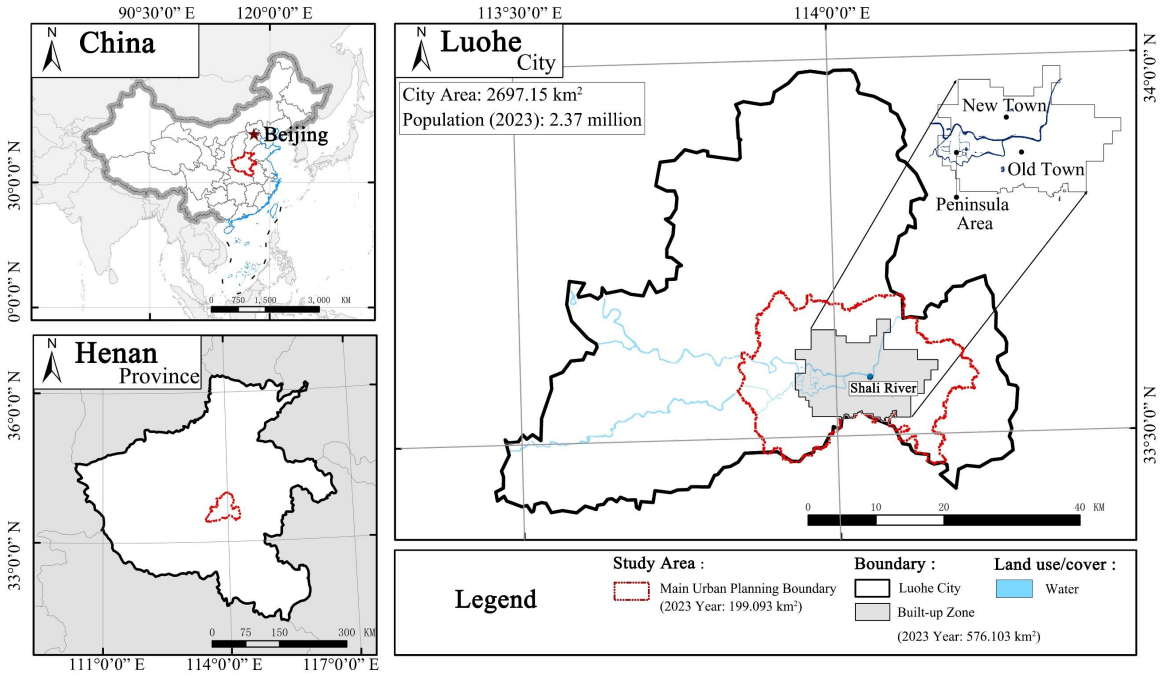

Figure 8 Location Map: Study Area (GS (2020) 4619).

3.1.2 Representativeness and uniqueness

The economic and urbanization levels of Luohe City represent many of China's lesser-known cities (Wang et al., 2023), showcasing a typical Chinese urban development model guided by policies and resource investment. In planning theory, the point-axis system has profoundly impacted urban planning in China (Manchun LI, 2019). This theory highlights the differential impacts of infrastructure, such as traffic and landscape, on location and thereby introduces the inescapable heterogeneity of location theory on urban development. Historically, Luohe's urban development was driven by the livestock trade brought about by river transportation. The historical street at the city core is Niuhang Street, a street where cattle were bought and sold. In the context of Transit-Oriented Development (TOD) theory, the heterogeneous transportation network introduces new driving factors for open spaces, vegetation, economies of scale, and market competition, highlighting the critical role of roads and transportation in the city's economy (Calthorpe, 1993).

Luohe City has distinct characteristics. Its flat terrain, lack of significant natural landscapes or historical relics, and limited large green spaces around the urban area make Luohe an ideal subject for analyzing the relationship between urban land development and human activities. Overall, Luohe not only represents the general development patterns of ordinary Chinese cities but also demonstrates unique characteristics under specific conditions, providing a distinctive

perspective on changes in human-land relationships during urbanization.

3.1.2.1 Urbanization &land development

Urbanization is not a stable linear process; rather, it resembles a stepwise zigzag pattern (Figure 9 (b)). This is primarily because urban expansion often follows a cycle of agglomeration, dispersion, and re-agglomeration. As the existing growth areas gradually face constraints from boundary effects, the development and construction of new growth poles are often driven by policy, resulting in a wave-like progression at the macro level (China, 2000-2010) (Wang et al., 2023). This characteristic is observed not only in China but also in other Asian countries, such as Japan, and in European countries, such as Hungary (Figure 9 (a)). The steady-state and mutation phases of urban development can be distinguished by changes in the proportion of built-up land or the rate of change in different types of land (Figure 9 (b)).

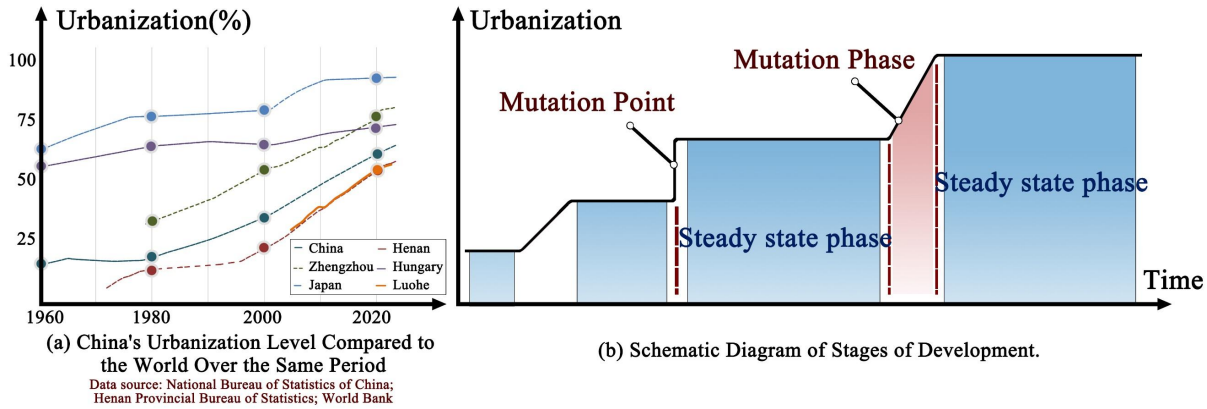

Figure 9 Schematic Diagram of Stages of Urban Development.

Based on MODIS land cover classification data, the study shows changes in the area of Farmland, Green Infrastructure (GI), and Artificial Surfaces (AS) in Luohe City from 2001 to 2022 (expressed in terms of pixel count). Overall, over the past 20 years, the area of AS in Luohe City has steadily expanded, while farmland has gradually decreased. Correspondingly, green space initially decreased and then increased, indicating that urban development generally follows a path of “Destruction followed by recovery”.

The standardization of pixel counts for the three types of land shows that the stages of land development in Luohe City can be further differentiated into: (1) The first phase (2001-2013) was an urban development phase. During this period, the area of AS increased relatively slowly from 2001 to 2010, but began to accelerate from 2010 to 2013. Before 2013, farmland area remained relatively stable while GI was limited, indicating that urban development occurred at

the expense of green space. In 2013-2014, there was a mutation period in land development, marking the transition to the second phase. (2) The second phase (2014-2018) was a GI restoration phase, during which the growth of AS further accelerated. Influenced by the "Returning farmland to forest" policy, GI area began to recover while farmland area started to decline rapidly. Between 2014 and 2018, GI area surpassed the initial levels of 2001, indicating that Luohe City began to simultaneously focus on the development of social and ecological functions. (3) After 2018, the proportions of urban GI and farmland changed significantly again, and Luohe City entered the third phase. The third phase (2018 to present) is characterized by ecological construction, with a continued rapid increase in the area of AS. Meanwhile, the further implementation of the "Returning farmland to forest" policy accelerated the growth of GI, although farmland area continued to decline rapidly. Nevertheless, as of 2022, farmland still occupies a significant proportion of the planned area (pixel count: 1516; proportion: 65.74%), indicating that the city still has substantial land potential.

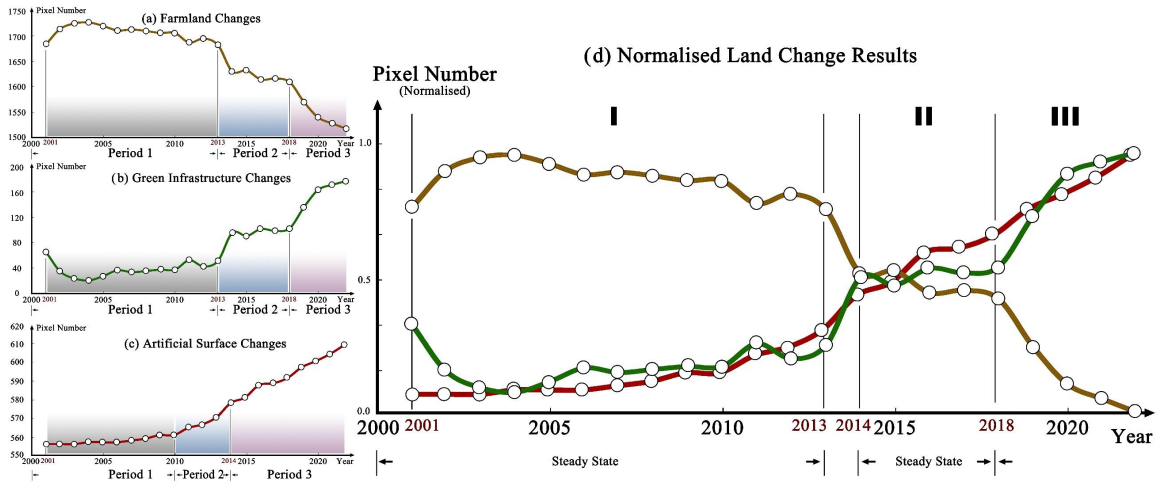

Figure 10 MODIS-based Land Area Changes in Luohe, 2001-2022.

Therefore, studies on urban development and land function assessment should consider the period from 2014 to the present as a steady-state phase, while future land simulations should focus on the steady-state phase from 2018 to the present.

3.1.2.2 Risk of lack urban vitality

It is worth noting that changes in the human-land relationship in Luohe also reflect dynamic processes of both synchronous and asynchronous development in the urbanization process, corresponding to the current trend of a disconnect between population growth and urban construction in China. This could well represent potential future issues in human-land relations.

Therefore, the study of Luohe can provide an illustrative case for issues related to land development and resident vitality in these cities.

The risk of Luohe's current lack of urban vitality comes from two main sources: 1 the first is the year-on-year decline in the resident population. 2 The second is the asynchronous development of population/construction land in terms of quantity. These can be glimpsed in the changes in the relationship between population and land in the last 20 years.

The human-land relationship in Luohe City can be understood in two distinct phases. First, from 2000 to 2010, the rate of population growth surpassed urbanization, prompting development strategies centered on expanding construction land to ensure sufficient living space for the growing population. Second, after 2010, according to data from the Henan Province Yearbook, the growth rates of both the population and urban built-up area appeared to align, suggesting a period of synchronized, coupled development between human and land resources.

However, following the 2020 national census, which involved direct household visits and reliable individual registration, the Henan Province Yearbook revised the population data for the prior decade in 2021. This revision revealed that Luohe City had, in fact, experienced a steady population decline from 2010 to 2020, contrasting with the rapid expansion of urban land. This divergence reflects an asynchronous development trend, highlighting potential risks of urban "sprawl" and diminished vitality. Luohe may thus exemplify the broader challenges of population decline and urban contraction, signaling critical future scenarios for cities across China.

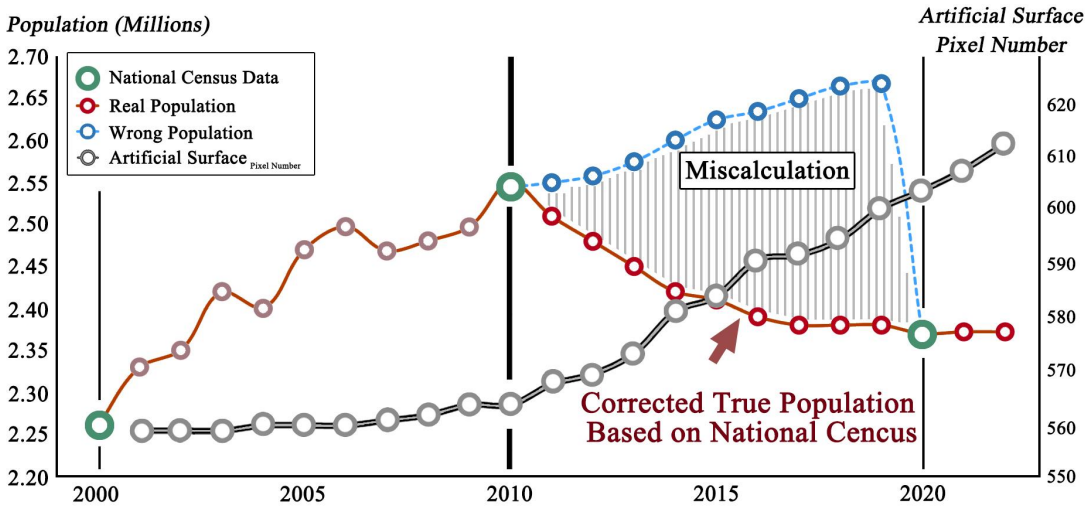

Figure 11 Changes in Population and AS Area in Luohe, 2000-2022.

3.1.2.3 Urbanization & built-up area expansion

From 2014 to 2023, the area of built-up areas in Luohe City increased from 143.84 km² (24.97% of the study area) to 199.09 km² (34.56% of the planned area), an increase of 55.25 km², representing a growth rate of 38.41%. Morphologically, this expansion exhibited a pronounced TOD pattern, with new built-up spaces expanding in a star-shaped pattern along national and provincial roads. Specifically, small patches around major landscapes either disappeared or merged into the main body, with the built-up area expanding preferentially in one or more directions, a phenomenon described as the axial strip extension model (Cheng et al., 2021).

The center of gravity of the built-up area converged near the intersection of rivers and railways, indicating that the city as a whole expanded along these axes, highlighting the locational importance of transport and waterways. The center of gravity shift map revealed Luohe City's development trend over the past decade: constrained by the city boundary to the south, the built-up area expanded predominantly to the northeast. The direction and rate of center of gravity shifts remained relatively stable, indicating that the city's development policies and driving factors have been relatively consistent over the past ten years.

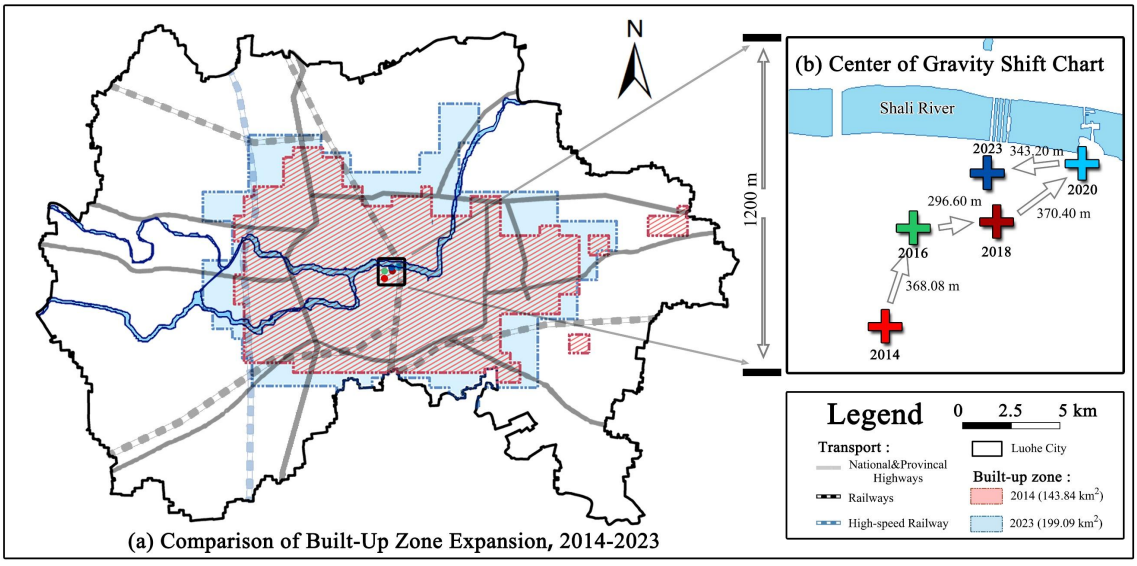

Figure 12 Built-up Area Boundaries and Center of Gravity Shifts.

3.2 Data acquisition and preprocessing

This section specifically includes: (1) introduction to the data sources; (2) preliminary processing after data acquisition; and (3) the calculation of basic remote sensing indices.

3.2.1 Data sources and collection

The data in this study is divided into three main parts: (1) human mobility data used for assessing urban vitality; (2) satellite remote sensing data and related products used for land assessment; (3) other data, including road network, Google Map, and urban yearbooks and so on.

3.2.1.1 Baidu heat map data

The human mobility data used in this study is derived from the human activity heat map feature provided by Baidu Map. It quantifies mobile signals based on real-time geographic information provided by smartphone users of Baidu products (such as Baidu Map, Baidu Search, and Baidu Music), making it one of the most influential big data sources in China. While this dataset cannot directly reflect the actual number of human activities, it has been proven to be a reliable indicator of the real-time distribution of human activity intensity, serving as a proxy for depicting the spatial distribution of the population in real time(Z. Fan et al., 2021).

The human mobility data collection spans 4 weeks (i.e., 4 activity cycles) distributed across four seasons: Spring (April 11-16, 2023); Summer (July 11-16, 2023); Autumn (October 11-16, 2023); Winter (January 15-21, 2024). During the sampling period, no extreme weather events occurred. The data features high temporal resolution (hourly) and spatial resolution (200 m*200 m).

3.2.1.2 Remote sensing satellite datasets

This study primarily utilizes atmospherically corrected Landsat-8/9 surface reflectance (L8/9 SR) data, collected every 16 days. The Landsat-8/9 satellites carry the Operational Land Imager (OLI) and Thermal Infrared Sensor (TIRS), providing global coverage with 11 spectral bands: 30 m resolution for the main spectral bands, 15 m for the Panchromatic band, and 100 m for the Thermal bands.

For nighttime light (NTL) data, the study uses the Suomi NPP Visible Infrared Imaging Radiometer Suite (VIIRS) from the Earth Observation Group. VIIRS Day/Night Band (DNB) data offers higher spatial resolution (463.83 m) and a higher light saturation threshold than DMSP/OLS and has been available since 2012. The NTL data for this study is sourced from monthly composite data from the NPP-VIIRS satellite.

3.2.1.3 Finished product datasets

MODIS (Moderate Resolution Imaging Spectroradiometer) is a primary sensor aboard NASA's EOS satellites Terra (launched in 1999) and Aqua (launched in 2002). MODIS provides high spectral resolution and a wide spectral range, offering multiple data products. These include raw (L0), corrected (L1), and application-specific (L2-L4) datasets, covering land, atmosphere, and ocean, with a total of 44 standard data types. This study primarily uses MODIS land data products. Gross Primary Productivity (GPP) data is from the MOD17 dataset with a 500m resolution, and land cover data comes from the MOD12 dataset, also with a 500m resolution. The MODIS land classification has been consolidated as follows.

Table. 1 MODIS Land Consolidation.

MODIS ID	Description	Merge
9	Savannas: tree cover 10-30% (canopy >2m)	Green Infrastructure
10	Grasslands (a very small amount): dominated by herbaceous annuals (<2m).	Green Infrastructure
12	Croplands: at least 60% of area is cultivated cropland.	Farmland
13	Urban and Built-up Lands: at least 30% impervious surface area including building materials, asphalt and vehicles.	Artificial Surface
14	Cropland/Natural Vegetation Mosaics (a very small amount): mosaics of small-scale cultivation 40-60% with natural tree, shrub, or herbaceous vegetation.	Farmland

Given that human settlement density is a key indicator for land assessment and urban vitality, this study incorporates the WorldPop population density dataset. This dataset offers global spatial population distribution data with a 100m spatial resolution and annual temporal resolution from 2000 to 2020. However, two challenges arise: (1) Post-2020 population data requires fitting and extrapolation, and (2) for specific study areas, outlier removal and linear correction of regional population data are needed, with no-data areas addressed using an IQR moving window method. Detailed procedures will be explained in the methods section.

3.2.1.4 Terrain & other data

A Digital Elevation Model (DEM) is a digital representation of the Earth's surface, typically obtained via satellite for large-scale coverage due to cost considerations. This study uses the Copernicus DEM 30m (COP-DEM) dataset, a product of the Copernicus program—a collaboration between the European Space Agency (ESA) and the European Union. The Copernicus DEM provides a global elevation model with 30m resolution, derived from

TANDEM-X and SRTM data, sampled between 2010 and 2015, and released in 2019.

The above remote sensing datasets were processed using the Google Earth Engine platform (GEE, https://code.earthengine.google.com/, accessed in April 2024). Road network data were obtained from OSM (https://www.openstreetmap.org/, accessed in April 2024) and subsequently manually corrected using Google Maps. Text and yearbook data were sourced from the Henan Provincial Bureau of Statistics (https://tjj.henan.gov.cn/tjfw/tjsj/). Details of the specific dataset are given below:

Table. 2 Data Set Acquisition Paths and Descriptions.

Name	Source	Time	Resolution	Temporal Resolution
Landsat-8	LANDSAT/LC08/C02/T1_L2	2014 – 2022	30m	16 Days
Landsat-9	LANDSAT/LC09/C02/T1_L2	2023 – 2024	30m	16 Days
GPP	MODIS/006/MOD17A2H	2014 – 2022	500 m	Multi-Day
	MODIS/061/MOD17A2H	2023 –2024	500 m	8 Days
LULC – MODIS	MODIS/061/MCD12Q1	2001 – 2022	500 m	Yearly
NTL	NOAA/VIIRS/DNB/MONTHLY_V1/VCMCFG	2014 –2024	463.83 m	Monthly
POP	WorldPop/GP/100m/pop	2000 – 2020	100 m	Yearly
COP – DEM	COPERNICUS/DEM/GLO30	2010.12 – 2015.01	30 m	-
Roads	OSM, https://www.openstreetmap.org/	2018 –2024	-	-
Yearbooks	Henan Provincial Bureau of Statistics（https://tjj.henan.gov.cn/tjfw/tjsj/）	-	-	-

3.2.2 Data processing

3.2.2.1 De-cloud and data synthesis

Cloud Removal and Data Synthesis: The 2023 L8/9 SR dataset was utilized, and pixels corresponding to Dilated Cloud (Bit 1), Cloud (Bit 3), and Cloud Shadow (Bit 4) were excluded based on the QA_PIXEL band. To address null values and ensure data stability, the annual median was calculated for each pixel. This process combined multiple scene images into a single annual composite dataset.

Data Synthesis and Correction: The raw NTL data were provided as monthly composites, and GPP/NDVI data were provided as 8-day/16-day composites. Both datasets were processed into annual data by calculating the mean value for each pixel. Given the common “blooming” effect in these data, a mask was generated based on the 30 m land classification data (described in detail later) to exclude NTL/GPP values over the water surface. Finally, the Baidu human

mobility data were used as the baseline resolution (200m*200m) of all the data for resampling, and the resolution was unified.

3.2.2.2 Basic remote sensing indicators

Various remote sensing indices have been developed using the Landsat satellite bands to monitor and analyze land cover and environmental changes. These indices help identify and quantify features like vegetation growth, building density, water bodies/moisture distribution, and land surface temperature. Since these indices will be frequently referenced and integrated in subsequent sections, they are pre-calculated here. The abbreviations for the bands used in the formulas correspond to Landsat 8/9: Blue (B2), Green (B3), Red (B4), NIR (B5), SWIR1 (B6), SWIR2 (B7), and TIR1/2 (B10/B11).

(1) Vegetation Indicators

NDVI (Normalized Difference Vegetation Index). NDVI is one of the most commonly used indices to reflect changes in vegetation greenness by utilizing the differing absorption rates of NIR and Red spectral bands in green vegetation. It is closely related to plant biomass, leaf area index, and vegetation coverage, making it a comprehensive indicator of vegetation density and health. **EVI (Enhanced Vegetation Index).** EVI addresses NDVI's saturation issues in areas with high vegetation and improves atmospheric and background noise correction. It performs better in densely vegetated and atmospherically influenced regions.

FVC (Fractional Vegetation Cover). FVC represents the vertically projected area of green vegetation canopy per unit area. Traditionally measured with fisheye lenses, remotely estimated FVC relies on techniques such as mixed pixel decomposition. This study uses a pixel binary model (Peng et al., 2016), assuming that pixel information is composed of vegetation and bare soil. After recalculating NDVI data, the formula for FVC is:

$$\mathrm{FVC} = \frac{(\mathrm{NDVI} - \mathrm{NDVI_{soil}})}{(\mathrm{NDVI_{vg}} - \mathrm{NDVI_{soil}})} \quad (1)$$

where $\mathrm{NDVI_{soil}}$ and $\mathrm{NDVI_{vg}}$ are the NDVI values for bare soil and fully vegetated areas, typically at the 5% and 95% cumulative percentiles.

LAI (Leaf Area Index). LAI (Baret & Guyot, 1991) measures the total area of plant leaves per

unit ground area, indicating the three-dimensional vegetation volume. It is essential for processes such as evapotranspiration and photosynthesis. The empirical formula for LAI (Boegh et al., 2002), is:

$$\mathrm{LAI} = 3.618 * \mathrm{EVI} - 0.118 \tag{2}$$

LAI values typically range from 0 to 3.5, with higher values indicating more substantial vegetation volume.

SAVI (Soil-Adjusted Vegetation Index). SAVI improves NDVI by minimizing soil brightness influences through a soil correction factor, making it more effective in areas with low vegetation cover, such as urban or arid regions. The formula for SAVI is:

$$\mathrm{SAVI} = ((\mathrm{NIR} - \mathrm{Red})/(\mathrm{NIR} + \mathrm{Red} + \mathrm{L})) * (1 + \mathrm{L}) \tag{3}$$

Where L is the soil correction factor, generally set to 0.5. SAVI values range from -1.0 to 1.0.

(2) Building Indicators

NDBI (Normalized Difference Built-up Index). This index is used to identify and quantify the density and coverage of urban buildings. **IBI (Index of Building Intensity).** This index incorporates water and vegetation background information into the NDBI, effectively suppressing background signals from water bodies and vegetation. It is used to assess urban density by considering factors such as building height, density, and coverage (Xu, 2008). The formula for IBI is:

$$\mathrm{IBI} = \frac{(\mathrm{NDBI} - (\mathrm{SAVI} + \mathrm{MNDWI})/2)}{(\mathrm{NDBI} + (\mathrm{SAVI} + \mathrm{MNDWI})/2)} \tag{4}$$

MNDWI will be introduced later.

(3) Water and Moisture Indicators

MNDWI (Modified Normalized Difference Water Index). This index improves upon the NDWI by adjusting the wavelength combinations used, thereby enhancing water body detection and distinguishing them from other surface types. The MNDWI better reveals subtle water features, such as suspended sediments and water quality changes. Additionally, MNDWI effectively distinguishes shadows from water bodies, addressing challenges in water extraction

due to the presence of shadows (Han-Qiu, 2005) . **NDBSI (Normalized Difference Built-up and Soil Index).** This index indicates surface "dryness," derived by averaging the IBI and the Soil Index (SI), which reflects exposed or sparsely vegetated land in the study area. The formula is:

$$\mathrm{NDBSI} = \frac{\mathrm{IBI} - \mathrm{SI}}{2} \tag{5}$$

$$\mathrm{SI} = ((\mathrm{SWIR1} + \mathrm{RED}) - (\mathrm{NIR} + \mathrm{BLUE}))/((\mathrm{SWIR1} + \mathrm{RED}) + (\mathrm{NIR} + \mathrm{BLUE})) \tag{6}$$

WET: WET reflects the moisture content of water bodies, soil, and vegetation, which is closely related to the ecological environment. High WET values positively impact vegetation growth, disaster prevention, and regional ecological protection. The formula for WET is:

$$\mathrm{WET} = \mathrm{L1} * \mathrm{Blue} + \mathrm{L2} * \mathrm{Green} + \mathrm{L3} * \mathrm{Red} + \mathrm{L4} * \mathrm{NIR} + \mathrm{L5} * \mathrm{SWIR1} + \mathrm{L6} * \mathrm{SWIR2} \tag{7}$$

Where L1-L6 are correction coefficients corresponding to each band, for the OLI sensor: L1= 0.1511，L2= 0.1973，L3= 0.3283，L4= 0.3407，L5= -0.7117，L6= -0.4559.

(4) Thermal Indicators

LST (Land Surface Temperature). This metric measures the actual temperature of the land surface, derived from TIR band data. LST is increasingly important in various studies assessing surface conditions, such as urban climate, evapotranspiration, and vegetation stress. This study uses the Statistical Mono-Window (SMW) algorithm to derive LST from the TIR bands of Landsat 8/9 SR (Ermida et al., 2020).

3.3 Data testing and dimensionality reduction methods

3.3.1 Principal component analysis

Principal Component Analysis (PCA) is a commonly used dimensionality reduction technique that projects high-dimensional data into a lower-dimensional space while preserving as much variance information as possible. After normalizing the original data, the covariance matrix, eigenvalues, and eigenvectors are calculated. The top k eigenvectors with the largest eigenvalues are selected as principal components, as they explain the most variance in the data. The original data is projected onto these principal components, resulting in reduced-dimensionality data. Through linear transformation, the original variables are converted into a few uncorrelated new

variables (principal components), each of which is a linear combination of the original variables (Smith, 2002).

Two key metrics are considered: the proportion of total information and the eigenvalue. The proportion of total information refers to the ratio of the variance explained by the top k principal components to the total variance, reflecting the amount of original data information retained. Eigenvalues represent the amount of variance explained by the corresponding eigenvectors (principal components); the larger the eigenvalue, the more significant the principal component. Selecting the top k eigenvectors with the largest eigenvalues helps retain the primary information in the data.

In this paper, PCA is a mandatory step to calculate the RSEI (to be presented later). It is also used to screen representative landscape pattern indices.

3.3.2 Normalization method

In this paper, different normalization methods are applied to different types of indicators. The normalization of positive indicators is denoted as "nor+," while the normalization of negative indicators is denoted as "nor-." The specific formulas are as follows:

$$nor^{+} = \frac{X - X_{min}}{X_{max} - X_{min}} \tag{8}$$

$$nor^{-} = \frac{X_{max} - X}{X_{max} - X_{min}} \tag{9}$$

where X is the original data point, X_{min} is the minimum value, and X_{max} is the maximum value in the dataset. The normalization method adjusts the magnitude of different indicators so that they can be compared on the same scale, eliminating the effects of different magnitudes in the raw data. In this way, the normalized data can more accurately reflect the relative importance of each indicator in the comprehensive evaluation.

3.3.3 Inter-quartile range test

Compared to the Z-test and robust Z-test, the IQR (Inter-quartile Range) test does not assume the normality of the original data, making it more broadly applicable. The IQR is insensitive to outliers, as it relies only on the middle 50% of the data, making it a reliable statistic for describing data dispersion and identifying outliers, especially in the presence of extreme values.

In identifying outliers in raster data, spatial heterogeneity should be considered; thus, a moving window IQR test is employed. An N*N pixel window is defined, and the 25th and 75th percentiles of each pixel's local area are calculated, representing the lower quartile (Q1) and upper quartile (Q3), respectively. The IQR, defined as the difference between Q3 and Q1, is used to delineate the normal value range, set from Q1 - 1.5 * IQR to Q3 + 1.5 * IQR. Values outside this range are considered outliers.

$$IQR = Q3 - Q1 \tag{10}$$

In this paper, IQR is combined with the moving window method for removing outliers in raster datasets (e.g., population data) to ensure data robustness.

3.4 Land functional assessment framework

Land use often manifests in both explicit and implicit forms (Long, 2012; Song & LI, 2019). During periods of low human activity, area serves as the primary driving factor and represents the explicit outcome of human activities. However, as human activity increases, the forms and functions of land use, the social/ecological benefits generated per unit of land, as well as the patch morphology, distribution, and connectivity at the class scale undergo significant changes. These are implicit expressions of the outcomes of human activity.

Based on this understanding, we constructed a comprehensive framework to evaluate the spatial heterogeneity of land functions, considering both the social and ecological functions of land. This framework integrates quantity, quality, and structure: **(1) The multi-source data principle.** This approach not only effectively avoids data collinearity issues but also comprehensively assesses the diversity and complexity of land functions from multiple dimensions, which is particularly crucial in complex urban environments. **(2) The comprehensive indicators principle.** While ensuring the distinctiveness of the indicators, we use comprehensive indicators derived from the combination of multiple indices to enhance the simplicity and interpretability of the assessment system. The use of comprehensive indicators also reduces redundant information while improving the overall efficiency of the assessment.

Table. 3 Land Function Assessment Framework and Indicators.

Goal Layer	Framework	Rule Layer	Index Layer
Land Social	Quantity	Spatial Service	Artificial Surface Rate (ASR)

Function (LSF)		Urbanization Level	LST and EVI regulated NTL city index (LERNCI)
	Quality	Transportation Accessibility	Weighted Integration (WI)
		Settlement Situation	Worldpop Population Density (POP)
	Structure	Artificial Surface Patch Morphology	Artificial Surface -Landscape Shape Index (ALSI)
		Artificial Surface Patch Aggregation	Artificial Surface -COHESION (ACO)
	Quantity	Basic Green Space Service	Green Infrastructure Rate (GIR)
Land Ecological Function (LEF)	Quality	Vegetation Cover	Vegetation Quality (VQ)
		Ecological Benefits	Remote Sensing Ecological Index (RSEI)
	Structure	Green Infrastructure Patch Morphology	Green Infrastructure -Landscape Shape Index (GLSI)
		Green Infrastructure Patch Aggregation	Green Infrastructure -COHESION (GCO)

3.4.1 Random Forest-based land classification

Random Forest has been widely applied in land classification studies across global cities (Nguyen et al., 2020; Zhou et al., 2020). In this paper, we use spectral, indicator, nightlight, terrain, and textural features—a total of five types of features—to aid in classification. Based on annual composite data from Landsat 8/9 SR, this approach aims to address the common challenges of interpreting multispectral images and data redundancy by highlighting key information about land use types, enhancing image interpretability, and improving monitoring accuracy. PCA was employed to compress the B2-B7 spectral bands into three principal components, which were used as spectral features (X. Wang, Yao, et al., 2023).

NDVI, NDBI, MNDWI, and SI were employed as index features, each emphasizing specific land use characteristics such as green infrastructure, artificial surfaces, water bodies, and farmland (bare soil). Since urban development and expansion tend to occur in flatter areas, terrain features such as DEM and slope were also included.

Due to the potential confusion between green infrastructure and farmland, texture features were added to aid analysis. These texture features were derived from the panchromatic band (B8, resolution: 15m) using the Gray-Level Co-occurrence Matrix (GLCM), extracting the GLCM mean and variance. In Luohe City, the regular textures of farmland ridges contrast with the more

natural textures of planned green infrastructure, aiding in their differentiation.

Additionally, nightlight features were incorporated. NTL intensity helps locate artificial surfaces and differentiate green infrastructure from farmland, as green infrastructure are more likely to be situated around human settlements. Using the Random Forest classifier, we derived LULC data for 2018-2024, categorized into: 1) Artificial Surface (AS), 2) Green Infrastructure (GI), 3) Water, and 4) Farmland.

Table. 4 LULC Classification Accuracy.

Year	Overall Accuracy	Kappa Accuracy
2018	87.04%	81.41%
2019	84.56%	79.57%
2020	86.43%	81.61%
2021	87.03%	81.55%
2022	87.94%	83.69%
2023	89.95%	86.43%
2024	88.44%	84.40%

LULC is classified data. To facilitate the calculation of factor weighting and raster overlays, a 200m grid was constructed to compute the land use proportion within each grid, referred to as the land use rate. This study focuses on the Artificial Surface Rate (ASR), which indicates the physical basis of the land's social functions; and the Green Infrastructure Rate (GIR), which indicates the physical basis of the land's ecological functions.

3.4.2 Vegetation quality assessment

To evaluate the heterogeneity of vegetation quality (VQ), we adopted three indicators: LAI, FVC, and GPP, based on the National Ecological Environment Standard (HJ 1172-2021, China). These indicators are combined with equal weights to represent the quality of natural vegetation within an ecosystem, reflecting the condition of vegetation and the overall ecosystem.

$$VQ = \frac{nor^{+}(FVC) + nor^{+}(LAI) + nor^{+}(GPP)}{3} \quad (11)$$

3.4.3 Ecological benefit assessment

The Remote Sensing-based Ecological Index (RSEI) is widely used due to its visibility, objectivity, and comparability (XU, 2013). RSEI combines greenness (NDVI), wetness (WET),

dryness (NDBSI), and heat (LST) indicators for the period of May to October. After normalizing these indicators and processing them through PCA, the first principal component (PC1) is extracted. This PC1 is further normalized to obtain the objective ecological index.

$$\mathrm{RSEI} = 1 - nor^{+}\ (\mathrm{PC1}\ (\mathrm{NDVI}, \mathrm{WET}, \mathrm{NDBSI}, \mathrm{LST})) \tag{12}$$

The difference between "PC1" and "1-PC1" is merely a change in the direction of the eigenvector, not its value, which affects the RSEI results.

This study utilizes the RSEI and VQ to jointly assess the "quality" dimension of LEF, incorporating improvements to the RSEI to address its limitations in multi-layer vegetation observation (Y. Liu et al., 2023). While greenness indices like the EVI (X. Wang et al., 2008) , NPP (D. Fan et al., 2021) are commonly used to improve RSEI, they overlook the complex vertical structure of green infrastructure. Variations in understory vegetation, canopy density, and leaf density can significantly impact ecological assessments (C. Liu et al., 2008). The VQ index, which measures vegetation in three dimensions—horizontal area, vertical density, and productivity—provides a more detailed evaluation.

3.4.4 NTL downscale

NTL has been widely used to monitor urbanization and expansion. However, its low resolution limits its effectiveness in local urban areas, often requiring cross-satellite corrections to enhance spatial detail (Liao & Liang, 2024). Typically, scholars first try to solve the pixel saturation problem in DMSP data. These models provide the possibility of downscaling the NTL data for NPP-VIIRS.

Some researchers have incorporated vegetation data for NTL correction. For example, Zheng & Chen (Z. Zheng & Chen, 2019) integrated nighttime light data with NDVI to propose the Human Settlements Index (HSI). Zhuo et al. (Zhuo et al., 2015) used EVI to develop a desaturation method for modifying saturated NTL pixels, though it overlooked human factors in urban structure. Zheng et al. (Y. Zheng et al., 2021) proposed the Enhanced Nighttime Light Urban Index (ENUI) by incorporating NDWI and NDBI, reducing background light but distorting NTL intensity. Liu et al. (Y. Liu et al., 2017) introduced the LST and EVI Regulated NTL City Index (LERNCI), which integrates LST and EVI to better reflect economic and human activities:

$$\mathrm{LERNCI} = \mathrm{nor}^{+}\left(\left(\frac{\mathrm{LST}}{\mathrm{LSTAVGs}} + \frac{\mathrm{EVIAVGs}}{\mathrm{EVI}}\right) \times \mathrm{NTL}\right) \quad (13)$$

Here, LSTAVGs and EVIAVGs represent average values of LST and EVI in the urban core. Weighted light reflects urbanization and development intensity, which is strongly correlated with economic growth and energy consumption.

3.4.5 Population fitting and outlier removal

Given the relative stability of population growth in the time series and considering data consistency, we created a spatiotemporal cube using historical data from 2000 to 2020, constructing an OLS (Ordinary Least Squares) model for pixel-wise prediction of the post-2020 population distribution. We also obtained district-level population data from the city almanac for each year, calculated scaling factors, and linearly corrected the raster data:

$$\mathrm{Total\ POP} = \sum_{i=1}^{n} \mathrm{POP}_{I} \quad (14)$$

$$\mathrm{POP}_{\mathrm{Corrected}} = aX+b \quad (15)$$

Here, POPi is the population count for the i_{th} pixel, and Total POP is the total population within the district administrative boundaries constituting the study area. In this formula, $\mathrm{POP}_{\mathrm{Corrected}}$ is the corrected population data, and a is the weighted coefficient for the year, derived from the district-level permanent population from the almanac divided by Total POP. In linear population correction, if X is 0, the pixel is considered uninhabited, and b is set to 0.

The calculated pixel values may show anomalies, such as values below zero or extremely high values. Then, the Moving Window IQR was employed to remove outliers. The moving window threshold was set to a 10*10 pixels (1000*1000 m) square.

3.4.6 Space syntax - Integration

Space Syntax, a theory and method developed by Bill Hillier and Julienne Hanson in 1984, analyzes spatial structures to interpret human social systems. It views cities as spatial entities defined by topological structures. By abstracting roads as independent elements, this approach removes social attributes to focus purely on spatial relationships, facilitating the study of human activities, economic development, spatial structure, and land use (Hiller, 2007). This theory shifts the understanding of road network accessibility from "perceptual feeling" to "rational analysis".

In this study, roads are used to segment urban spaces, as road networks typically correlate with the quality of commercial, medical, cultural, and educational services. However, road grades and importance vary, so we employ a segment map and the "Integration" variable to measure road space accessibility. The weighted integration index (WI) is calculated through road length weighting using Depthmap10 software, and vector road network files are converted to raster via ArcGIS Pro 2.8. Integration is defined by the number of paths (N) and the topological depth (TD) of paths, expressed by the formula:

$$\mathrm{WI} = \frac{\mathrm{N}\left[\log_2\left(\frac{\mathrm{N}+2}{3}-1\right)+1\right]}{(\mathrm{N}-1)|\mathrm{TD}-1|} * \mathrm{Weighted} \tag{16}$$

Areas with high WI usually correspond to main urban roads with high traffic flow. Unlike road network density, the integration model includes TD, which reflects the number of turns needed to reach a destination. A higher TD indicates more turns, increasing travel difficulty. The inclusion of TD enhances the analysis of road "turning" costs, aligning with the continuous movement of pedestrians and vehicles. Road length weighting further emphasizes networks with fewer turns (SHENG et al., 2015).

3.4.7 Landscape pattern index

Previous studies show that landscape scale, shape, quantity, type, and spatial configuration significantly influence ecological security (Ma et al., 2019) and correlate with human activities (L. Fan & Zhang, 2022; M. Huang et al., 2022). Landscape patterns describe the texture of land patches: finer textures represent smaller divisions of functions, while coarser textures indicate larger divisions. Sharp textures reflect rigid functional boundaries, whereas blurred textures indicate more natural transitions between functions. Coarse textures characterize the spatial interweaving of functions, which facilitates the mixed use of land and its associated benefits. (D. Wang et al., 2019).

Based on previous studies (J. Wu, 2000), we initially selected indices such as Aggregation Index (AI), Patch Density (PD), Largest Patch Index (LPI), Landscape Shape Index (LSI), Edge Density (ED), Effective Mesh Size (MESH), and Patch Cohesion Index (COHESION) to capture key landscape pattern characteristics. These indices were calculated using FRAGSTATS 4.2 (McGarigal et al., 2002, 2012) with a moving window method. Principal component analysis

(PCA) was employed, and only indices with contributions greater than 0.90 to the first principal component (PC1) were selected (Table 2, Bartlett's test passed).

Table. 5 Primary Landscape Pattern Index.

Type	Name	Description
Aggregation and Patch Distribution	AI	Examines the connectivity between patches of each landscape type. Values range from 0 to 100, with lower values indicating more dispersed landscapes.
	PD	Represents the density of a specific patch type within a landscape, reflecting the degree of fragmentation of a particular land type.
Patch Characterization	LPI	Values range from 0 to 100, used to identify dominant patch types in a landscape.
	LSI	Measures the complexity of patch shapes within a landscape; higher values indicate more complex shapes.
	ED	The total length of all patch edges per unit area, reflecting the density and fragmentation of patch boundaries.
Spatial Connectivity	MESH	The ratio of the sum of the squared patch areas to the total landscape area, used to compare the average patch size within a landscape. When the total landscape area is constant, an increase in effective mesh size indicates an increase in the area of that type, reflecting its greater proportion in the landscape.
	COHESION	Reflects the aggregation and dispersion state of patches within the landscape, with values ranging from 0 to 100; higher values indicate greater aggregation.

From this process, the LSI for artificial surfaces and green infrastructure, and COHESION, which describes patch aggregation, were identified as key indicators.

Table. 6 Factor Loading Factors.

	PC1	ED	LPI	LSI	MESH	PD	AI	COHESION
Factor Loadings	AS	0.852	0.731	0.902	0.584	0.666	0.915	0.964
	GI	0.916	0.719	0.912	0.52	0.723	0.861	0.949

3.4.8 Weighted model & comprehensive overlay

3.4.8.1 CRITIC objective weighted

The issue of multicollinearity among indicators needs careful consideration. Therefore, the Criteria Importance Through Intercriteria Correlation (CRITIC) model is used to weight the aforementioned indicators (Diakoulaki et al., 1995). By weighting and combining these indicators, we obtain the final weighted coefficient. This method imposes a penalty on highly

correlated data. The specific formula is as follows:

$$W_j = \frac{C_j}{\sum_{j=1}^{p} C_j} \tag{17}$$

The CRITIC method is based on multi-criteria decision-making (MCDM). It could ensure the weights by combining the indicator variability S_j (i.e., the degree of dispersion of this indicator), the indicator conflict R_j (i.e., the irrelevance between different indicators), and the information-carrying capacity C_j (obtained by multiplying S_j and R_j). These indicator features were calculated within one data group (p group) of the j indicator. It is highly advanced in dealing with covariance and collinearity between the different indicators of urban studies.

3.4.8.2 AHP subjective weighted

Given that residents are the ultimate beneficiaries of urban land development, subjective weights are incorporated into the analysis. Subjective weights are determined using the Analytic Hierarchy Process (AHP), a structured decision-making tool that requires minimal mathematical input, offering a straightforward approach to addressing multi-objective, multi-criteria, or complex unstructured decision problems (Saaty, 1987) . Using SPSSPro to construct pairwise comparison matrices, the weights for each indicator are calculated. The consistency of the AHP model is assessed using the Consistency Ratio (CR), denoted by the λ index. The λ index gauges the rationality of the AHP model; a value less than 0.1 signifies an acceptable consistency level, confirming the model's reliability.

3.4.8.3 Land social/ecological function

The calculation formula for the final valuation result of the land function is as follows:

$$\mathrm{LSF} = \mathrm{W}_1 * \mathrm{ASR} + \mathrm{W}_2 * \mathrm{POP} + \mathrm{W}_3 * \mathrm{LERNCI} + \mathrm{W}_4 * \mathrm{WI} + \mathrm{W}_5 * \mathrm{ALSI} + \mathrm{W}_6 * \mathrm{ACO} \tag{18}$$

$$\mathrm{LEF} = \mathrm{W}_7 * \mathrm{GIR} + \mathrm{W}_8 * \mathrm{VQ} + \mathrm{W}_9 * \mathrm{RSEI} + \mathrm{W}_{10} * \mathrm{GLSI} + \mathrm{W}_{11} * \mathrm{GCO} \tag{19}$$

W is the mean of the subjective and objective weights of the corresponding indicator.

3.5 Land coupling & functional area identification

With urbanization advancing, land development evaluation has shifted from focusing solely on development levels to assessing coupling coordination degree (CCD) for functions mixed (L. Li

et al., 2022). Land function coupling relationships include intra-group and inter-group couplings, with this study focusing on inter-group couplings between LSF & LEF, calculated using the traditional CCD model.

Landscape analysis follows two paradigms: (1) the "Patch-Corridor-Matrix" paradigm, which emphasizes spatial relationships but struggles to connect patterns with ecological processes (L. Chen, Liu, et al., 2008; Hess & Fischer, 2001); and (2) the "Source-Sink-Flow" paradigm, which incorporates spatial flows to better understand these processes (L. Chen, Fu, et al., 2008; FENG et al., 2024). In this study, the traditional CCD model was combined with tools such as gravity model, Gaussian Two-Step Floating Catchment Area (2SFCA) (Yang et al., 2022) and complex network algorithms such as the Minimum Spanning Tree (MST), which enhances the long-distance relationship and is applied in the analysis of intra-group coupling.

3.5.1 Inter-group coupling of land function

3.5.1.1 Coupling coordination degree model

The coupling coordination model assesses coordinated development among subsystems, with the coupling degree (C) representing the interaction between systems and the coordination degree (T) measuring the quality of this interaction (L. Li et al., 2022). The formula is:

$$C = 2 * \left\{ \frac{(u_1 \cdot u_2)}{(u_1 + u_2)^2} \right\}^{1/2} \tag{20}$$

where U1 and U2 are the normalized LSF and LEF values. To exclude low-quality coupling (i.e., low-low system balance), the coordination index T is introduced and combined with the C index to derive the CCD value:

$$T = W_1 * U_1 + W_2 * U_2 \tag{21}$$

$$CCD = \sqrt{C * T} = \sqrt{2\left\{ \frac{(u_1 \cdot u_2)}{(u_1 + u_2)^2} \right\}^{1/2} * (W_1 * U_1 + W_2 * U_2)} \tag{22}$$

To clarify, the CCD calculated using the traditional coupling coordination model is labeled as CCD, where W represents the corresponding system's weight. In this study, the weights for the land social function (LSF) and land ecological function (LEF) systems are assumed to be equal. CCD values range from 0 to 1, representing the degree of coordinated development. Higher CCD

values indicate better coordination between the systems, with the scale ranging from extremely unbalanced (CCD = [0.0, 0.1]) to highly coordinated (CCD = [0.9, 1.0]) (Table.7).

Table. 7 CCD and Its Corresponding Level

Imbalance	**Level**	**1**	**2**	**3**	**4**	**5**
	CCD	(0,0.1]	(0.1,0.2]	(0.2,0.3]	(0.3,0.4]	(0.4,0.5]
	Type	Extreme imbalance	Severe imbalance	Moderate imbalance	Mild imbalance	Little imbalance
Coordination	**Level**	**6**	**7**	**8**	**9**	**10**
	CCD	(0.5,0.6]	(0.6,0.7]	(0.7,0.8]	(0.8,0.9]	(0.9,1]
	Type	Bare coordination	Primary coordination	Intermediate coordination	Good coordination	Excellent coordination

Grids with CCD values below 0.5 are classified as decoupling areas, while those above 0.5 are functional coupling areas.

3.5.1.2 Regional functional identification

Furthermore, areas are categorized based on the C_i index (Raux et al., 2016), which measures the ratio of LSF to LEF. If the C_i value of a specific land function in the grid exceeds 50%, the grid is marked as a single-function area of that type (S. Tang & Ta, 2022). If the function ratio is maintained around 1:1, the unit is considered a mixed-function area. Specifically:

$$C_i = \text{LSF pixel}_i / (\text{LEF pixel}_i + \text{LSF pixel}_i) \tag{23}$$

$$\text{Land Function} = \begin{cases} \text{if } C - CCD < 0.5, \text{ Decoupling Area} \\ \text{if } C - CCD \geq 0.5, \begin{cases} \text{and } C_i < 0.45, \text{ Ecological Area} \\ \text{and } 0.45 \leq C_i < 0.55, \text{ Mixed Area} \\ \text{and } C_i > 0.55, \text{ Social Area} \end{cases} \end{cases} \tag{24}$$

Areas are classified as ecological, social, or mixed-function zones based on C_i values.

3.5.2 Intra-group coupling of land function

3.5.2.1 Distance-considered CCD model

Significant inequalities exist in the spatial distribution of resident activities, as evidenced by spatial equity research. A study conducted in Singapore reveals that approximately 80.60% of residents have access to only 14.35% of regional park recreational opportunities, and 80.62% have access to only 26.46% of the environmental quality in these parks (R. Guo et al., 2024).

This inequality often manifests in a "Pareto distribution" of services, where a small fraction of land provides services to the majority of nearby residents. Therefore, land social function (LSF) and ecological function (LEF) can be simplified into a functional network consisting of localized peak points.

To calculate self-coupling relationships, the following steps are proposed: **(1) Peak point selection**: Using a 1000x1000 m moving window, select the pixel with the highest functional value within the window as the regional control point, considered as the primary service providers. **(2) Construct coupling relationships**: The GIS "construct sightline" function is used to connect these peak points. Further, coupling links are filtered based on a predetermined distance threshold (d0), which is calculated using the incremental spatial autocorrelation model. **(3) Incorporate distance factors**: Gaussian decay function weights are applied to each self-coupling relationship to reflect the distance decay effect between peak points. **(4) Select coupling relationships**: Based on the Minimum Spanning Tree (MST) model, the strongest self-coupling relationships are selected from all potential coupling relationships. The formula for calculating the distance-considered CCD (d-CCD) is:

$$\mathrm{d-CCD} = Max\left(\sqrt{2\left\{\frac{(\mathrm{u}_1 \cdot \mathrm{u}_2)}{(\mathrm{u}_1 + \mathrm{u}_2)^2}\right\}^{\frac{1}{2}} * (\mathrm{W1} * \mathrm{U1} + \mathrm{W2} * \mathrm{U2}) * G(d_{kj}, d_0)}\right) \tag{25}$$

$$G(d_{kj}, d_0) = \begin{cases} \dfrac{e^{-\frac{1}{2}\times(\frac{d_p}{d_0})^2} - e^{-\frac{1}{2}}}{1 - e^{-\frac{1}{2}}}, d_{kj} \le d_0 \\ 0, d_{kj} > d_0 \end{cases} \tag{26}$$

Where U1 and U2 represent the land function values corresponding to the LSF/LEF peak points, respectively. W1 and W2 are the weights of these peak points, reflecting their importance in the functional network. In this study, equal weights are assigned. Each peak point may have several neighboring peak points, leading to multiple possible coupling relationships. $G(d_{kj},d_0)$ is a Gaussian decay function based on the distance (d_{jk}) between peak points (Yang et al., 2022). By leveraging the Pareto distribution characteristic, the Minimum Spanning Tree (MST) model is used to simplify the calculations, selecting the strongest coupling relationship from all long-range coupling results. This ensures that there is at most one edge connecting any two peak points, with the edge weight being the previously calculated d-CCD value. The model's output

ranges between 0 and 1, reflecting the strength of the coupling coordination degree, consistent with traditional CCD models.

3.5.2.2 Minimum spanning tree

The Minimum Spanning Tree (MST) model is an algorithm used to optimize network connections. Its goal is to construct a tree that connects a given set of points (nodes), while minimizing the total cost of all edges in the tree and ensuring maximum connectivity among the nodes. Common algorithms for constructing MSTs include Kruskal's and Prim's algorithms. The MST model is widely utilized in GIS, network design, and ecological network analysis (Avram & Bertsimas, 1992).

In this study, the MST is used to select links between points with the highest CCD, assuming that the total cost of connections is minimized. By constructing an MST network and analyzing the CCD strength of its edges, we can identify patterns of land function aggregation (clustering) and isolation (dispersion) in space, thereby optimizing the connections between functional points.

The MST network is constructed using the Geo-MST Python plugin in QGIS 3.14 (Çalışkan & Anbaroğlu, 2020). Preparation includes constructing the network using the GIS "construct sightline" function and filtering out connections that exceed the distance threshold. Based on the d-CCD model, each edge is assigned a d-CCD value, and the corresponding cost of that edge is 1/d-CCD. The plugin employs Kruskal's algorithm, which follows these steps: In the Geo-MST plugin, edges are sorted in descending order based on their weights (i.e., cost values). The algorithm examines each edge one by one to determine whether its endpoints belong to the same set. If the endpoints are not in the same set, the edge is added to the MST, and the sets of the two endpoints are merged. If the endpoints are already in the same set, the edge is ignored to avoid forming a cycle. These steps are repeated until all edges have been evaluated.

By integrating the MST model, the coupling coordination degree analysis in this study can more accurately capture the self-coupling interactions between land functions, optimizing the pathways for providing urban ecological and social services.

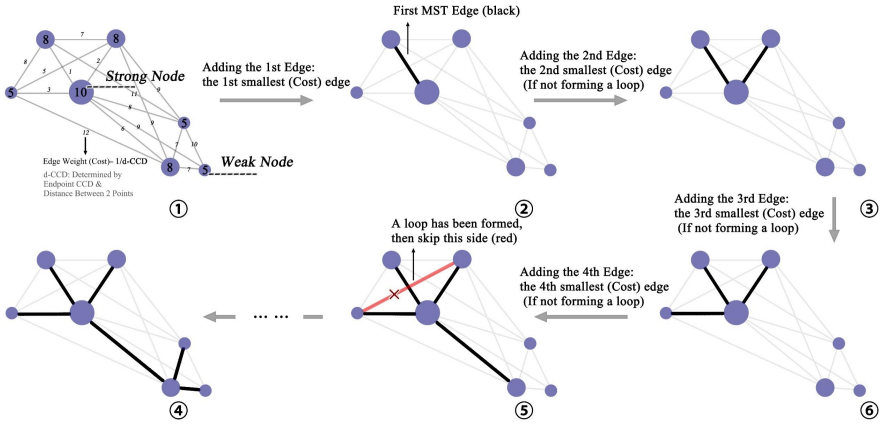

Figure 13 MST Schematic (Kruskal).

3.6 Urban vitality assessment

3.6.1 Human mobility intensity and self-organizing map

Based on traditional human mobility indicators, this paper introduces the application of the Self-Organizing Map (SOM) model. It is an unsupervised neural network technique for visualizing and interpreting large, high-dimensional datasets (Penn, 2005). In this study, the SOM model was used to segment the 24-hour day into distinct periods, revealing the city's typical behavioral pattern characterized by a 16-hour active period and an 8-hour rest period. This method is combined with the K-means algorithm for a two-stage clustering process. In the first stage, SOM acts as an initial clustering method, determining a reasonable range for cluster number N and assigning initial cluster centers. Subsequently, based on sample similarity, K-means is employed to optimize the clustering achieved by SOM (WANG et al., 2019). The clustering effectiveness is then evaluated using the Davies-Bouldin Index (DBI).

The analysis was performed using the R-kohonen package. The specific process is as follows: (1) Hourly Human Mobility data for 24 hours across four weeks (a total of 28 days) were input into the SOM model. To achieve optimal network performance, the number and combination of neurons were selected based on the lowest quantization error (QE) and topographic error (TE). (2) The weights obtained from the SOM clustering results were used as the initial cluster centers. The optimal number of clusters for K-means was determined using the DBI. Finally, Human Mobility Intensity (HMI) for both workdays (Monday to Friday) and weekends (Saturday and Sunday) was calculated as the hourly mean of human mobility during active periods:

$$\text{Human Mobility Intensity: HMI} = \frac{\sum_{i=1}^{n} v_i}{n} \tag{27}$$

where v_i is the human mobility data at the i_{th} hour of the active period, and n is the total number of hours within the active period (16 hours in this study). The HMI value reflects the average level of human mobility during active periods, calculated separately for both workdays and weekends, with higher values indicating higher population density and activity intensity within the area.

3.6.2 Human mobility data & self-correction

3.6.2.1 Atypical activity adjustment coefficient

Using HMI as the base value for UV assessment, it is important to note that human activities in certain urban areas may not align with the typical behavioral patterns identified by SOM. This discrepancy is particularly common in night-shift workplaces, such as some industrial zones, or nighttime recreational venues like bars and night markets:

$$\text{Activity Ratio: AR} = \frac{\frac{\sum_{t=1}^{m} v_t}{m}}{\text{HMI}} \tag{28}$$

where v_t is the HMI at the t_{th} hour of the rest period, and m is the total number of hours in the rest period (8 hours in this study). The term $(\sum_{t=1}^{m} v_t)/m$ reflects the average human mobility during the rest period on workdays and weekends. An AR value greater than 1 indicates that the area does not follow the typical activity pattern. The larger the AR value, the more the area tends toward activity during the rest period. The Atypical Activity Adjustment Coefficient (AAAC) was then calculated to adjust the HMI accordingly. The AAAC for the active period on workdays and weekends was computed as follows:

$$\text{Atypical Activity Adjustment Coefficient: AAAC} = \begin{cases} if\ \text{AR} \leq 1, 1 \\ if\ \text{AR} > 1,\ \text{AR} \end{cases} \tag{29}$$

Therefore, for areas with an AR less than or equal to 1, the AAAC is set to 1, indicating no adjustment to the HMI. For areas with an AR greater than 1, the HMI is adjusted proportionally to the AR value.

3.6.2.2 Temporal characteristics weighting of HMI

In addition to HMI, three indicators were calculated to comprehensively measure the spatiotemporal patterns of UV: Leisure Activity Ratio (LAR), Human Mobility Variability (HMV), and Human Mobility Consistency (HMC). Tang and Ta (S. Tang & Ta, 2022) use the Night Rate to indicate the tendency for leisure activities within an area. A higher night rate signifies more human activities during the night, reflecting the extent of nighttime economic and social activities. However, in this study, the intensity and proportion of nighttime activities are better represented by the AAAC. The Night Rate indicator mainly shows the tendency for leisure activities during post-work or evening periods on rest days. Therefore, the indicator was renamed LAR. LAR for workdays and weekends was calculated as follows:

$$\text{Leisure Activity Ratio}: \text{LAR} = \frac{\sum_{21}^{23} v}{\sum_{21}^{23} v_i + \sum_{9}^{11} v_i} \tag{30}$$

Jacobs contrasts natural residents with "birds of passage," temporary and non-invested neighborhood dwellers who "have no idea who is watching the street or how to watch it." Jacobs warns that while a neighborhood can absorb a large number of these individuals, "if everyone in the neighborhood becomes like them, they will gradually realize that the street is not safe."

Activity variability is defined as the difference in human mobility numbers at different times, represented by the Standard Deviation (STD) of hourly human flow data throughout a 24-hour period (L. Tang et al., 2022). This is considered a negative indicator, as higher STD values indicate greater fluctuations in activity intensity across the day. To account for significant differences in average human mobility numbers across different areas, the Coefficient of Variation (CV) was used to enhance data comparability. HMV for active periods on workdays and weekends was calculated as follows:

$$\text{Human Mobility Variability}: \text{HMV} = \text{CV} = \frac{\text{STD}}{\text{Mean}} \tag{31}$$

where Mean represents the average human activity over 24 hours.

Lastly, the measurement of activity consistency utilized 2.5 times the Median Absolute Deviation (MAD) to calculate the number of hours with outlier activity intensity at each sampling point

daily. The MAD is a measure of statistical dispersion, which can be more robust against outliers in a dataset than the standard deviation. The formula for calculating the MAD, based on a set of observations, is as follows:

$$\mathrm{MAD} = \mathrm{Median}(|X_i - \mathrm{Median}(X)|) \tag{32}$$

Where: X_i represents each individual observation in the dataset. Median(X) is the median of the observations. $|X_i - \mathrm{Median}(X)|$ represents the absolute deviation of each observation from the median. To calculate the number of hours with outlier activity intensity, the median absolute deviation is scaled by a factor (in this case, 2.5) to determine the threshold for identifying outliers. Here's the adjusted formula for outlier detection:

$$\mathrm{Threshold} = 2.5 * \mathrm{MAD} \tag{33}$$

Activity intensities that exceed this threshold can be considered outliers. This value is then normalized by the total number of global outliers for that specific day (Sulis et al., 2018). HMC for active periods on workdays and weekends was calculated as follows:

$$\text{Human Mobility Consistency}: \mathrm{HMC} = \frac{\text{Region\_outliers}}{\sum \text{Daily\_outliers}} \tag{34}$$

3.6.2.3 CRITIC model and multi-scenario urban vitality intensity

By weighting and combining the three indicators, we obtain the final weighted coefficient for the temporal characteristics of HMI. After weighting, the HMI is corrected to derive the Urban Vitality Intensity (UVI):

$$\mathrm{UVI} = \mathrm{HMI} * \mathrm{AAAC} * (W_1 * \mathrm{nor}^{+}(\mathrm{LAR}) + W_2 * \mathrm{nor}^{-}(\mathrm{HMV}) + W_3 * \mathrm{nor}^{+}(\mathrm{HMC})) \tag{35}$$

where W1, W2, and W3 are the comprehensive weights corresponding to each indicator, obtained by mean value of subjective and objective weights, as described in the previous section. Compared to a single dependent variable, the UVI in this study is distinguished by its occurrence time and is categorized into UVI under non-volitional human activity scenarios (i.e., workday UVI) and UVI under volitional human activity scenarios (i.e., weekend UVI).

3.7 Factor selection and driver analysis

This section focuses on constructing a regression model with multi-scenario UVI as the dependent variable (Y) and various land evaluation factors as independent variables (X). The

Optimal Parameters-based Geographical Detector (OPGD) model is constructed, combined with the Multi-Scale Geographically Weighted Regression (MGWR) model to explore regression coefficients and bandwidth of influence.

3.7.1 Spearman correlation

The Spearman's rank correlation coefficient is a rank-based measure suitable for continuous or discrete ordinal data. Its primary advantage is that it does not require data to follow a normal distribution and can handle nonlinear relationships. The robustness of the Spearman correlation coefficient against outliers and non-normal data makes it particularly effective when handling nonlinear, asymmetrical, or outlier-prone data (Fieller et al., 1957). The formula for calculating the Spearman correlation coefficient is:

$$r = 1 - \frac{6\sum d_i^2}{n(n^2-1)} \tag{36}$$

where r represents the Spearman correlation coefficient, d_i^2 is the rank difference for the i_{th} observation, indicating the difference in rankings between two variables, and n is the total number of observations. By calculating the sum of the squared rank differences and standardizing by the sample size, the degree of correlation between variables is determined. The Spearman correlation coefficient ranges from -1 to 1, where 1 indicates a perfect positive correlation, -1 indicates a perfect negative correlation, and 0 indicates no correlation.

3.7.2 Optimal parameters geographical detector

3.7.2.1 Geographical detector

Spatial heterogeneity captures the inherently uneven distribution of spatial phenomena. Spatial stratified heterogeneity analysis explores this variability by examining differences in spatial variance both within and across distinct strata of explanatory variables. Among methods used for this purpose, the geographical detector model is particularly effective and widely applied in analyzing spatially stratified heterogeneity (Y. Song et al., 2020). Based on the theory of spatial differentiation, these methods detect the determinants of dependent variables and evaluate the relative importance of influencing factors (J. Wang & Xu, 2017; J.-F. Wang & Hu, 2012). The driving strength of an independent variable X on a dependent variable Y is represented by the q value; the larger the q value, the greater the influence of X on Y.

$$q = 1 - \frac{\sum_{h=1}^{L} N_h \sigma_h^2}{N\sigma^2} = 1 - \frac{SSW}{SST}$$
$$SSW = \sum_{h=1}^{L} N_h \sigma_h^2, SST = N\sigma^2 \quad (37)$$

where N is the number of samples in the study area, L is the number of categories of factor X, $\sigma 2$ is the total variance of Y in the study area, and σ_h^2 is the variance of Y within category h of factor X. SSW is the within-category sum of squares, and SST is the total sum of squares.

A larger q-value (ranging from 0 to 1) indicates a stronger explanatory power of factor X for the variation in Y (Cen et al., 2024).

In addition to assessing the spatial relationships between independent and dependent variables, the model also identifies interactions between multiple X-variables, determining the direction, strength, and linearity of their combined effects. It evaluates whether the joint effect of two factors, X1 and X2, increases or decreases the explanatory power for the dependent variable Y.

The method calculates the q-values for factors X1, X2, and their interaction $q(X1 \cap X2)$, which is derived by overlaying the spatial layers where X1 and X2 intersect. The relationships are classified as follows (Table.8):

Table. 8 The Interactive Types of Two Factors & the Interactive Relationship.

Description	Interaction
$q(x_1 \cap x_2) < \text{Min}(q(x_1), q(x_2))$	Weakened, nonlinear
$\text{Min}(q(x_1), q(x_2)) < q(x_1 \cap x_2) < \text{Max}(q(x_1), q(x_2))$	Weakened, unique
$q(x_1 \cap x_2) > \text{Max}(q(x_1), q(x_2))$	Enhanced, bilinear
$q(x_1 \cap x_2) = q(x_1) + q(x_2)$	Independent
$q(x_1 \cap x_2) > q(x_1) + q(x_2)$	Enhanced, nonlinear

This analysis allows the identification of how different factors interact to influence the dependent variable, helping to refine understanding of land function clustering and dispersion.

3.7.2.2 Optimal parameter

Geographical detectors require the discretization and reclassification of various independent variables X, as different discretization methods and classification numbers can significantly impact the relationship between driving factors and geographical phenomena. Using inappropriate methods may lead to inaccurate reflections of these relationships. Common

classification methods include equal interval, natural breaks, quantiles, geometric interval, and standard deviation classification. The number of classifications typically ranges from 3 to 7, depending on the study area's characteristics and the researcher's understanding. In traditional geographical detectors, the choice of discretization method and scale selection relies on subjective judgment and experience.

However, the Optimal Parameters-based Geographical Detector (OPGD) model improves upon this by selecting the optimal discretization method, number of spatial layers, and spatial scale parameters, enhancing spatial analysis. In this study, the OPGD model is used to iteratively optimize discretization to determine the most effective classification method and the optimal number of categories for each driving factor X, thereby maximizing its explanatory power on the dependent variable Y (Cen et al., 2024).

The model calculates the q-value for each driving factor across different classification methods and numbers of categories. The number of classifications is set between 3 and 7 due to the computational complexity. The combination of method and classification number that yields the highest q-value is chosen for discretization. All operations are performed in R Studio using the "GD" package.

3.7.3 Multiscale geographically weighted regression

To overcome the limitation of the geographical detector, which can measure driving strength but not the specific direction of influence, the MGWR model is employed. MGWR reveals spatial heterogeneity in both the strength and direction of driving factors, while also providing insights into the bandwidth of factor influence. This model demonstrates high explanatory power, especially in multi-scenario analyses.

The UVI is used as the dependent variable Y, and various land socio-ecological function sub-indicators serve as the independent variables X. Unlike the Ordinary Least Squares (OLS) model, which establishes a global regression, the Geographically Weighted Regression (GWR) model accounts for spatial variability, capturing local variations in the relationships between variables. However, for phenomena involving processes operating at multiple spatial scales, a fixed scale is insufficient (Fotheringham et al., 2009). The MGWR model extends GWR by structuring it as a generalized additive model, allowing the estimation of local parameter

standard errors. This enables the relationship between the response and explanatory variables to vary across both space and scale, thus addressing overfitting issues under a uniform bandwidth and resolving nonlinearities (Cen et al., 2024):

$$y_i = \sum_{j=1}^{k} \beta_{bwj}(u_i, v_i)x_{ij} + \epsilon_i \quad (38)$$

For each sampling point i, MGWR constructs the coordinates (u_i, v_i). y_i is the value of the dependent variable at point i; bwj represents the bandwidth used for the regression coefficient of variable j. β is the regression coefficient, and ϵi is the random disturbance term.

This study uses the quadratic kernel function and the Akaike Information Criterion (AIC) for model selection. Land assessment indicators are pre-screened using Spearman correlation, OLS, and the VIF test. The qualified factors are then input into the MGWR model to compute driving coefficients and spatial bandwidths.

3.8 Spatial autocorrelation

In this study, global and local spatial autocorrelation methods were used to assess the spatial aggregation or dispersion status of the factors, following the first law of geography: “ ” Everything is interconnected, but things close together are more closely connected than things far away’. By calculating global and local Moran's I indices, it is possible to quantify the pattern of clustering or dispersion of spatial units within the study area.

3.8.1 Global Moran's I

This study utilizes both global and local spatial autocorrelation methods to assess the spatial clustering or dispersion of individual factors, following Tobler’s First Law of Geography: "Everything is related to everything else, but near things are more related than distant things." Global Moran's I is a common measure for global spatial autocorrelation, indicating whether spatial units are clustered or dispersed across a study area (P. A. Moran, 1948):

$$I = \frac{n}{S_0} \times \frac{\sum_{i=1}^{n}\sum_{j=1}^{n} w_{ij}(y_i - \bar{y})(y_j - \bar{y})}{\sum_{i=1}^{n}(y_i - \bar{y})^2} \quad (39)$$

Where $S_0 = \sum_{i=1}^{n}\sum_{j=1}^{n} w_{ij}$, n is the total number of spatial units, y_i and y_j represent the attribute values of spatial units i and j, $\bar{y}$ is the mean attribute value of all spatial units, and w_{ij} is the spatial weight. Moran's I values range from -1 to 1, with positive values (0 to 1) indicating

spatial clustering (positive spatial autocorrelation), and negative values (-1 to 0) suggesting spatial dispersion (negative spatial autocorrelation).

3.8.2 Local Moran's I

While global Moran's I captures overall clustering patterns, Local Moran's I identifies specific areas with clustering or dispersion, highlighting spatial dependence and heterogeneity at finer scales (Anselin, 1995). The specific formula is:

$$I = \frac{\sum_{j=1}^{n} w_{ij}(y_j - \bar{y}) * n^2(y_i - \bar{y})}{\sum_{j=1}^{n} w_{ij} \sum_{j=1}^{n} (y_i - \bar{y})^2} \quad (40)$$

Based on the calculation results, the correlation between a unit and its neighboring units can be classified into five types: "high-high" clustering, "high-low" clustering, "low-low" clustering, "low-high" clustering, and "insignificant" clustering.

4 RESULTS AND DISCUSSIONS

4.1 Urban vitality assessment

4.1.1 HMI description & spatio-temporal distribution

In analyzing seasonal Human Mobility Intensity (HMI), it was found that spring exhibits the highest mean HMI, with a value of 2.506. The mean HMI gradually declines through summer (2.400), autumn (2.172), and winter (2.077). Across all seasons, there are minimal differences in HMI between rest days and workdays. In spring and autumn, human activity is slightly higher on rest days, while in summer and winter, it is slightly higher on workdays. This suggests that seasonal variations affect human activity patterns, but overall, the disparity between rest days and workdays remains small.

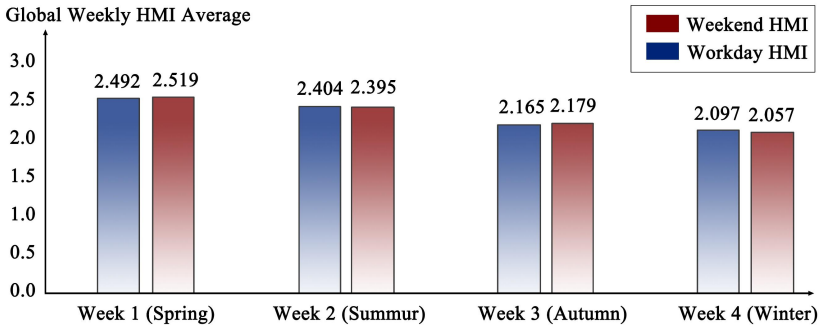

Figure 14 Seasonal Temporal Characteristics of HMI.

In a more detailed hourly analysis of the HMI across all seasons, a consistent pattern emerges. In Luohe City, human activity typically increases around 5:00 a.m., reaching a peak by 7:00 a.m., and maintains a steady level throughout the day before declining after 10:00 p.m. Interestingly, the lowest HMI does not occur immediately after midnight but is recorded at around 4:00 a.m. The analysis also reveals that this daily activity pattern remains stable across both workdays and weekends, reflecting consistent daily work and life rhythms of the city's residents.

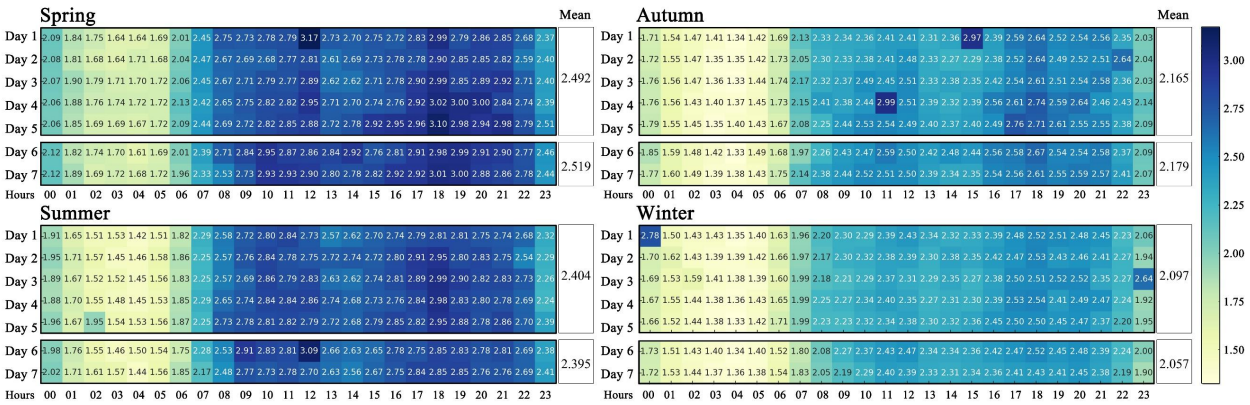

Figure 15 Weekly Temporal Characteristics of HMI.

By examining the spatial patterns of human activity during the week with the highest average HAI (spring), the analysis of weekdays (Mondays) and weekends (Saturdays) highlights different characteristics. Data presented in three-hour intervals reveal that on rest days, the spatial distribution of high HMI values is significantly broader between 9:00 a.m. and 12:00 p.m. On workdays, however, high HMI values are more concentrated in specific areas. In both cases, the highest HMI values are clustered within the built-up areas of the city. Outside these areas, HMI is only prominent between midnight and 9:00 a.m. This reflects Luohe's urban "agglomeration and diffusion" cycle, where residents aggregate in a fixed area for activities during fixed hours, and spread out over a wider area at night for rest.

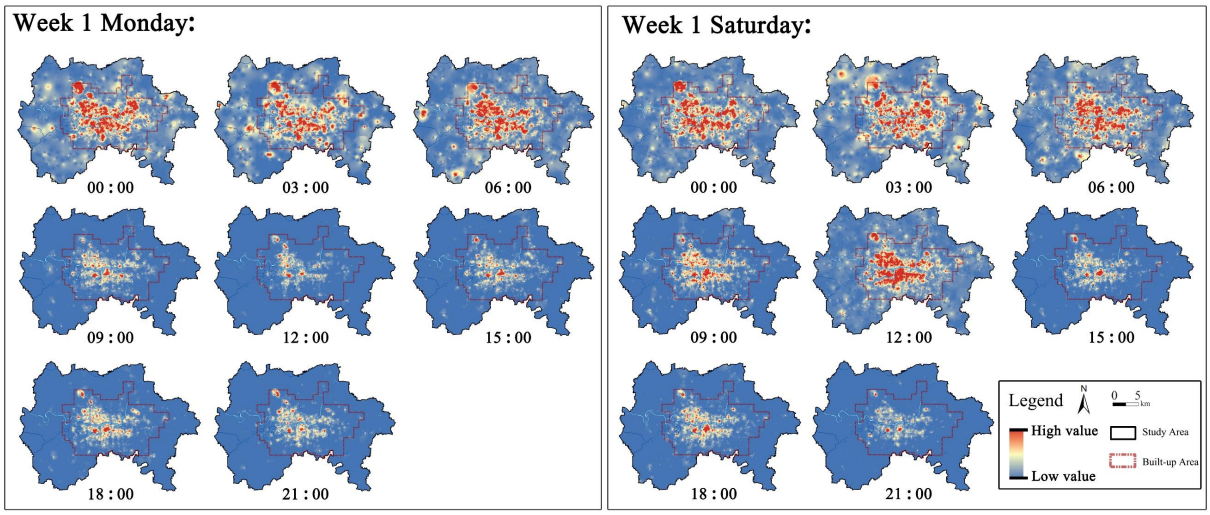

Figure 16 Daily Temporal Characteristics of HMI.

This spatial analysis suggests that, compared to overall activity intensity, the spatial heterogeneity of HMI under different temporal scenarios offers more valuable insights into human activity patterns. Specifically, spatial variability provides a clearer understanding of how different areas experience varying levels of human activity during rest and workdays.

4.1.2 Identification of typical activity patterns

The Self-Organizing Map (SOM) analysis identified two key human activity clusters in the city:

-- Cluster 1 represents the active period from 08:00 to 23:00, with an average activity level of 2.650.

--Cluster 2 represents the rest period from 00:00 to 07:00, with an average activity level of

1.696.

The SOM achieved optimal training performance with 24 neurons (4×6), yielding a quantization error (QE) of 0.230 and a topographic error (TE) of 0.133. The clustering results, based on the Davies-Bouldin Index (DBI), highlighted five clusters, with the lowest DBI achieved at this setting.

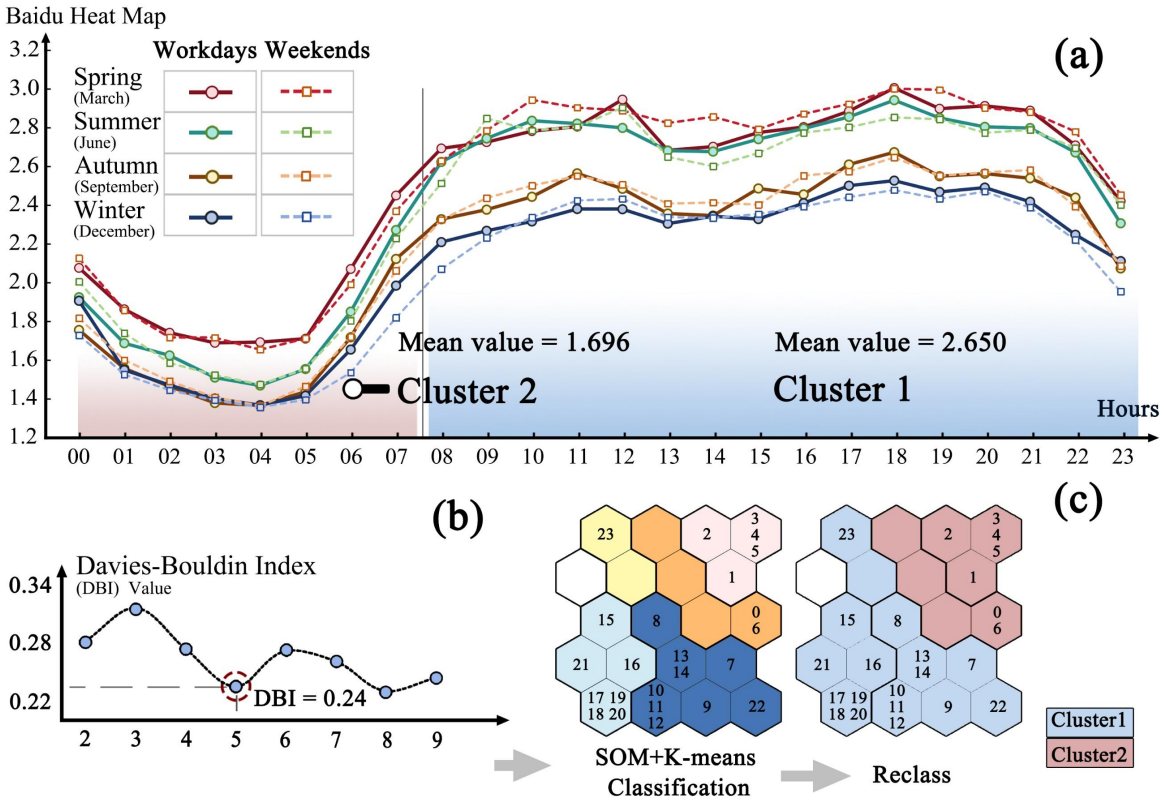

Figure 17 SOM Clustering Analysis.

4.1.3 Activity patterns & correction factors

Analysis of the AAAC shows that while most areas adhere to the typical activity pattern, the number of areas deviating from the pattern increases on weekends, despite only a slight decrease in overall mean activity levels. Notably, areas such as factories and villages surrounding the built-up zone exhibit a stable reverse-typical activity pattern, unaffected by the distinction between rest and workdays.

Among the three correction coefficients, LAR specifically highlights areas inclined towards nighttime leisure activities while suppressing areas such as highways, national roads, and provincial roads. Accordingly, this partially overlaps with the areas of high fluctuation identified by the HMV. HMV analysis indicates that, compared to farmland areas, changes in human flow

intensity are more frequent within built-up areas. Therefore, on a macro level, built-up areas exhibit high temporal fluctuations in human activity across a large scale. Meanwhile, both LAR and HMV show strong spatial clustering tendencies, effectively mitigating the "road boom" and "passing bird" effects caused by traffic flow.

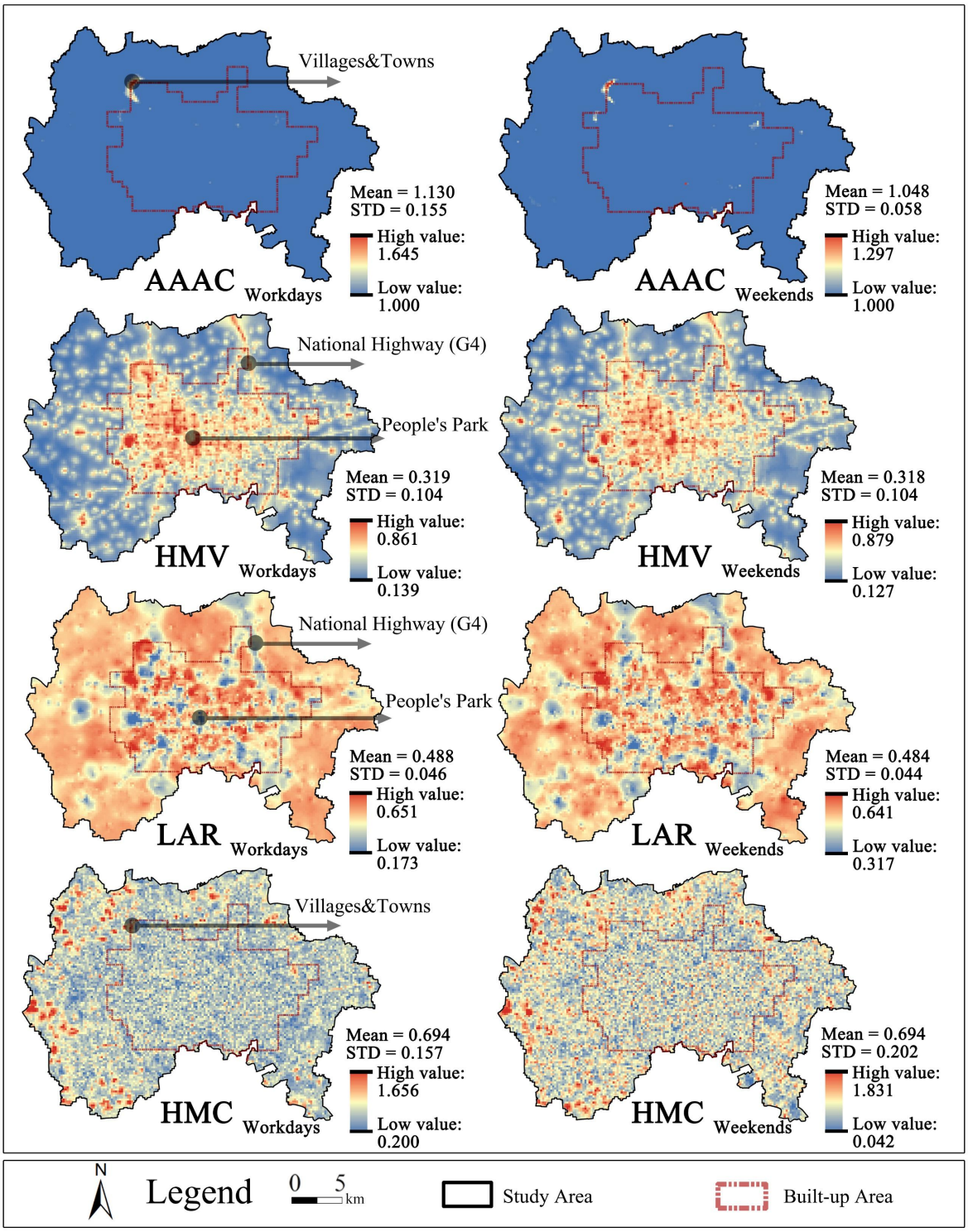

Figure 18 Spatial Characteristics of Correction Coefficients.

The spatial aggregation of the indicators decreased on weekends compared to workdays. Based

on the hour-by-hour HMI analysis, residential activity on weekends is spread over a wider area, so the characteristics/attributes from the activity are attenuated in the furniture department.

Table. 9 Indicators of Spatial Autocorrelation of Factors.

Correction Factor	Type	Moran's I	Z-value
AAAC	Workday	0.838	133.504
	Weekend	0.641	115.571
HMV	Workday	0.875	155.437
	Weekend	0.859	151.769
LAR	Workday	0.854	147.971
	Weekend	0.845	141.596
HMC	Workday	0.497	81.857
	Weekend	0.340	53.507

4.1.4 Multi-scenario UVI calculations

The UVI calculations, performed across both workday and weekend scenarios, exhibit high Moran's I values (0.905 for workdays and 0.897 for weekends), indicating strong spatial clustering of urban vitality within Luohe City. The spatial analysis reveals that human activities are predominantly concentrated in the built-up areas, with minimal differences between the mean and standard deviation values of UVI between workdays and rest days (Mean = 1.396/1.395; STD = 1.087/1.089). However, some local variations in UVI distribution exist, particularly in regions like the peninsula, where differences become more apparent (Figure 19 (a1) - (a2)).

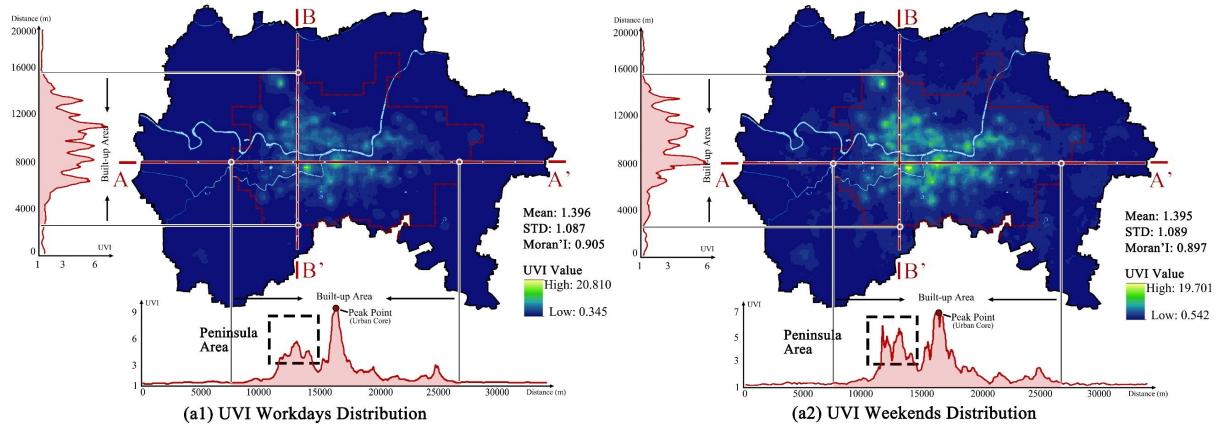

Figure 19 Spatial Characteristics of UVI.

Stability of UVI Hotspots: The multi-scenario analysis shows that spatial hotspots of UVI remain largely consistent across different scenarios, indicating that the differences in residents'

behavior patterns between workdays and weekends do not drive significant large-scale changes in UVI distribution. The High-High (HH) clusters—areas of high vitality—are stable within the built-up areas, showing no significant expansion toward surrounding towns. This stability implies that the majority of daily activities are concentrated in localized zones within the city, contributing to a consistent urban vitality pattern.

Clusters in Built-up and Surrounding Areas: Taking the built-up area on a rest day as an example, the distribution of spatial clusters indicates that Low-Low (LL) clusters (26.471%) and insignificant points (57.453%) dominate, while High-High (HH) clusters account for only 16.015% (795 clusters). This shows that most areas around the built-up area have low vitality. In terms of location, the core urban area within the built-up area is still the main hub of human activities.

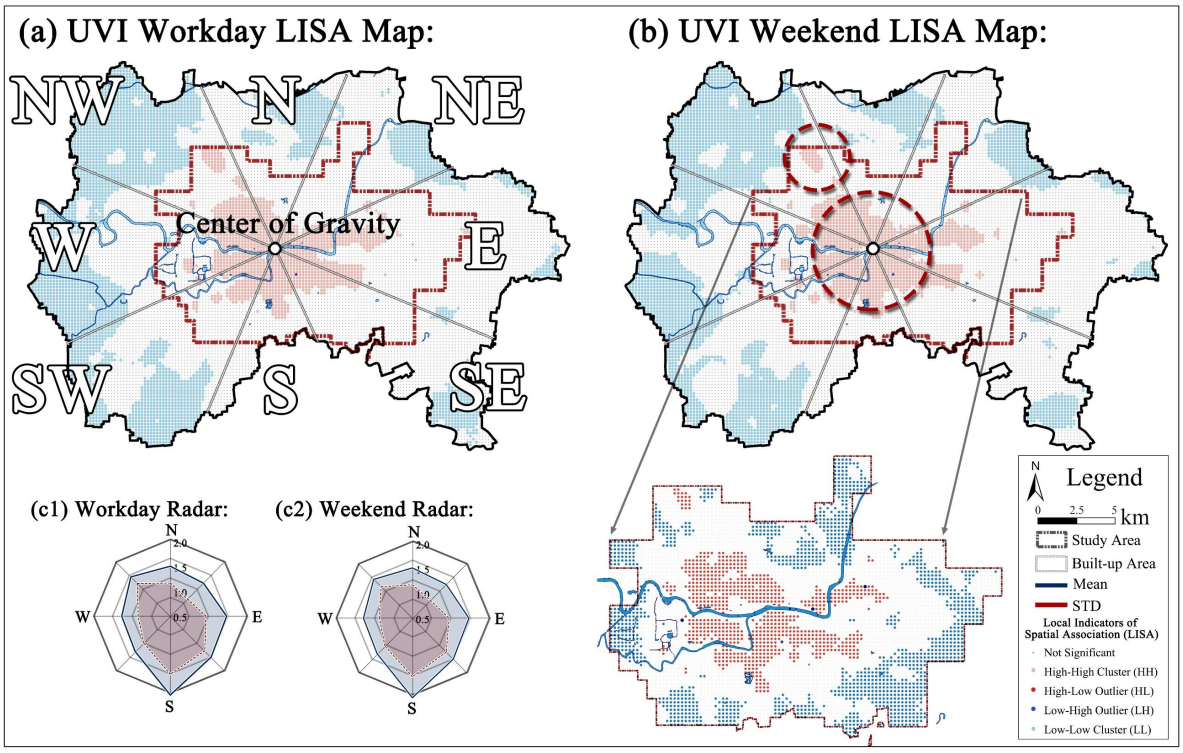

Figure 20 Hotspot Analysis Based on Multi-scenario Viability.

There are no significant changes in the spatial distribution of UVI between workdays and rest days. This pattern reflects that human activities are primarily centered in localized functional clusters capable of meeting residents' socio-ecological needs. Consequently, instead of large-scale movement, human activities are characterized by localized shifts under different scenarios.

4.2 Land function assessment

4.2.1 Land use and landscape index

The five features used to classify land in 2023 are shown in the Figure 21: Spectral Features, Indicator Features, Nightlight Features, Terrain Features, Textural Features.

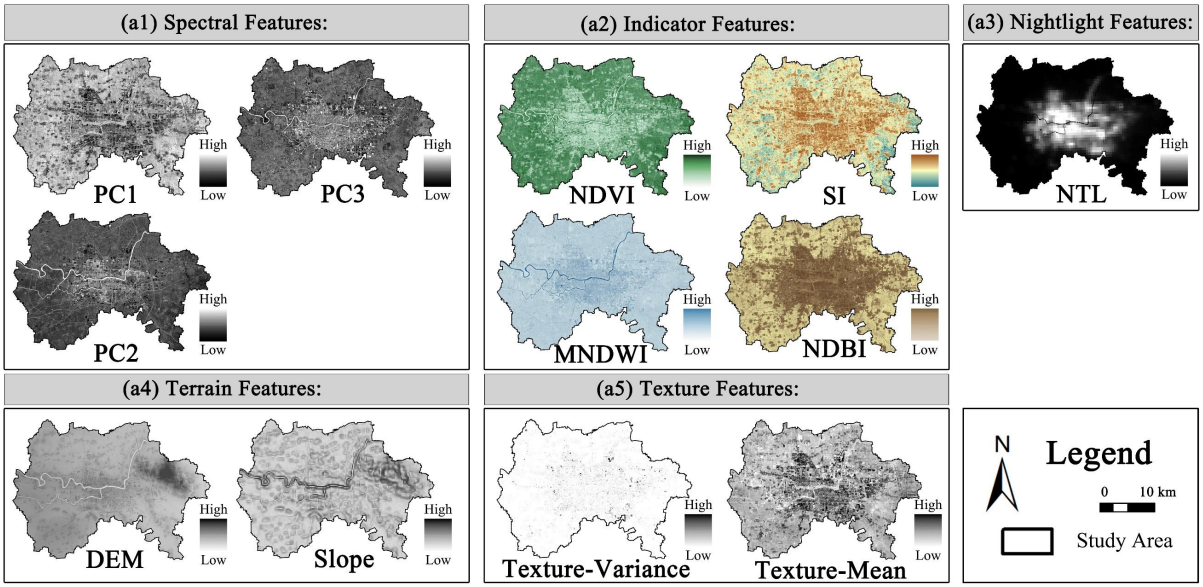

Figure 21 RF Feature Datasets.

The land use within Luohe City's planned urban area demonstrates a pattern of mixed urban and rural development. Farmland comprises the largest share (57.71%), followed by artificial surfaces (27.18%), green infrastructures (13.85%), and water bodies, which account for the smallest portion (1.26%). Significant amounts of farmland remain both at the boundaries and beyond the built-up areas. This characteristic is consistent with findings from studies on other developing medium-sized cities in China. A 200m grid was created to transform the classified AS and GI data into continuous land-use ratio data. Furthermore, the LSI and COHESION indices for AS and GI were calculated at the class level using LULC data to represent the morphological complexity and spatial clustering of land patches.

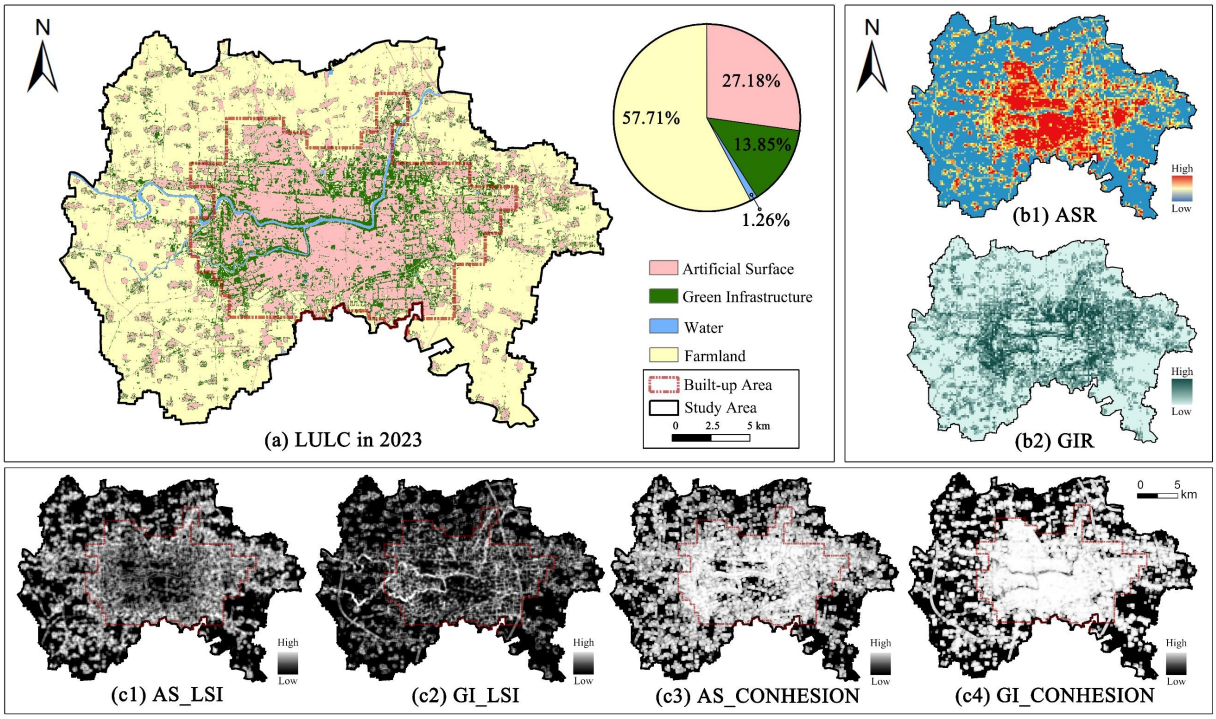

Figure 22 LULC and Land Use Ratio Results in 2023.

4.2.2 Quality assessment

4.2.2.1 Social function assessment

The social function of land is evaluated across three dimensions: the degree of urbanization, human settlement patterns, and transportation accessibility. The corrected nighttime light data, referred to as LERNCI, accurately identifies the urbanization level of the old town. The built-up area is expanding outward from a central core, with several sub-cores forming around the periphery. WI and POP are heavily concentrated in the built-up areas, underscoring disparities in urbanization, human settlement patterns, and transportation accessibility, and highlighting the pronounced urban-rural divide.

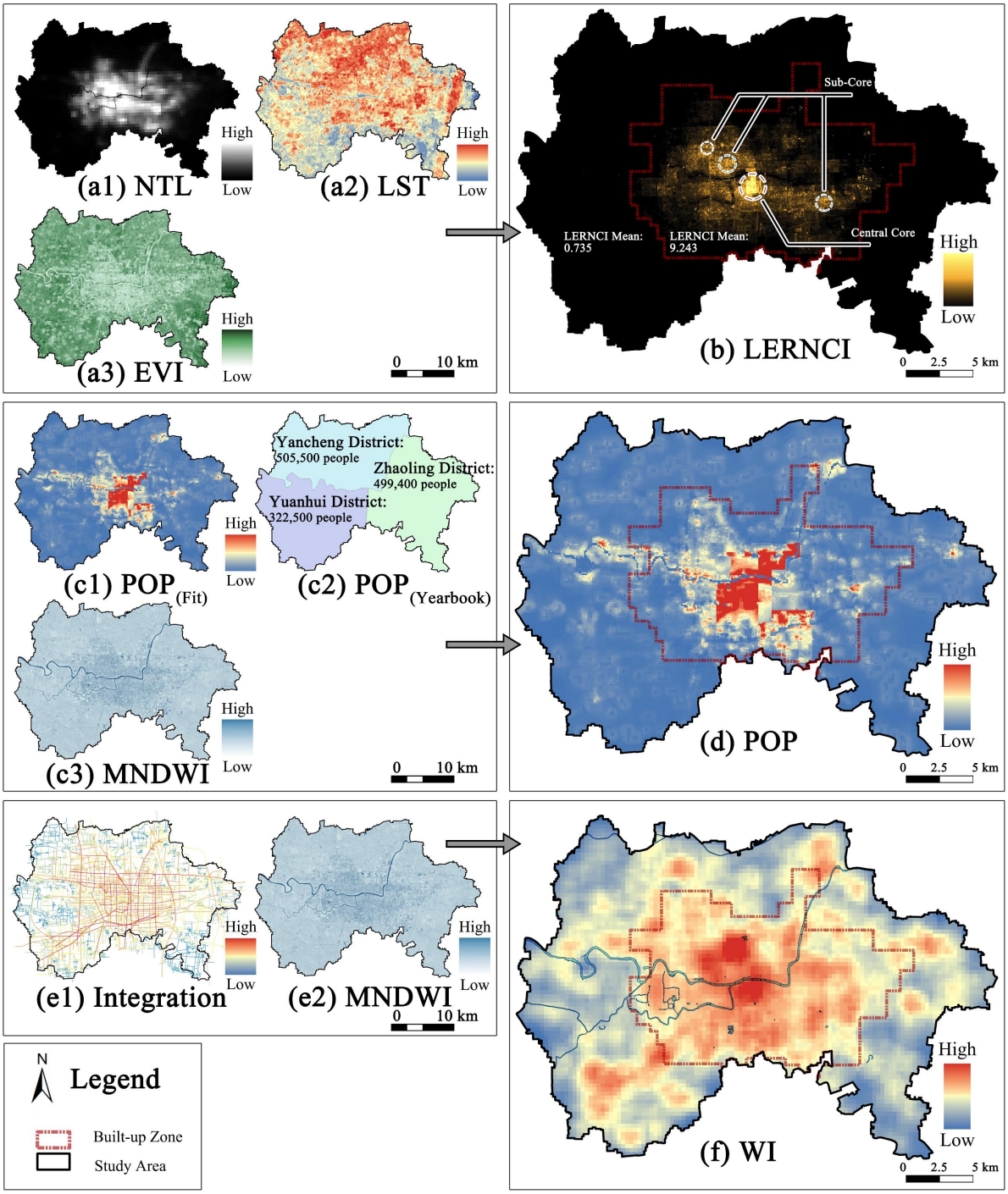

Figure 23 Qualitative Indicators of LSF.

4.2.2.2 Ecological function assessment

In the study area, large green patches are limited, requiring the evaluation to extend beyond a simple assessment of green space area. The VQ index effectively differentiates between farmland and green space based on vegetation quality. Results indicate that high-quality vegetation patches are predominantly found outside the built-up area, whereas vegetation quality within the built-up area is generally poor, with only a few scattered high-value regions. The RSEI offers a

comprehensive assessment of environmental conditions. RSEI values are lower in high-density built-up areas, whereas high-value regions are primarily concentrated on the outskirts and along riverbanks. Based on the results, incorporating RSEI into the assessment further reduces the weight assigned to farmland in the evaluation of LEF to some extent.

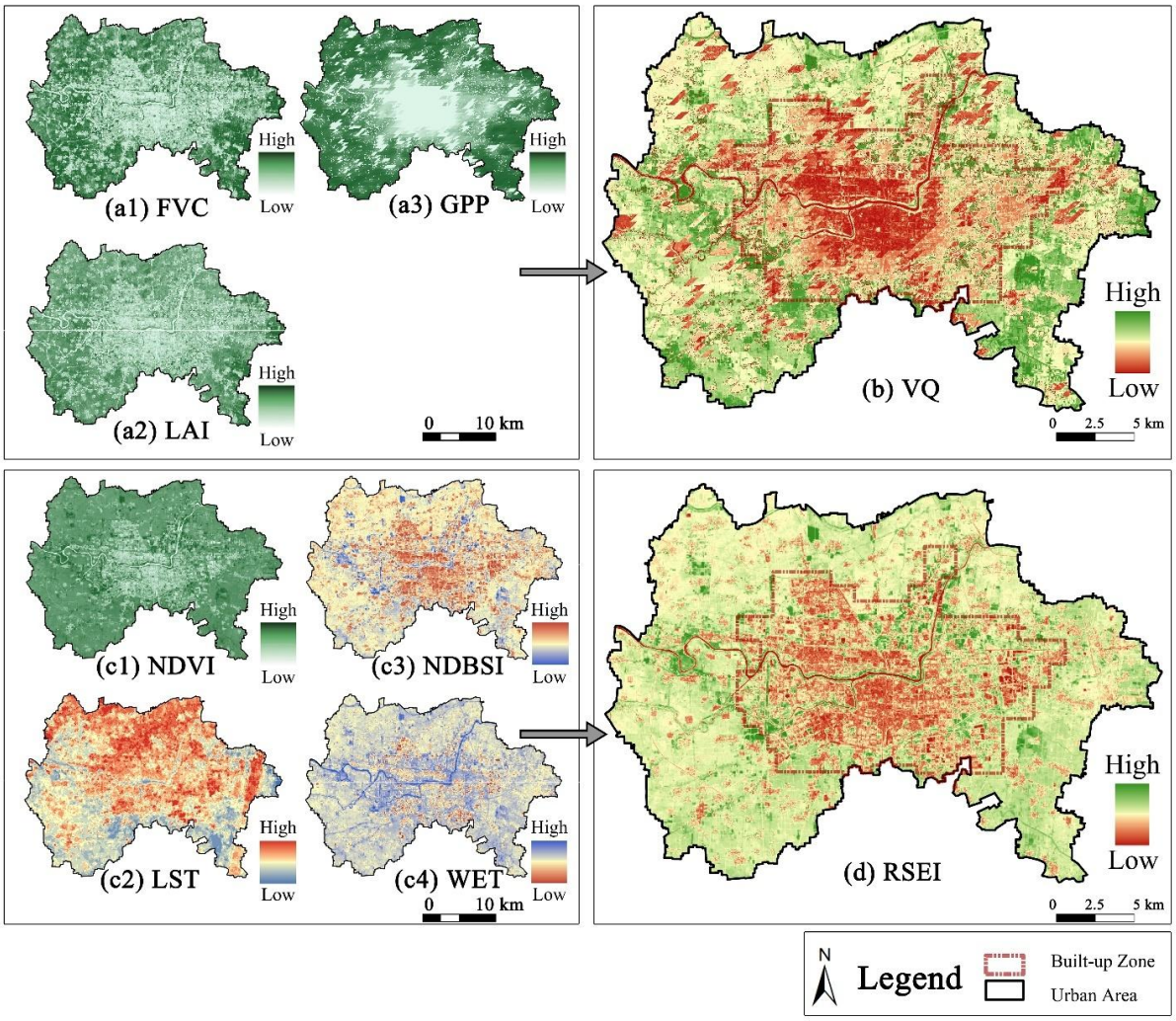

Figure 24 Qualitative Indicators of LEF.

4.2.3 Land functions & spatial characteristics

The table. 9 presents the subjective, objective, and composite weights, along with the spatial heterogeneity of various factors influencing land function, according to the land function evaluation framework. In the LEF/LSF system, the AHP evaluation consistency is $\lambda = 0.068 \leqslant 0.1$, demonstrating that the subjective weight assessment passed the consistency test and the weights are valid.

Table. 10 11 Factors Weights and Corresponding Moran's I.

Goal	Framework	Name	Objective	Subjective	Comprehensive	Moran's I	Z

Layer			Weight	Weight	Weight		
LSF	Quantity	ASR	0.258	0.150	0.204	0.767	133.838
		LERNCI	0.037	0.407	0.222	0.843	144.786
	Quality	HSD	0.098	0.130	0.114	0.812	136.931
		WI	0.109	0.176	0.142	0.981	167.147
	Structure	ACO	0.308	0.055	0.181	0.736	131.183
		ALSI	0.191	0.082	0.137	0.700	129.338
LEF	Quantity	GIR	0.133	0.444	0.288	0.641	114.039
	Quality	VQ	0.253	0.132	0.192	0.461	77.415
		RSEI	0.130	0.191	0.160	0.415	67.175
	Structure	GCO	0.282	0.131	0.206	0.711	125.488
		GLSI	0.203	0.102	0.153	0.731	135.439

LSF exhibits a strong clustering pattern (Moran's I = 0.869), while within the built-up area, its spatial distribution is relatively more balanced (Figure 25a). Similarly, LEF demonstrates a weaker clustering pattern (Moran's I = 0.689), with relatively sparse provision in the urban core. High-value areas form a ring encircling the urban core (Figure 25b).

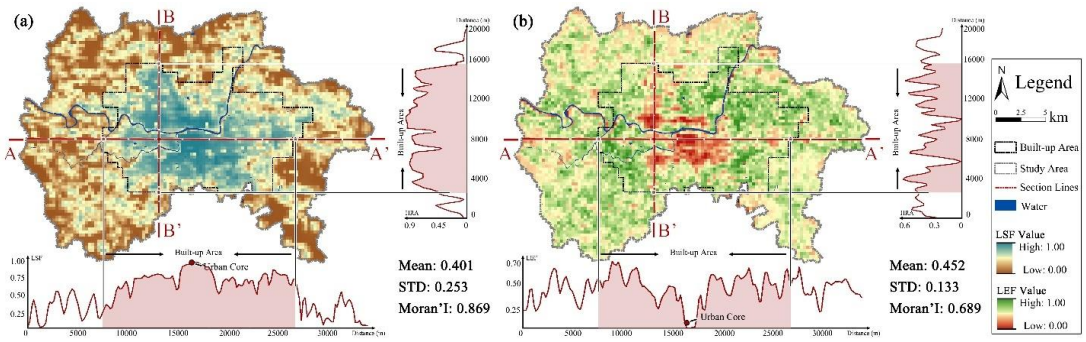

Figure 25 LSF and LEF Assessment and Profile Analysis.

The LISA maps for LSF and LEF reveal that HH and LL clusters dominate in quantity, indicating significant spatial polarization. The spillover effects of land socio-ecological functions are pronounced, with variations in local land function exerting considerable influence on land development in adjacent areas. The radar chart further illustrates the spatial distribution pattern, showing that LSF functionality is higher in the S/SE/E directions, following a vertical trend of "higher in the southeast and lower in the northwest." In contrast, LEF exhibits a nearly balanced ecological supply in all directions, reflecting a more horizontal distribution.

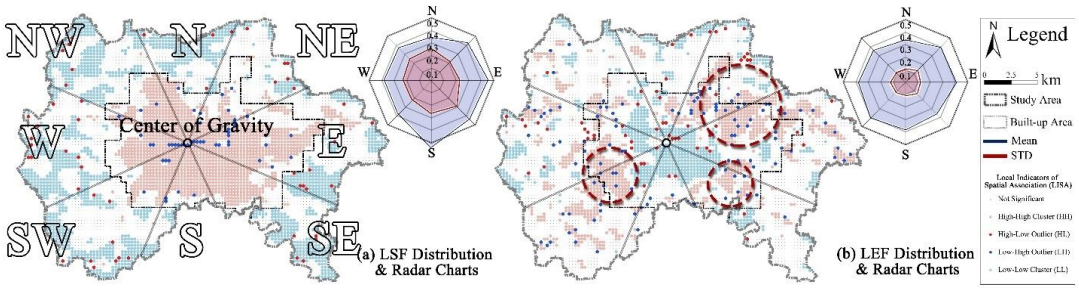

Figure 26 Spatial Clustering and Radar Chart of LSF and LEF.

The differing spatial clustering characteristics of LSF and LEF suggest a lack of synchronization in the spatial provision of ecological and social functions. Thus, the coupling relationship between social and ecological functions is spatially inconsistent.

4.3 Coupling coordination of land functions

Coupling and coordination between groups (CCD) measures the spatial mixing and equilibrium of socio-ecological function provision. Coupling and coordination within groups (d-CCD) is more concerned with the spatial correlation and aggregation of local peaks of functions within a single function.

4.3.1 Inter-group coupling & functional area identification

4.3.1.1 Multi-scale inter-group coupling analysis

In the multi-scale analysis, CCD results generally show an upward trend as the scale increases from 200m to 3000m. Specifically, at clustering scales of 600m, 2400m, and 3000m, the CCD values exhibit a higher level of coupling coordination, indicating that at these scales, the interaction between social and ecological functions is well-coordinated and integrated. This phenomenon suggests that these medium scales may represent the "key scales" for achieving effective coupling between social and ecological functions.

However, it is noteworthy that when the analysis scale exceeds 3000m, the CCD value drops sharply. This suggests that while increasing the scale within a certain range enhances the coupling coordination of the social-ecological system, when the scale becomes too large, the interactions and coupling between functions weaken. This may be due to the increased spatial distance between functional areas at larger scales, which weakens the interaction and coordination between them. Additionally, the regional and local nature of functions limits the effectiveness of coupling, as overly large scales may fail to maintain this close interaction.

The coupling coordination of social-ecological functions exhibits significant spatial scale dependence. At medium scales (such as 3000m), the coupling between social and ecological functions reaches its optimal state. Beyond this range, the interactions between functions weaken, and the level of coupling coordination declines accordingly.

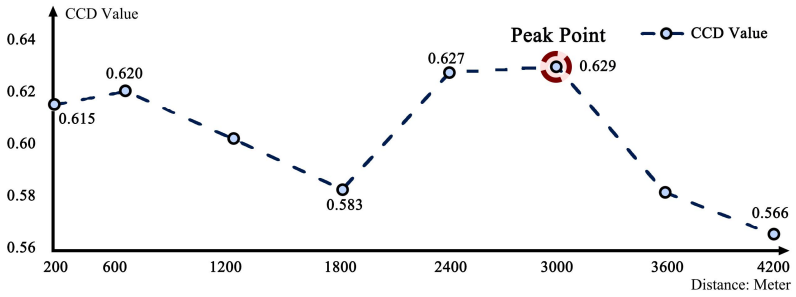

Figure 27 Multi-scale Inter-group CCD.

Spatially, the 3000m CCD results indicate that highly coupled pixels (0.9-1.0) are primarily concentrated in the eastern portion of the built-up area, especially in newly developed zones along the river or near transportation hubs (H-1). Moving outward from the center to the periphery, L-CCD values generally decline in concentric layers. Low-value areas are mainly situated along the western edge of the study area, consisting primarily of declining villages and farmland patches (L-1). Further frequency analysis shows that Level 6 areas represent the highest proportion, at 25.81%. Within the built-up area, Level 8 dominates the coupling areas, with 9 pixels representing 14.52%.

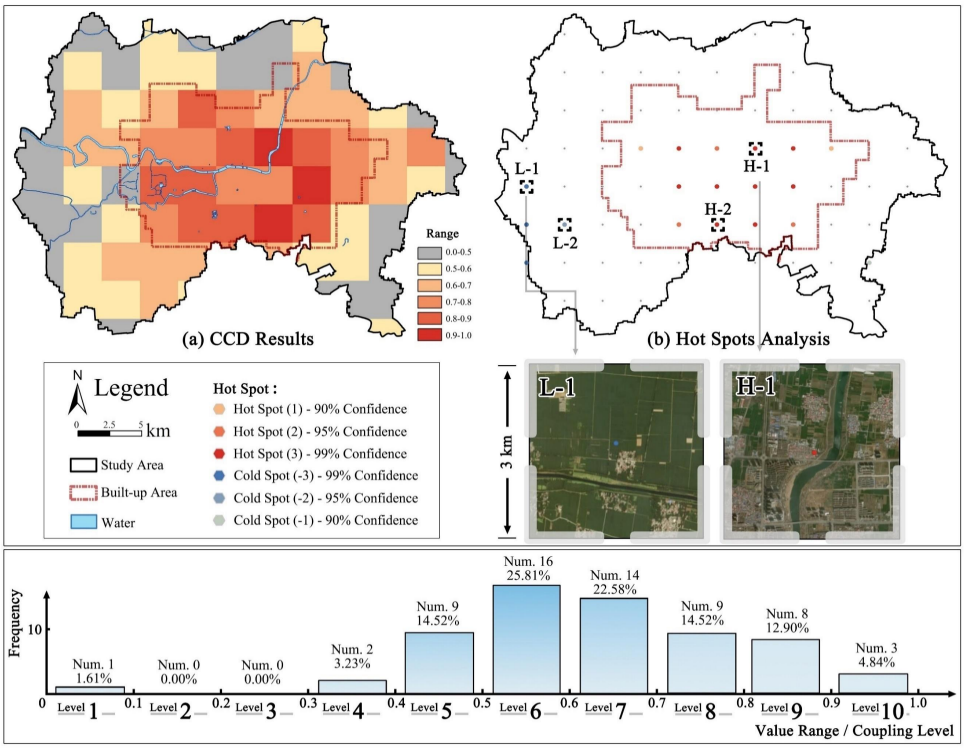

Figure 28 CCD Results & Sampling Point Expansions.

4.3.1.2 Functional area identification

Further screening of priority development areas within CCD regions (i.e., CCD levels [6,7]) was conducted, followed by an assessment of current land function tendencies in these areas. Based on the UVI's dependence on LSF/LEF, for social function zones, prioritizing the introduction of additional LEF is an effective strategy to enhance UVI. For ecological function zones, as LSF serves as the foundation and prerequisite for UV aggregation, further development of LSF is necessary.

The situation in mixed zones is more intricate. Generally, mixed zones within the built-up area exhibit nearly balanced socio-ecological functions, though both remain underdeveloped. Such zones are commonly found in built-up areas. In this case, simultaneous development of socio-ecological functions is recommended.

Mixed zones near the boundary of the built-up area are typically clusters of large towns. Given Luohe City's expansion and incorporation of surrounding towns over the past decade, priority should be placed on LSF development in these areas. Mixed-function zones located far from the built-up area are often situated at transportation hubs, such as regional nodes on national and provincial highways. In these areas, LSF development is constrained by land characteristics and should receive primary attention.

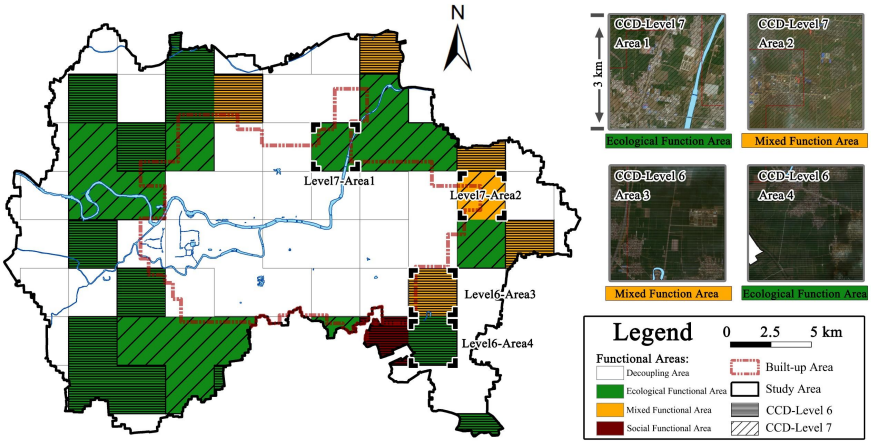

Figure 29 Functional Identification of the Area to be Optimized.

4.3.1.3 Historical trends in CCD

A comparison of global average CCD values from 2018 to 2024 reveals a significant decline in the coupling coordination of land functions during the 2019-2021 period. This sharp decline can likely be attributed to the negative effects of the COVID-19 pandemic and its associated measures on land function relationships, as reflected in a reduction in indicators such as nighttime lights, while vegetation indicators experienced some recovery, ultimately contributing to the overall drop in CCD values. Following the end of pandemic control measures in 2022, CCD values began to recover. Overall, CCD values showed a downward trend between 2018 and 2024. This suggests that, to maintain CCD stability and enhance the coupling coordination of land functions, planners should closely monitor the situation and implement appropriate measures.

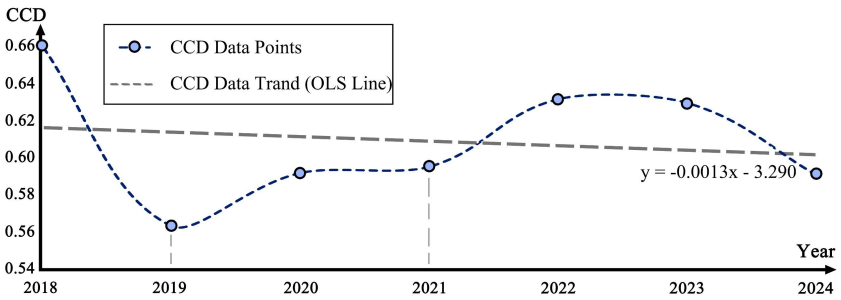

Figure 30 Historical Trends in CCD.

4.3.2 Intra-group coupling & MST networks

4.3.2.1 Multi-scale intra-group coupling analysis

This study first applies the moving window method (1km window) to extract peak points of local land functions (LSF/LEF). Incremental spatial autocorrelation analysis reveals that LSF exhibits

significant spatial clustering peaks at 2950 and 5500m ($Z > 0$, $P < 0.01$), while LEF demonstrates similar clustering at 2650m and 6100m. These threshold distances indicate pronounced spatial clustering effects of land function peak points at specific scales, reflecting the grouping characteristics of corresponding functions. Specifically, the 3000m threshold is typically considered the scale range for medium-sized blocks to urban districts, where residents can access various facilities on foot within 30 to 40 minutes—the maximum radius for walkable living circles in numerous urban planning strategies. The distances of 2650m and 2950m approximate the scale of walkable living circles, where both LSF and LEF can effectively form functional clusters.

Conversely, the 6000m threshold distance corresponds more closely to the scale of a small urban district or multiple functional areas, representing a larger urban structure. At this scale, the distribution and connections of urban and ecological functions grow more complex, typically necessitating public transportation or motorized travel, reflecting the integration and extension of functions across blocks or communities. At this scale, the LEF threshold exceeds that of LSF, indicating that ecological functions are more integrated overall, while local areas exhibit relatively dispersed characteristics.

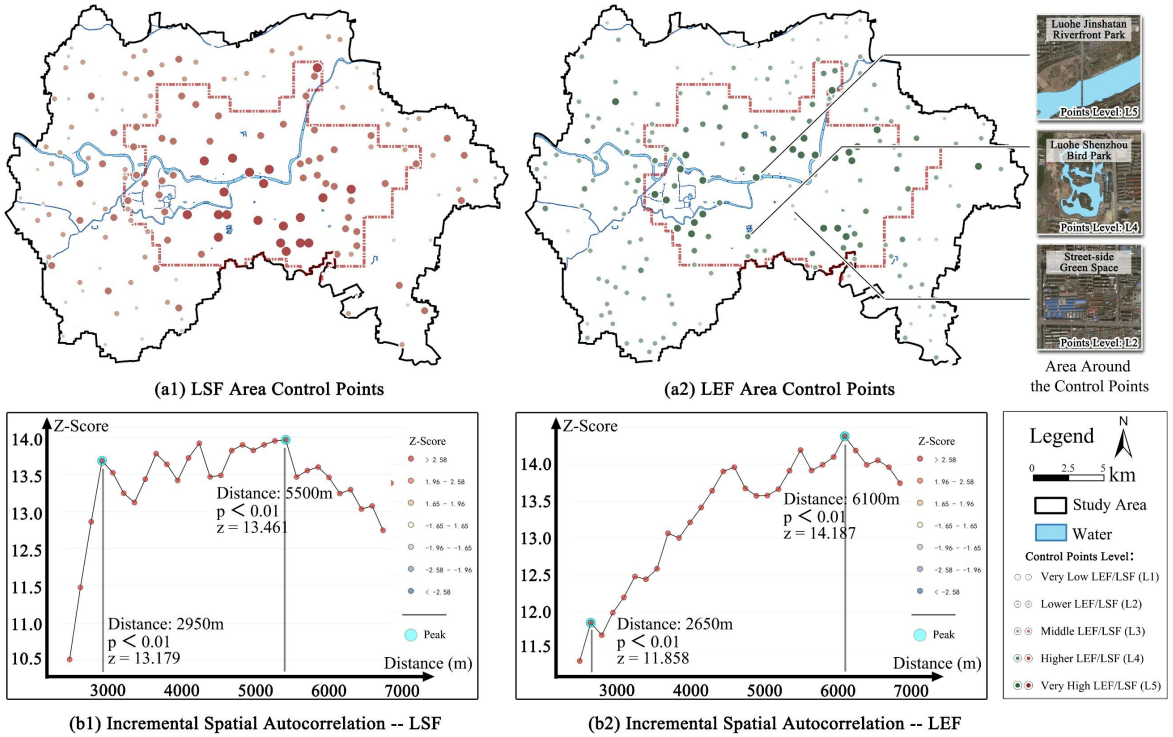

Figure 31 Local Peak Point Extraction and Functional Cluster Scale Analysis of LSF/LEF.

In summary, LSF and LEF exhibit both similarities and differences in terms of aggregation thresholds. The similarities are primarily reflected in the proximity of certain key thresholds, particularly in the range of 2650m to 2950m. This distance aligns with the scale of a pedestrian living circle, indicating that in medium-scale urban spaces, both social and ecological functions can effectively form functional clusters. The differences, however, lie in the aggregation effects at different scales. Specifically, LEF exhibits stronger aggregation effects at smaller scales (e.g., 2650m), suggesting that the provision of ecological functions demonstrates a strong local concentration within walking distances.

4.3.2.2 Network & functional groups

The network connectivity results based on the 3000m distance threshold are shown in Figure 32. The strength and quantity of these connections actually reflect the weighted density of the local peaks of social and ecological land functions, rather than the intensity of function provision.

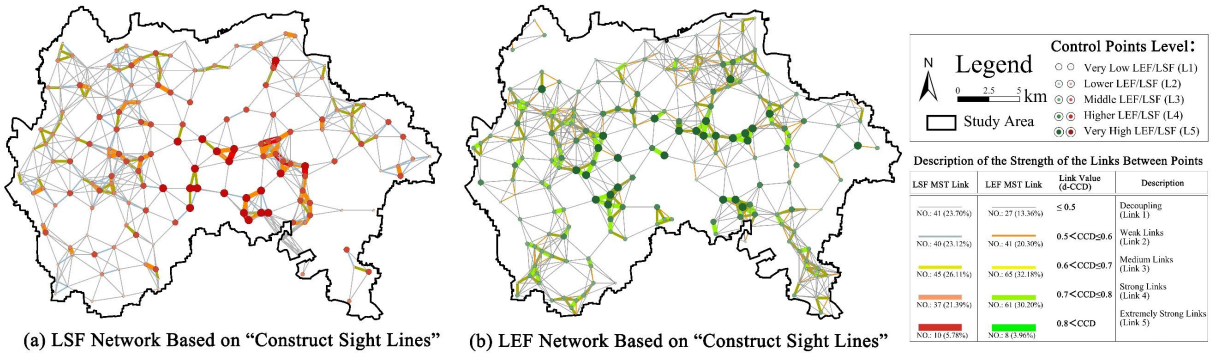

Figure 32 Network Based on "Construct-Sight-Lines".

A comparison of the MST networks of LSF and LEF reveals that strong/very strong links (Link Level 4/5) in LSF are primarily concentrated in the north-eastern part of the study area, distributed along the river in large clusters. In the northern new district, LSF peak points exhibit little clustering and are more scattered, with some links having d-CCD values below 0.5, indicating that LSF peak points in this area are nearly decoupled. The clusters in the peninsula area are relatively weaker, though the overall clustering trend is already apparent.

Converting the above network into a raster using the "line density" tool can more effectively identify local functional clusters.

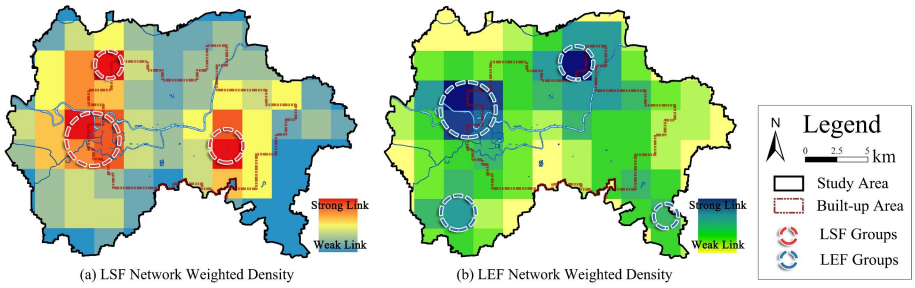

Figure 33 Functional Group Identification.

In the LEF network, very strong/strong links (Link 4/5) are predominantly located in the peninsula area, which houses the largest LEF functional cluster. The remaining functional clusters are mostly scattered along the built-up area's boundary in small formations. Both the old district and the northern new district contain peak points but lack significant functional clusters.

Overall, the LSF network demonstrates stronger coupling coordination between LSF peak points (Mean = 0.74) and exhibits weaker d-CCD fluctuations (STD = 0.02), resulting in more well-defined large spatial functional clusters that heavily rely on the river. In contrast, LEF peak points display weaker coupling coordination (Mean = 0.63) and stronger d-CCD fluctuations (STD = 0.13), with functional clusters more scattered in small groups along the built-up area's boundaries, and the main cluster located in the peninsula area.

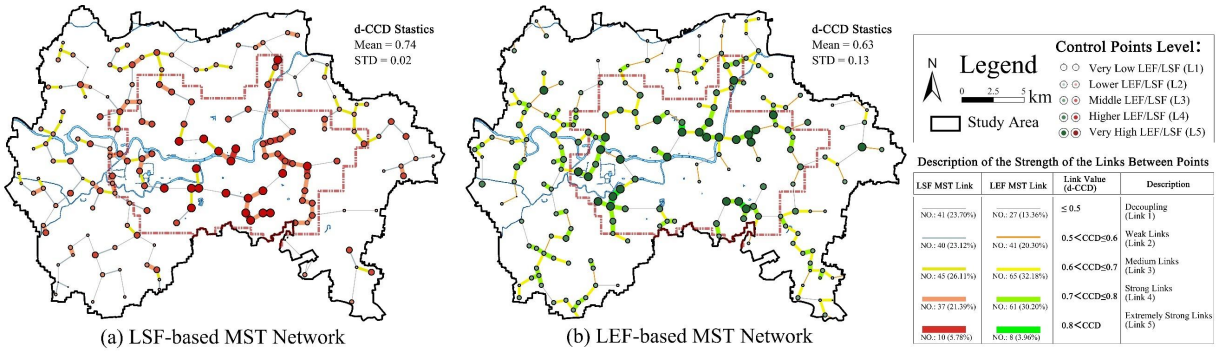

Figure 34 LEF/LSF-based MST Network.

4.4 Vitality & land coupling coordination

4.4.1 UVI correlation with inter & intra coupling

At the optimal scale for functional coupling and clustering (3km), the inter-group coupling coordination between urban vitality and land functions shows a significant correlation ($P \leqslant 0.01$). Specifically, the Spearman correlation coefficient between the UVI and inter-group coupling (CCD) is 0.697 on workdays and 0.723 on weekends. This indicates that, at this spatial

scale, the combination of social and ecological functions can effectively explain urban vitality, highlighting the crucial role of the synergy between social and ecological functions in driving urban vitality.

In contrast, urban vitality responds only marginally to intra-group coupling of individual functions (social or ecological). The intra-group coupling of social functions (LSF d-CCD) and ecological functions (LEF d-CCD) does not show significant correlations with urban vitality on either workdays or weekends. Specifically, the intra-group coupling of ecological functions (LEF d-CCD) shows an almost zero correlation with urban vitality, suggesting that the clustering of peak points for individual functions or local functional clusters does not significantly affect urban vitality (Table 11).

Table. 11 Correlation of Vitality & Land Function Coupling

	CCD	LSF d-CCD	LEF d-CCD
UVI Workday	0.697***	0.135	0.002
UVI Weekend	0.723***	0.149	0.026

From the above results, it is evident that the inter-group coupling coordination of social and ecological functions has a more direct impact on enhancing urban vitality compared to individual functions. The integrated coordination of social and ecological functions provides multi-dimensional support. For instance, ecological functions supply green spaces and a comfortable environment, while social functions stimulate active foot traffic and commercial activity. Their complementarity significantly enhances the overall vitality of the city.

While the over-concentration of individual functions may bring short-term localized improvements, its marginal effects are low and cannot directly or significantly drive vitality. Therefore, in urban planning and design, excessive emphasis on the dense development of single functions should be avoided, and more attention should be given to functional diversity and complementarity. Through rational spatial planning and the integration of functions, effective connections and interactions between social and ecological functions should be ensured to promote the overall enhancement of urban vitality.

4.4.2 Vitality mutation with CCD level

Based on the OLS regression results between UV and CCD ($y = 0.458x - 0.411$, $R^2 = 0.715$), it is clear that the higher the CCD level of the land, the higher the corresponding UVI. Urban vitality,

according to the classification of CCD levels, can be divided into three distinct stages:

Stage III (CCD levels [8,10]): This stage demonstrates the highest urban vitality (mean UVI = 4.224). The high degree of coupling coordination between social and ecological functions enhances resident vitality and reflects a high level of land function integration and optimization.

Stage II (CCD levels [4,7]): This stage demonstrates moderate urban vitality (mean UVI = 1.724). Regions with CCD levels above 5 ([6,7]) have established initial social-ecological coordination, showing strong optimization potential, while areas with CCD levels below 5 ([4,5]) display weaker or decoupled relationships, necessitating long-term efforts for land function improvement despite moderate vitality.

Stage I (CCD levels [1,3]): This stage represents the lowest urban vitality (mean UVI = 0.423), characterized by completely decoupled land functions or minimal system development, with limited optimization potential.

In conclusion, regions with CCD levels of [6,7] should be prioritized for development based on varying system development modes. These regions possess a strong foundation for land function development and account for 48.39% of the total area, indicating significant redevelopment potential.

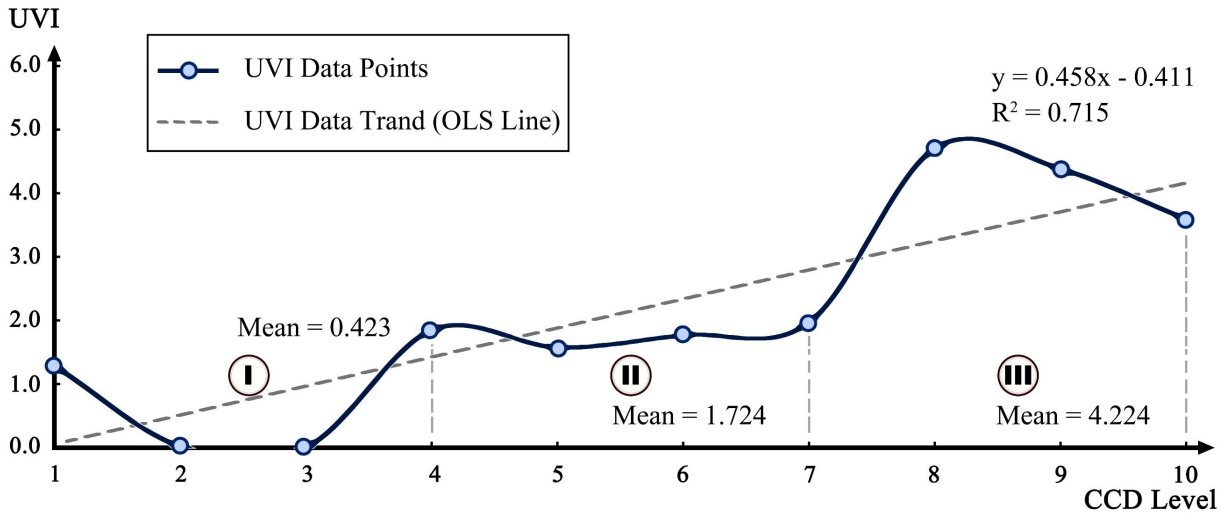

Figure 35 Viability Mutation Based on CCD Levels.

4.5 Analysis of UV dependence on land functions

According to the Spearman correlation model, at the 200m scale, both LSF/LEF and workday/weekend UVI exhibit significant positive correlations ($P < 0.01$), with LSF showing a

stronger correlation with UVI (Figure 36). To further validate the robustness of these correlations, the grid size was adjusted, and mean aggregation was applied to UVI, LEF, LSF, and their respective land function sub-indicators using fishnet data, enabling additional multi-scale analysis.

4.5.1 Multi-scale robustness analysis

The grid sampling ratios are set at 3, 6, 9...21. The spatial distribution of the grid and its relationship to the study area's boundaries are shown below.

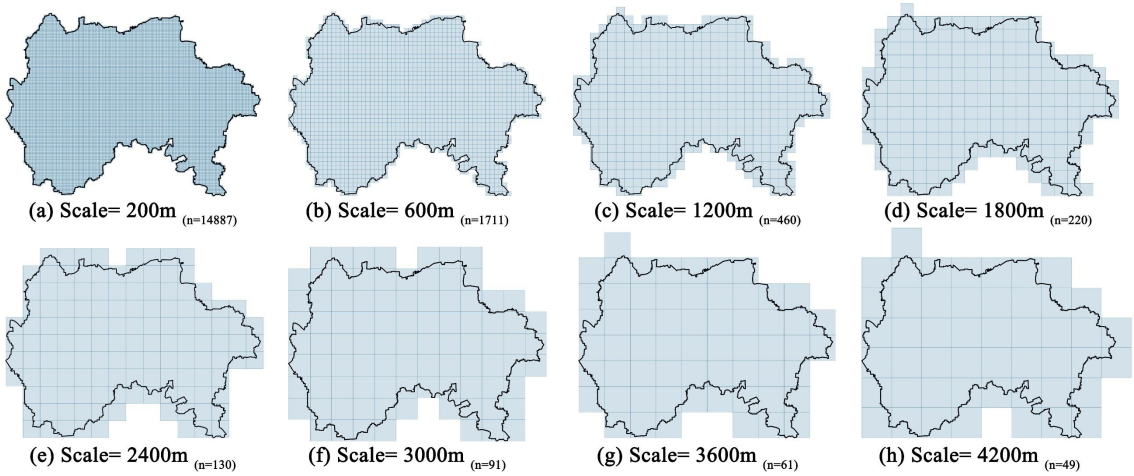

Figure 36 Multiscale Fishing Net.

As the scale expands from micro (200m) to macro (4200m), the correlation between UVI and land functions gradually intensifies. At scales of 200-1800m, the correlation between UVI and both LEF and LSF does not display significant differences between workdays and weekends. The correlation between UVI and LEF is weaker but remains significant, suggesting that urban vitality is relatively less dependent on ecological functions. At scales between 1800m and 4200m, the correlation begins to fluctuate. Differences in the correlation between UVI and both LEF and LSF on workdays and weekends become more pronounced. The correlation between UVI and LEF increases on workdays, while the correlation with LSF declines rapidly, both peaking at the 3000m scale.

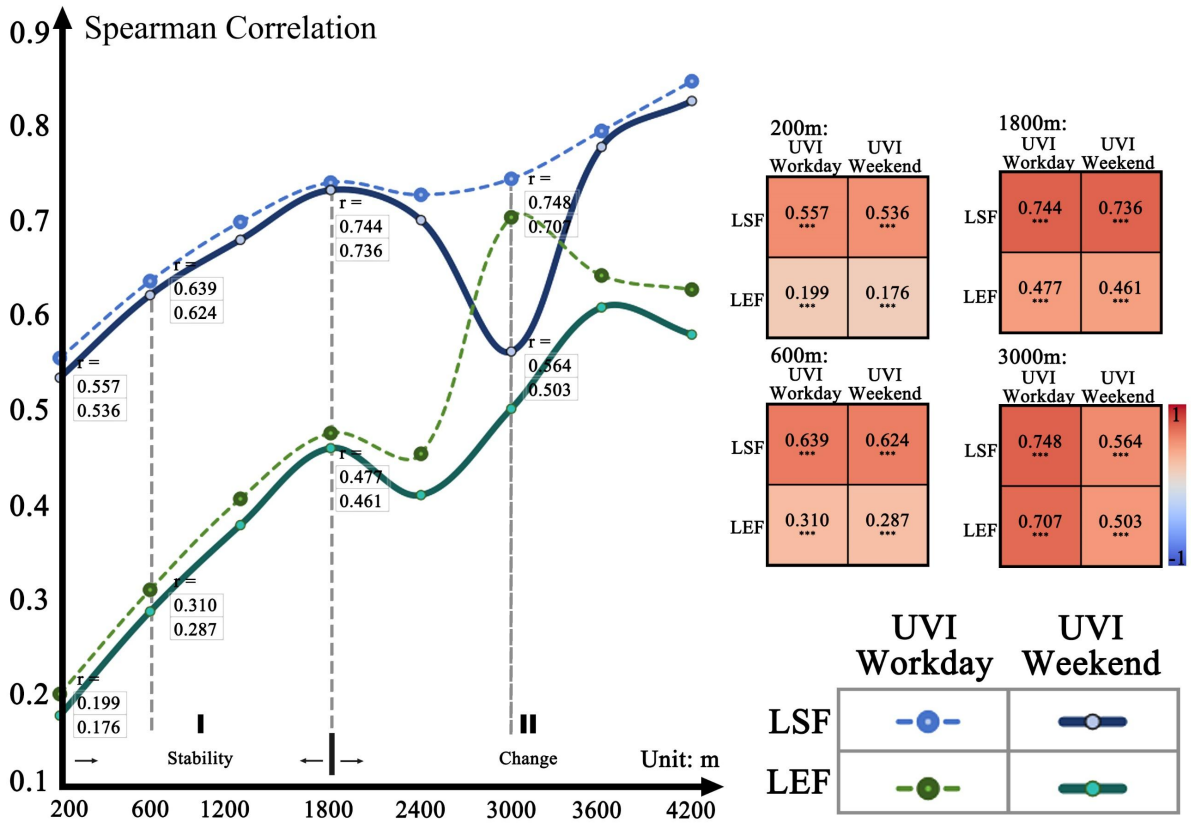

Figure 37 Multi-scale & Multi-scenario Vitality-Land Function Correlation Curves.

LSF and LEF are used as the X variables and UVI as the Y variable to construct the driving relationship through OLS. Across multiple scales, the F-statistics for the models remain significant, and R^2 increases gradually. Land functions indeed drive variations in UVI intensity, with greater explanatory power at macro scales, exceeding 80% at the 4200m scale.

Table. 12 Results of OLS Fitting Accuracy of UVI with LSF/LEF.

Scale	Vitality Scenarios	R^2	F
200	Weekend	0.324	F=3453.495 P=0.000***
	Workday	0.329	F=3525.688 P=0.000***
600	Weekend	0.461	F=731.854 P=0.000***
	Workday	0.466	F=745.918 P=0.000***
1200	Weekend	0.601	F=344.526 P=0.000***
	Workday	0.608	F=353.818 P=0.000***
1800	Weekend	0.684	F=234.569 P=0.000***
	Workday	0.685	F=236.28 P=0.000***
2400	Weekend	0.762	F=203.257 P=0.000***
	Workday	0.766	F=207.997 P=0.000***
3000	Weekend	0.783	F=158.626 P=0.000***

3600	Workday	0.782	F=157.49 P=0.000***
	Weekend	0.791	F=109.928 P=0.000***
4200	Workday	0.787	F=107.431 P=0.000***
	Weekend	0.802	F=93.45 P=0.000***
	Workday	0.805	F=94.874 P=0.000***

4.5.2 Current spatial dependency analysis

Based on the IQR test (with a whisker point of 1.5), the UVI is divided into six categories ranging from H1 (extremely low values) to H6 (extremely high values). We can observe the variations in each UVI category as the land ecological/social functions change (Figure 38, (b1) - (b2)). LSF and LEF are divided into three land function service categories—low, medium, and high—based on quantiles. Combining the two, we can classify nine service scenarios, such as high LSF and high LEF (HH), high LSF and medium LEF (HM), and others. LSF/LEF and UVI on workdays and weekends exhibit significant correlations, with minimal impact from the scenarios. The UVI distribution trends on workdays and weekends are largely consistent. We use the weekend UVI scenario as an example to examine its spatial response to land functions.

At the 600m scale, the scatterplot demonstrates a significant dependence of UVI on LSF, with UVI levels H2-H5 highly concentrated in areas with high LSF (LSF $\geqslant$ 0.50) and medium-high LEF (LEF $\geqslant$ 0.34). UVI at the H6 level responds only to LSF, but the point density becomes slightly sparse when LEF is less than 0.18. Spatially, extremely high UVI (H6) primarily appears in HH scenarios (H6 Number = 89), followed by HM (H6 Number = 73), and finally HL (H6 Number = 62). This indicates that urban vitality depends on a well-developed LSF, with additional demand for LEF. This trend is more pronounced when LSF is at the median level: H6 UVI primarily appears in MH scenarios (H6 Number = 11), followed by MM and ML scenarios. When LSF is insufficient, LEF loses its appeal, and UVI levels H2-H3 primarily occur in LH, LM, and LL scenarios.

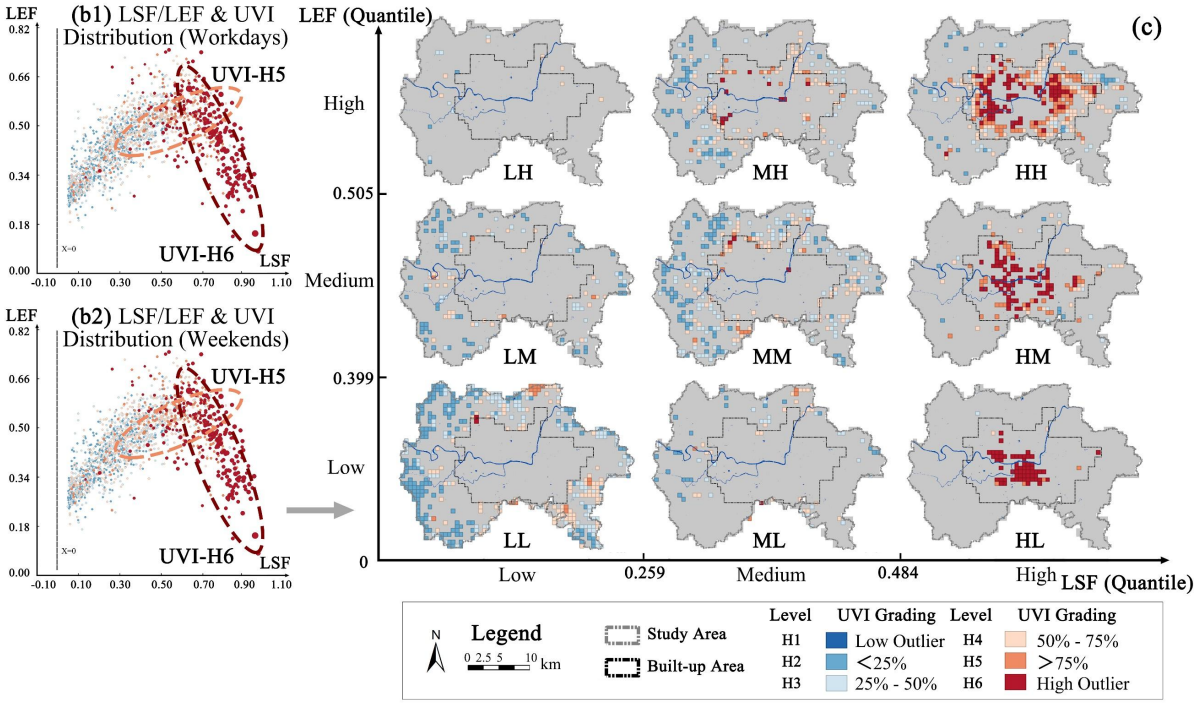

Figure 38 Spatial Correlation of Land Functions with UVI 600m.

At the 1800m scale, the scatterplot is further simplified. Spatially, the effect of high LSF becomes more pronounced, but the number of UVI points in HH, MM, and LL scenarios is significantly higher than in other scenarios with the same LSF. When LSF is consistent, a higher LEF is not always better; rather, LEF in a coupled state with LSF can better attract human flow and improve UVI.

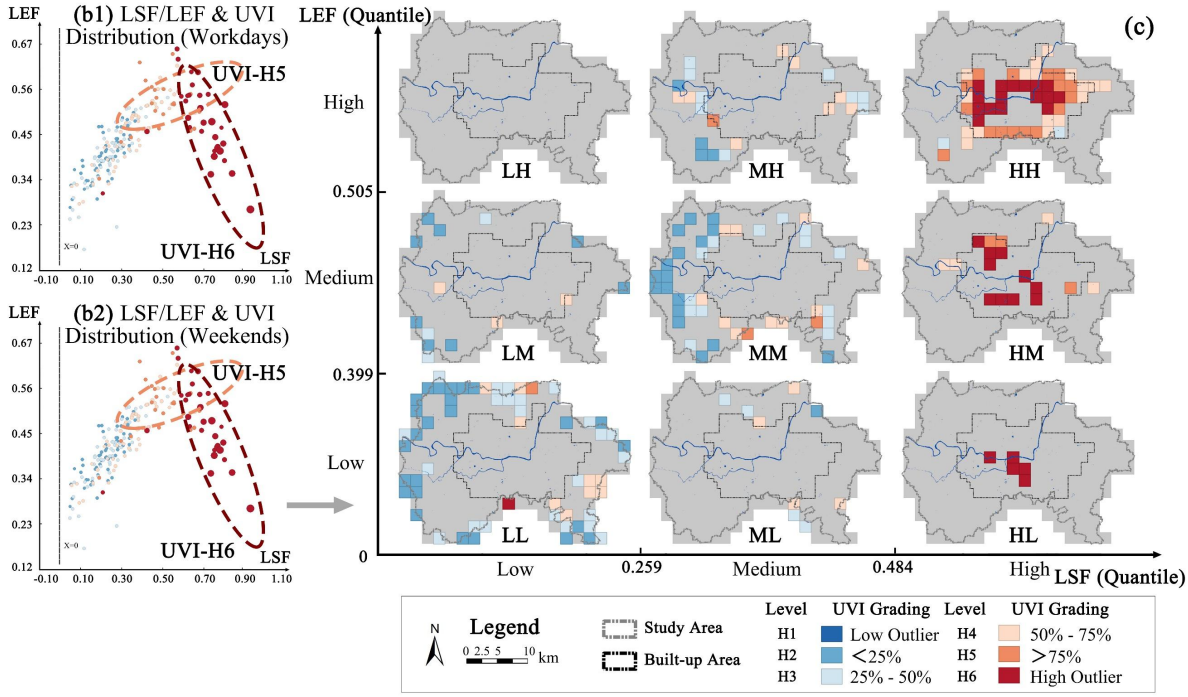

Figure 39 Spatial Correlation of Land Functions with UVI 1800m.

At the 3000m scale, the trends shown by the scatterplot become quite clear. The UVI for H1-H3, H4-H5, and H6 show distinct clustering tendencies, each following its own distribution pattern. The spatial correlation diagram further emphasizes the balanced relationship between LSF and LEF in attracting UVI.

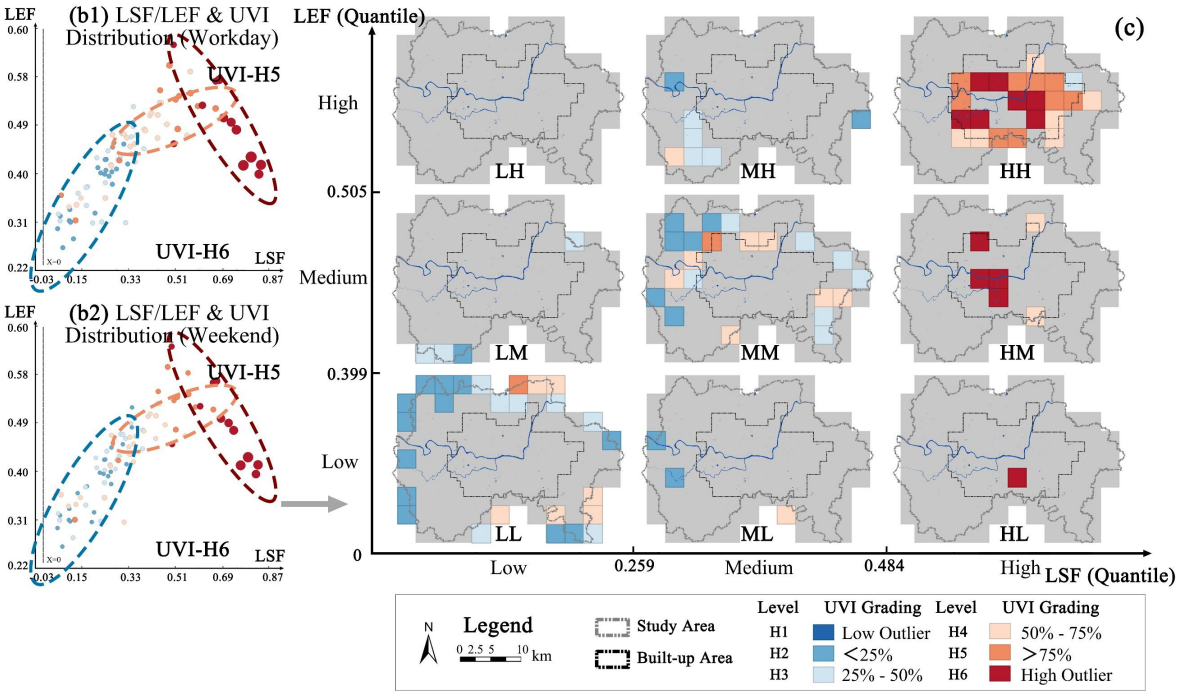

Figure 40 Spatial Correlation of Land Functions with UVI 3000m.

4.6 Driving analysis of land factor on UV

4.6.1 Factor screening based on correlation & VIF

The selection of the MGWR driving scale follows the principle of prioritizing the micro-scale range of 200-1800m to capture as much spatial detail as possible. Therefore, based on the analysis in section 4.4.2.1, the representative scale of 600m within the 200-1800m range is selected. At this scale, the correlation between various factors and UVI is analyzed as follows, with all results being statistically significant at p-value < 0.01.

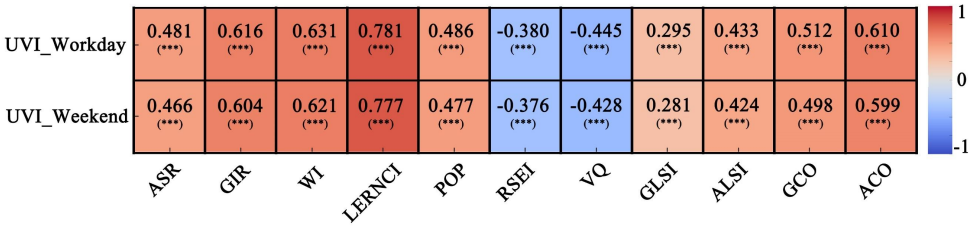

Figure 41 Correlation Between Land Factor & UVI.

Furthermore, as the OLS driving coefficients of the various indicators for UVI on workdays and weekends show little variation, the OLS model is constructed using UVI (Weekend) as an example, and factors with high multicollinearity (VIF ≥ 10) are removed based on the VIF test. At the current scale, the land cohesion indicators (GCO/ACO) were removed. The remaining factors are used to construct a fitting model with UVI.

Table. 13 VIF Values for Individual X Indicators in OLS.

Y	X1	X2	X3	X4	X5	X6	X7	X8	X9
UVI (Weekend)	ASR	GIR	WI	NTL	POP	RSEI	VQ	GLSI	ALSI
	2.679	5.831	2.924	3.659	1.904	5.25	3.134	6.333	7.946

4.6.2 Factor drivers and bandwidth variation

4.6.2.1 Factor bandwidth analysis

In the MGWR model, bandwidth indicates the spatial range within which a factor exerts a uniform influence, directly representing the scale of its influence. A larger bandwidth means that the factor's influence remains relatively consistent over a larger area. This study incorporated land function variables as explanatory factors, with the intercept term capturing the influence of other uncontrolled variables such as location, resident culture and city history. Based on the Jenks natural breaks method for bandwidth classification, we divided these locational factors into three distinct categories: (a) Global scale (bandwidth = [959, 1710]), covering 56.082%-100% of

the study area; (b) Semi-global factors (bandwidth = [290, 479]), covering 16.959%-28.012%; and (c) Local factors (bandwidth = 57), covering 3.333%.

From workdays to weekends, four factors maintained consistent bandwidths: LERNCI, POP, WI, GLSI. These persistent global factors served as constant drivers of UVI, while persistent local factors were significant drivers of UVI heterogeneity and remained unaffected by various scenarios. The bandwidth of the remaining five factors significantly changed depending on human activity scenarios (Table 12).

Table. 14 Bandwidth Changes of Driving Factors on Workdays/Weekends.

NO.	Name	Workdays	Weekends	Change
X1	ASR	479	57	Semi-global → Local
X2	LERNCI	57	57	Local → Local
X3	POP	1680	959	Global → Global
X4	WI	1710	1710	Global → Global
X5	ALSI	1710	57	Global → Local
X6	GIR	57	1710	Local → Global
X7	VQ	330	1710	Semi-global → Global
X8	RSEI	290	1710	Semi-global → Global
X9	GLSI	1710	1710	Global → Global
/	Intercept	57	1710	Local → Global

ASR and LERNCI were the main driving forces, with LSF also playing a significant role (LSF Mean(abs) = 0.148 ＞LEF Mean(abs) = 0.045). When disregarding factors with a change rate lower than 0.005, it was observed that in autonomous activity scenarios (Weekend), factors comprising LEF (GIR, VQ, RSEI) and factors comprising LSF (ASR) exhibited an increase in attractiveness, whereas the attractiveness of LERNCI and POP within LSF diminished (Table 13).

Table. 15 Driving Forces Mean Changes and Directions of Driving Forces on Workday/Weekend.

System	Variable	Workdays	Weekends	Change	Direction
LSF	ASR	0.207	0.217	0.010	+
	LERNCI	0.424	0.356	-0.068	-
	POP	-0.071	-0.080	-0.009	-
	WI	-0.034	-0.032	0.002	/
	ALSI	0.004	0.072	0.068	+
Mean (abs)		0.148	0.151	0.003	+
LEF	GIR	0.002	0.024	0.022	+
	VQ	-0.078	-0.024	0.054	+
	RSEI	0.091	0.090	-0.001	/
	GLSI	-0.054	-0.057	-0.003	/

Mean (abs)	0.045	0.039	-0.059	-
Intercept	-0.136	-0.195	-0.059	-

4.6.2.2 Coefficient analysis of bandwidth stabilization factors

(1) Persistent Global Factors

From workdays to weekends, all three persistent global factors exhibited negative driving forces. UVI decreased with increases in population, accessibility, and the complexity of green infrastructure patch morphology. The influence of WI was mild, while POP exerted the most significant impact.

Table. 16 Changes in Driving Forces of Persistent Global Factors on Workday/Weekend.

	Workdays					**Weekends**				
Variable	**Mean**	**STD**	**Min**	**Median**	**Max**	**Mean**	**STD**	**Min**	**Median**	**Max**
POP	-0.071	0.002	-0.074	-0.071	-0.068	-0.08	0.017	-0.099	-0.086	-0.032
IW	-0.034	0.001	-0.037	-0.034	-0.031	-0.032	0.001	-0.035	-0.032	-0.03
GLSI	-0.054	0.003	-0.058	-0.056	-0.048	-0.057	0.004	-0.061	-0.058	-0.05

(2) Persistent Local Factors

The only persistent local factor was LERNCI, acting as a positive driver. This indicates that UVI generally increased alongside the degree of urbanization. Notably, the driving force associated with LERNCI exhibited the highest mean value among all factors. This finding underscores the attraction of population aggregation and activities facilitated by well-developed infrastructure.

Table. 17 Changes in Driving Forces of Persistent Local Factors on Workdays/Weekends.

	Workdays					**Weekends**				
Variable	**Mean**	**STD**	**Min**	**Median**	**Max**	**Mean**	**STD**	**Min**	**Median**	**Max**
LERNCI	0.424	0.214	-0.735	0.405	1.187	0.356	0.246	-1.861	0.379	1.073

Figure42 illustrates the spatial distribution of the LERNCI coefficient. The coefficient of LERNCI showed both positive and negative driving effects. Within the urban core (Area-3), increasing LERNCI values were associated with rising UVI. In the peninsula area (Area-2), LERNCI showed minimal impact on UVI. However, on the urban fringe, especially in logistics and warehousing areas (Area-4) and northern rural clusters (Area-1), increased light appeared to be linked with decreased human activity.

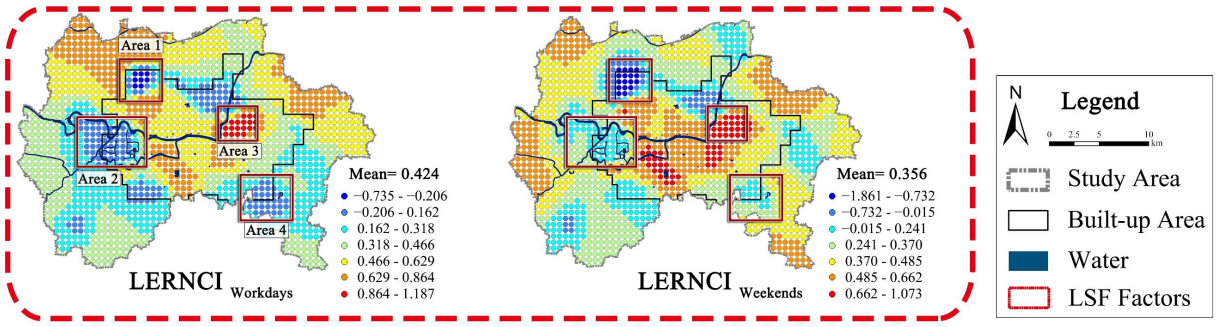

Figure 42 Persistent Local Driving Factors.

4.6.2.3 Coefficient analysis of bandwidth increase factors

An increased bandwidth implies an expanded spatial range of homogeneous influence. Notably, VQ and RSEI, previously categorized as semi-global factors of LEF, transitioned to global factors. Meanwhile, the GIR and the intercept exhibited a transition from local to global influence.

Overall, the driving force of RSEI remained stable across both workday and weekend scenarios. VQ's negative impact on UVI decreased significantly during weekends. The green infrastructure quantity factor, GIR, consistently acted as a positive driver of UVI, with a significant increase in its influence during weekends.

Table. 18 Changes in Driving Forces of Increased Bandwidth Factors from Workdays to Weekends.

	Workdays					Weekends				
Variable	**Mean**	**STD**	**Min**	**Median**	**Max**	**Mean**	**STD**	**Min**	**Median**	**Max**
VQ	-0.078	0.063	-0.25	-0.056	-0.011	-0.024	0.001	-0.026	-0.025	-0.023
RSEI	0.091	0.04	-0.012	0.093	0.165	0.09	0.002	0.086	0.09	0.094
GIR	0.002	0.109	-0.352	-0.009	0.79	0.024	0.001	0.023	0.024	0.027
Intercept	-0.136	0.185	-0.624	-0.16	0.712	-0.195	0.002	-0.199	-0.194	-0.192

The most notable change observed in the coefficients of RSEI, VQ, and GIR was the disappearance of cold spots within the built-up area during weekends. The localized negative driving effects of RSEI and GIR observed during workdays disappeared on weekends, resulting in an overall positive influence on UVI. Although VQ remained a negative driver, its impact weakened. This indicates a shift in green infrastructure function from landscape to recreational use. Notably, the increased demand for green spaces during weekends resulted in higher UVI in areas characterized by high LEF.

During workdays, the intercept served as a local factor, representing locational attributes such as the constraints imposed by commercial or work areas on human activity and UV. During weekends, the absence of these constraints under volitional human activity scenarios led to significant bandwidth changes in the intercept.

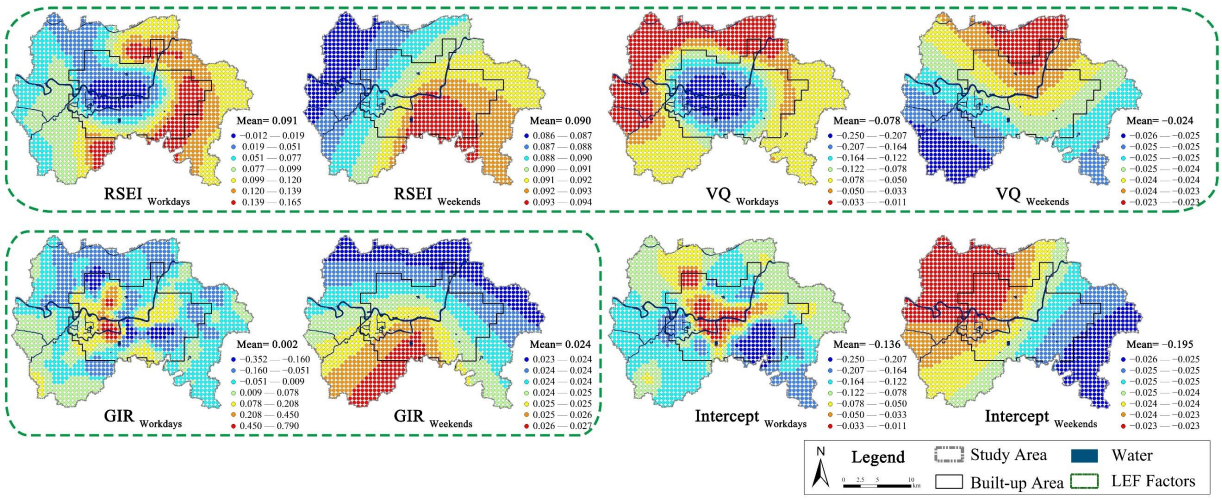

Figure 43 Driving Factors with Increased Bandwidth.

4.6.2.4 Coefficient analysis of bandwidth decrease factor

Several factors exhibited a decrease in bandwidth. ASR transitioned from a semi-global to a local factor, while ALSI shifted from global to local influence. ASR exhibited a stronger driving force compared to ALSI, but ALSI demonstrated greater variations in influence across different scenarios.

Table. 19 Changes in Driving Forces of Decreased Bandwidth Factors from Workdays to Weekends.

	Workdays					Weekends				
Variable	**Mean**	**STD**	**Min**	**Median**	**Max**	**Mean**	**STD**	**Min**	**Median**	**Max**
ASR	0.207	0.042	0.155	0.192	0.287	0.217	0.192	-0.083	0.154	0.892
ALSI	0.004	0.001	0.001	0.004	0.007	0.072	0.221	-0.616	0.024	1.462

Both on workdays and weekends, ASR showed a strong positive driving force in the core areas, with increased heterogeneity and a significant increase in the maximum driving force (from 0.287 to 0.892), highlighting a preference for urban built-up areas. During weekends, UVI was more attracted to the ASR of the built-up area, which suppressed surrounding townships. This also explained the change in ALSI coefficients, transitioning from global positive driving to significant local positive driving (maximum from 0.007 to 1.462), with the emergence of local negative driving effects (Figure 44).

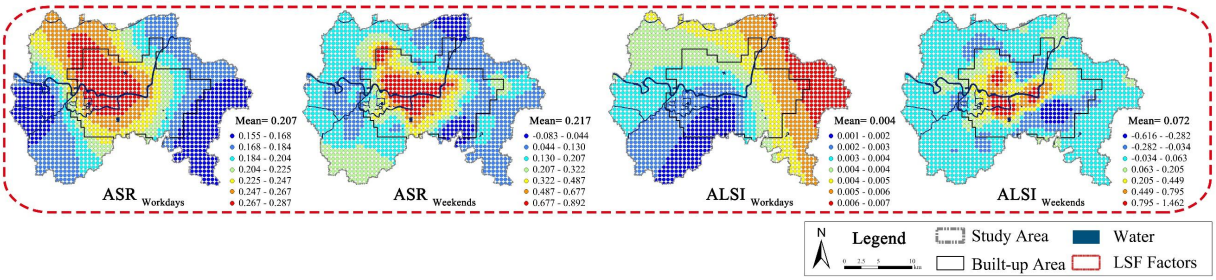

Figure 44 Driving Factors with Decreased Bandwidth.

4.6.3 Factor interaction analysis

The interaction between various land assessment factors is further explored using the OPGD. To achieve the optimal model performance, the best factor discretization parameters are identified through an exhaustive search.

4.6.3.1 Optimal discrete parameter

The explanatory power of each driving factor varies significantly across different discretization methods and classification numbers, which may introduce bias into the study's results. The study typically selects the combination with the highest q-value as the optimal discretization parameter. These optimal parameters better describe the influence of driving factors on geographical phenomena. The optimal classification method for the X1_GIR factor is Quantile, with 7 as the best number of classes. For the X2_ASR factor, the optimal classification method is Equal, with 6 as the best number of classes. The detailed discretization results for each factor are as follows:

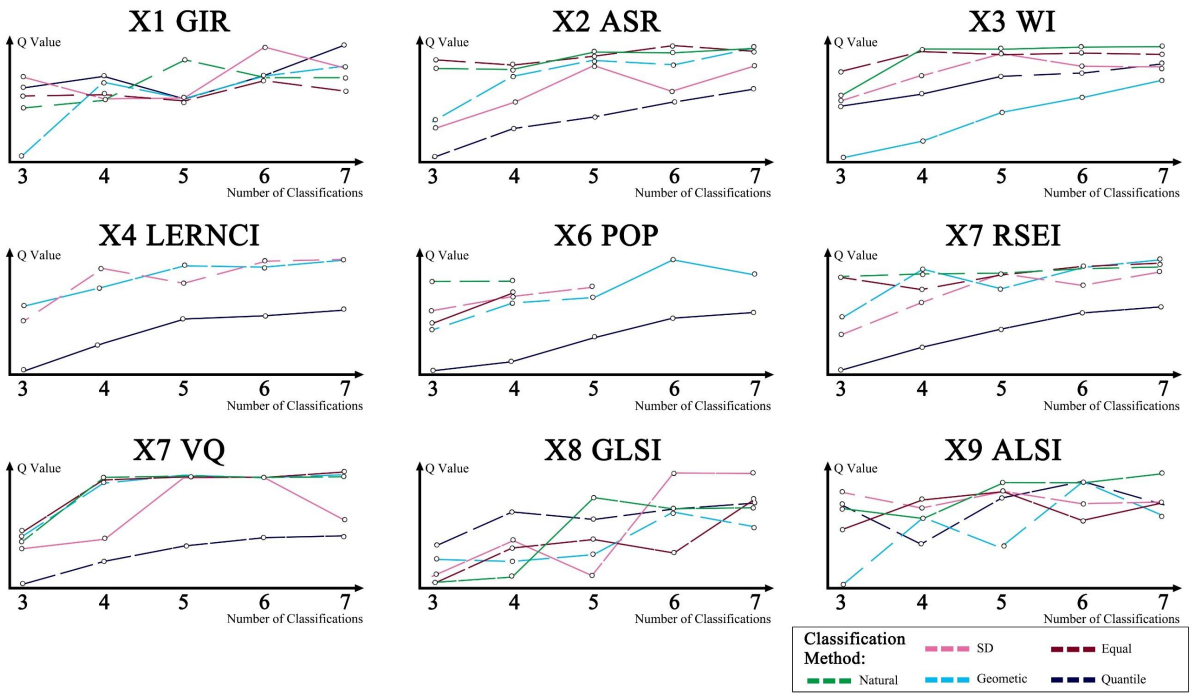

Figure 45 Optimal Discrete Optimization (Weekend).

During the discretization process, the optimal discretization parameters for workdays and weekends were consistent, showing a high degree of uniformity. At this point, they exhibited the highest explanatory power for the independent variables, with all p-values passing the significance test.

Table. 20 Factor Discrete Parameters at 600m Scale

Land Factors	Discretization Method	Classification
X1_GIR	Natural	7
X2_ASR	Natural	6
X3_WI	Equal	7
X4_LERNCI	Natural	5
X5_POP	Natural	7
X6_RSEI	SD	6
X7_VQ	Natural	7
X8_GLSI	Quantile	7
X9_ALSI	SD	6

4.6.3.2 Urban vitality: key factor interactions

Based on the analysis results from the OPGD, LERNCI (urbanization level) was identified as the strongest core factor, consistent with the findings from the MGWR model. The interaction combinations of LERNCI with other factors generally exhibit high q-values, indicating its strong

explanatory power for UV. Since the OPGD does not provide the positive or negative direction of the factors' influence on Y, we adopt the MGWR results for driving factor analysis, marking positive drivers as (+) and negative drivers as (-), (Figure 46).

On workdays, the strongest factor interaction combination is LERNCI (+) and ASR (+), with a q-value of 0.703, indicating a significant positive impact on UV. This is followed by LERNCI (+) and VQ (-) (q-value of 0.698), and LERNCI (+) and POP (-) (q-value of 0.686). On weekends, the ranking of factor combinations changes, with LERNCI (+) and VQ (-) (q-value of 0.699) becoming the strongest combination, followed by LERNCI (+) and GLSI (-) (q-value of 0.695), and LERNCI (+) and ASR (+) (q-value of 0.693), (Figure 46).

This shift suggests that on weekends, the attractiveness of high urbanization and high lighting factors to urban vitality decreases. The combination of LERNCI and POP, related to residential factors, drops from third to fourth place, replaced by the combination of LERNCI and GLSI. In contrast, vegetation-related factors (VQ and GLSI) show a significant increase in driving force on weekends, reflecting the enhanced explanatory power of ecological functions for UV on weekends. Compared to workdays, the q-value gap between factor interactions on weekends narrows, indicating more diversified driving factors.

For example, population density (POP) independently shows a negative impact on UV, likely due to high population density often leading to overcrowding and resource strain. However, when combined with the urbanization factor (LERNCI), despite the negative impact of POP on UV, urbanization can mitigate these negative effects by improving infrastructure and enhancing resource allocation efficiency. On the one hand, this nonlinear relationship suggests that while POP alone negatively affects UV, under high levels of urbanization, these negative effects may be alleviated or offset by the positive effects of urbanization, thereby enhancing overall urban vitality. On the other hand, this also highlights a potential risk for planners: relying too heavily on single-factor development may suppress UV, emphasizing the importance of functional diversity and integrated planning, (Figure 46).

4.6.3.3 Nonlinear enhancements in factor combinations

Most factor combinations exhibit bilinear enhancement ($q(A \cap B) > \max(q(A), q(B))$), meaning that the interaction of two factors has greater explanatory power for UV than either factor alone.

This suggests that the combination of these two factors produces an enhancement effect. For instance, the previously mentioned combination of LERNCI (+) ∩ POP (-) demonstrates this phenomenon. In this case, the synergy between the two factors shows that their combined influence explains the target phenomenon more effectively than when they act independently.

However, some factor combinations show nonlinear enhancement ($q(A \cap B) > q(A) + q(B)$), where the combined effect of the two factors on the target phenomenon is much greater than the sum of their individual effects. For example, factors such as GIR (Green infrastructure ratio) and GLSI (green infrastructure landscape shape index) are not typically strong attractors of resident activity on their own, but when combined with other factors, they often exhibit this nonlinear enhancement. This phenomenon typically indicates the presence of a complex nonlinear interaction between factors, where the combined effects are not simply additive, but generate additional explanatory or driving power.

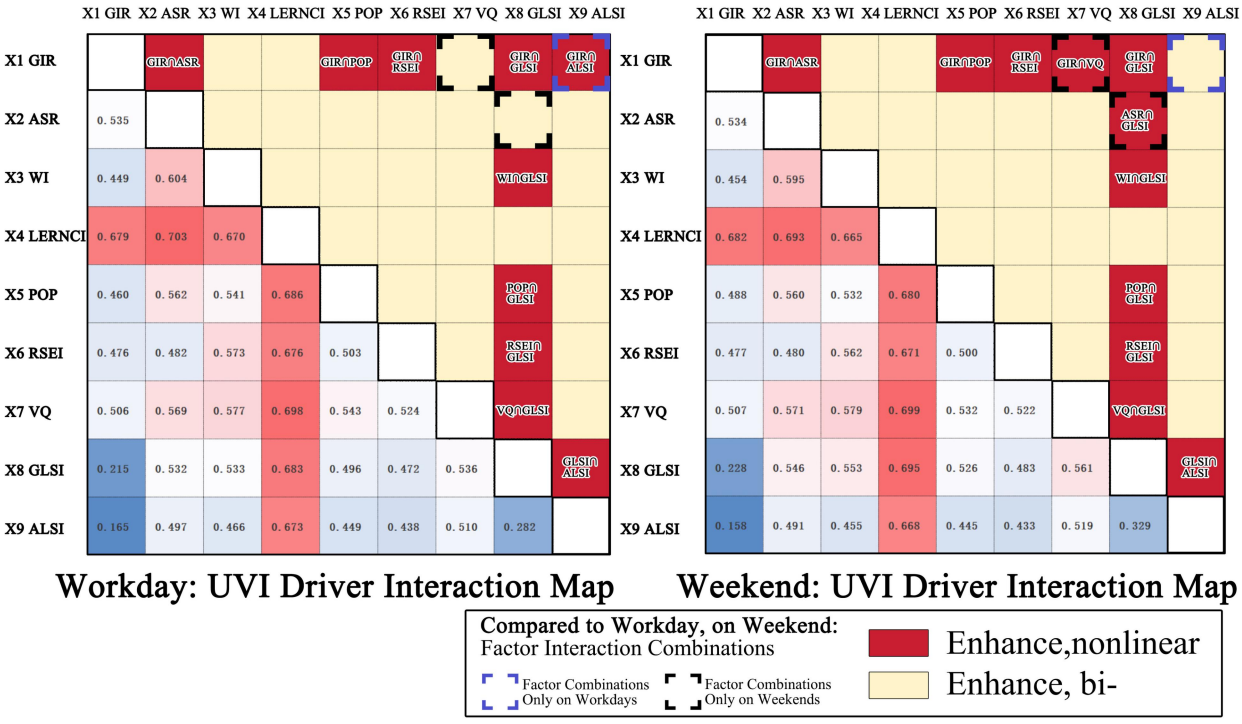

Figure 46 Factor Interaction Results for Multi-scenario UV.

Nonlinear enhancement combinations show some variation between workdays and weekends (Figure 46). For instance, the combinations of GIR (green infrastructure ratio) with ASR (artificial surface ratio), POP (population density), RSEI (remote sensing ecological index), or GLSI (green infrastructure landscape shape index) exhibit nonlinear enhancement across different scenarios. The combination of GIR ∩ VQ (vegetation quality) demonstrates nonlinear

enhancement only on weekends, suggesting that resident activities are more influenced by the natural environment and vegetation quality during this time. On the other hand, the combination of GIR ∩ ALSI (artificial surface landscape shape index) shows similar effects only on workdays, indicating that on workdays, resident activities are more influenced by the combined effects of urban artificial surface morphology and green infrastructure.

Similarly, the combinations of GLSI (green infrastructure landscape shape index) with GIR, WI (weighted road network integration), POP, RSEI, VQ, and ALSI also demonstrate nonlinear enhancement across different scenarios. Notably, the GLSI ∩ ASR combination shows nonlinear gain only on weekends. Considering the previously discussed priority of UV's dependency on land functions, LSF serves as a prerequisite for the effectiveness of LEF.

These results reveal the complex interactions between factors and their multidimensional impact on urban vitality, especially under different social and environmental scenarios. Therefore, urban planning policies should consider these complex factor interactions and optimize the coordination of multiple factors to balance positive and negative effects, maximizing urban vitality.

5 NEW SCIENTIFIC RESULTS

Thesis 1: A self-calibrating urban vitality (UV) assessment method and a multi-source data-based land function evaluation framework are proposed.

Current Situation: Many studies rely on static indicators or single data sources, failing to capture the dynamic spatiotemporal fluctuations in urban human activities. Existing UV assessments overlook variations between workdays and weekends, while conventional land function evaluations—predominantly one-dimensional—do not fully reflect the multifunctional and interrelated nature of urban land.

Innovation: This study integrates high-temporal-resolution human mobility data from Baidu LBS with the SOM algorithm to self-calibrate UV assessments, effectively distinguishing workday and weekend activity patterns. Simultaneously, this study leverages multi-source satellite data (Landsat, MODIS, and VIIRS) to develop a comprehensive evaluation framework for land functions, spanning quantitative, qualitative, and structural dimensions. Moreover, a novel method is introduced to capture spatial heterogeneity and the intricate interactions among land functions. Collectively, these innovations overcome the limitations of static, one-dimensional approaches and provide a robust, data-driven framework that simultaneously advances urban vitality assessment and land function evaluation for sustainable urban planning.

Related Results: Result (1) shows significant spatial spillover and distinct workday/weekend UV patterns. High-temporal Baidu LBS and multi-source satellite data capture dynamic urban activity and land functions, validating our integrated assessment framework.

Thesis 2: Revealing the multi-scale dependence between urban vitality and land social/ecological functions.

Current Situation: Although studies increasingly recognize the role of land social functions (LSF) in enhancing UV, the role of ecological functions (LEF) is often overlooked. Furthermore, many studies focus on single-scale analyses, which miss the variability and stability of these relationships across spatial scales.

Innovation: This study evaluates the robustness of the relationship between LSF/LEF and UV across multiple spatial scales, uncovering a multi-scale dependence. The findings highlight that

LSF is a stronger driver of UV across scales, and the research quantifies UV's dependence on both LSF and LEF across these scales.

Related Results: Result (2) reveals optimal LSF/LEF coupling at 3000 m and scale-dependent UV sensitivity. LSF exerts stronger influence than LEF, confirming multi-scale dependence of land functions on urban vitality.

Thesis 3: Quantifying the correlation between urban vitality and land function CCD..

Current Situation: Although early studies (e.g., Jacobs) recognized a link between mixed land functions and urban vitality, quantitative research on their coordinated integration remains limited. Most studies focus on physical mixing, overlooking the significance of balanced integration in enhancing urban vitality.

Innovation: This study extends traditional mixing approaches (e.g., land use and POI integration) by employing OLS regression, which confirms a positive correlation between conventional functional mixing and urban vitality (coefficient = 0.458, $R^2 = 0.715$). Crucially, to quantify the intricate relationship between CCD and urban vitality, both the traditional CCD model and an enhanced d-CCD model—integrating Gaussian decay functions and Minimum Spanning Tree networks—are utilized. The findings reveal a nonlinear, threshold-driven relationship, demonstrating that balanced functional integration significantly amplifies urban vitality and providing specific thresholds to inform high-efficiency urban development strategies.

Related Results: Result (3) finds CCD peaks at 3000 m with a stable correlation (~0.7) and nonlinear threshold effects, confirming the importance of balanced functional integration for UV.

Thesis 4: Analyzing the driving effects and bandwidths of land function factors on urban vitality in different scenarios in Luohe.

Current Situation: Traditional studies often overlook the variation in urban vitality across different temporal scenarios and the specific roles and influence ranges of various land function factors within these scenarios.

Innovation: This study employs the MGWR model to analyze the driving effects and bandwidths of land function factors on UV under different scenarios in Luohe. The research highlights how land factors exert significant driving forces on UV across different temporal contexts, such as

workdays and weekends. Moreover, the study reveals variations in the bandwidths of each factor's influence on UV across different scenarios, demonstrating the diversity of land function factor impacts. This multi-scenario analysis offers insights into the varied influence of land function factors.

Related Results: Results (4 & 5) show that LSF has a consistently stronger influence on UV, while MGWR analysis detects key drivers (e.g., ASR, LERNCI) with variable influence ranges across scenarios.

Thesis 5: Uncovering the nonlinear enhancement effects among land function factors.

Current Situation: Most current research focuses on the single linear effects of factors on UV However, urban vitality is the ultimate geographic outcome of a city as a complex system. The complex interactions among factors in geographic processes and the potential compound effects they generate should not be overlooked.

Innovation: Through OPGD analysis, this study uncovers the complex interactions among land function factors and their bilinear/nonlinear enhancement effects when combined. For example, the combinations of LERNCI (+) and ASR (+), as well as LERNCI (+) and VQ (-), demonstrate significant nonlinear enhancement effects in specific scenarios. These findings suggest that urban planning and land use optimization should fully consider the interactions between factors to achieve more effective improvements in urban vitality. Furthermore, the continuous intensification of single factors may suppress vitality. As a complex system, enhancing urban vitality should begin with the coupling of social and ecological functions at both the factor and functional levels, taking into account the coordinated development of multiple factors. This study offers a new scientific perspective for understanding the interactions between land function factors and their overall impact on urban vitality.

Related Results: Result (6) shows significant nonlinear enhancement among land function factors. OPGD confirms that combinations (e.g., LERNCI ∩ ASR, LERNCI ∩ VQ) amplify UV, emphasizing coordinated integration.

Note: The above result codes are consistent with the order of results in section 6.1 below.

6 CONCLUSION AND PROSPECTS

6.1 Summary of the dissertation

Since the mid-20th century, global urbanization has accelerated, making cities the primary spaces for human habitation, where vitality has become a crucial indicator of sustainable development and urban quality. Urban vitality (UV) not only reflects the dynamic interactions and supply-demand coordination within the urban system, particularly the balance between human and land relationships, but also indicates the efficiency with which residents utilize urban space and resources, as well as the city's attractiveness to populations, capital, and other productive factors. However, in the face of novel human activity data brought about by the information age, current urban vitality assessment systems seldom delve deeply into the dynamic temporal changes in this data and its coupling/driving relationships with land functions.

Therefore, this dissertation proposes a novel UV assessment method, aimed at leveraging high temporal and spatial granularity data to systematically evaluate and analyze the spatial patterns of urban vitality and its interrelationships with land functions, thereby providing a scientific basis for optimizing urban planning and enhancing sustainable urban development. The specific objectives are: 1) to assess urban vitality and describe its spatial patterns; 2) to evaluate the socio-ecological functions of urban land and calculate the intra-group and inter-group coupling coordination degrees; 3) to analyze the impact of land coupling coordination on urban vitality; 4) to explore the multi-scale spatial response relationships between urban vitality and land social function (LSF) and land ecological function (LEF); and 5) to assess the driving effects and scopes of land function factors on urban vitality under different scenarios, and to further describe the interactions among these driving factors.

This study encompasses 4 aspects: urban vitality assessment, land function evaluation, and exploration of human-land relationships. **(1)** Urban vitality assessment: Based on Human Mobility Data provided by Baidu LBS services, the Self-Organizing Map (SOM) method is employed to identify typical activity patterns. Self-calibration is conducted by analyzing the temporal distribution characteristics of human activities (stability, volatility, day-night ratio), leading to the construction of an Urban Vitality Index (UVI) under various scenarios (workday/weekend). **(2)** Land function evaluation: Landsat satellite data is utilized to perform

supervised classification using the Random Forest (RF) model to obtain land classification data, and landscape pattern indices are calculated based on FRAGSTATS 4.2. Integrating multi-source satellite data from MODIS and VIIRS, a comprehensive function evaluation is conducted from three dimensions: quantity, quality, and structure of the land. **(3)** Under a socio-ecological (SE) framework, the coupling coordination degree (CCD) model was first used to calculate inter-group coupling coordination relationships. Furthermore, by integrating the Minimum Spanning Tree (MST) model and the Gaussian decay function, the traditional CCD was weighted to further calculate intra-group coupling coordination relationships for LSF (land social function) and LEF (land ecological function). **(4)** Exploration of human-land relationships: The relationship between urban vitality and land is explored at three levels: land coupling, land functions, and land factors. At the land coupling level, an Ordinary Least Squares (OLS) model is used to fit the relationship between UVI and land CCD, and historical data from 2018 to 2024 is calculated to show future trends. At the land function level, the stability and priority of UV's multi-scale dependence on LSF and LEF are studied through IQR classification and spatial response analysis. At the land factor level, a Multi-Scale Geographically Weighted Regression (MGWR) model is employed to analyze the driving strength and scope of land function sub-factors on urban vitality under different scenarios. The OPGD is used to reveal interactions among various land function factors and their nonlinear enhancement effects on UV.

The results obtained are as follows: **(1) Urban vitality and land functions exhibit significant spatial spillover effects within the built-up areas.** The distribution of urban vitality in Luohe is highly unbalance, with high-vitality areas concentrated in the built-up zone. LSF (land social function) and LEF (land ecological function) also tend to cluster in this area, but their spatial distributions are not synchronized. Moran's I analysis reveals a significant spatial autocorrelation between urban vitality and socio-ecological land functions, showing a polarization effect, where high/low vitality areas exert positive/negative influences on surrounding regions. **(2) LSF and LEF exhibit optimal coupling at the 3000m scale.** The CCD reaches its highest value at a scale of 3000 meters, closely aligning with the aggregation thresholds of LSF and LEF (2650m/2950m). This reflects the current urban functional clusters and living circle scale in Luohe. **(3) Inter-group coupling of LSF-LEF contributes more to urban vitality than intra-group coupling of single functions.** The d-CCD indicators for both LSF and LEF show

no significant correlation with the urban vitality index (UVI). However, the correlation between CCD and UVI remains stable around 0.7 across different scenarios, and UVI peaks when the CCD level is $\geqslant$ 8 ($0.7 \leqslant CCD < 1.0$). Historical data shows a declining trend in land coupling in Luohe, indicating potential risks of low vitality in the future due to functional decoupling. **(4) LSF has a stronger influence and priority over LEF in affecting UV.** Multi-scale analysis shows that the correlation between LSF and urban vitality is consistently higher than that of LEF. High LSF is a prerequisite for high vitality, while the effectiveness of LEF depends on the sufficient provision of LSF. (**5) The MGWR analysis identifies ASR and LERNCI as the main drivers of urban vitality, with weekend human activity increasing demand for GIR and VQ.** Factors such as VQ, RSEI, GIR, ASR, and ALSI exhibit varying spatial influence ranges (i.e., bandwidth) across different scenarios. **(6) The interaction of land factors in shaping UV.** OPGD analysis reveals nonlinear enhancement effects between driving factors, such as the combinations of LERNCI ∩ ASR and LERNCI ∩ VQ. Considering the interaction of these factors helps mitigate the risk of localized low vitality caused by the over-strengthening of single factors.

The study's results indicate that the formation of urban vitality is closely related to the socio-ecological characteristics of land functions, showing complex interactions across different spatial scales. Optimizing and coordinating land functions play a crucial role in enhancing urban vitality, providing new theoretical foundations and practical references for future urban planning. Future research should further integrate multi-source data and advanced analytical methods to explore the dynamic changes in urban vitality and its driving mechanisms, thereby providing scientific support for building more livable and vibrant urban environments.

6.2 Discussion & recommendations

Long et al. proposed a new future-oriented design paradigm known as Data Augmented Design (Y. Long et al., 2021). This approach aims to conduct scientifically informed, problem-oriented planning through data and image analysis. Building on this foundation, the present study seeks to apply Data Augmented Design to effectively integrate research methods and findings into future urban planning and design.

6.2.1 UV growth poles & polycentric construction

a. To enhance UV, it is recommended to prioritize the establishment of growth poles within developed areas to stimulate vitality in the surrounding regions.

Jacobs's insights emphasize that vitality extends beyond mere activity intensity, encompassing diversity and consistency in urban activities and the people involved (Jacobs, 1961). Urban life follows a dynamic pattern, with fluctuating activity levels over time (Dogan & Lee, 2024). Based on Moran's I analysis, areas with high UV have a significant positive impact on adjacent regions. However, the HMC index for Luohe reveals that while roads and parks attract temporary flows of people, they struggle to sustain long-term vitality. The built-up area lacks zones of sustained high-intensity human activity, indicating the absence of vitality growth poles. In other cities, such poles are typically driven by large shopping malls (Hami et al., 2018), theme parks (Yue et al., 2019), or green spaces (Nambuge et al., 2020). However, in Luohe, such "time-killing" high-traffic areas have yet to be established.

Through the MGWR model, local driving factors (e.g., ASR and LERNCI) have been identified as key determinants of vitality distribution. Based on this, establishing growth poles in areas with significant driving effects (e.g., Zone 3 in the northeast riverside area) would not only leverage the positive influence of LSF growth on UV but also effectively stimulate vitality in surrounding regions.

b. Building a polycentric vitality-landscape structure represents a more long-term planning vision.

However, growth pole construction should not be limited to the concentration of resources in a single area. Although Jacobs emphasized the importance of small blocks and high density for vitality (Jacobs, 1961), research shows that these factors have a limited or even negative impact on UV at Luohe's current stage of urbanization. Therefore, a singular focus on growth poles will not resolve the issue.

Data indicates that Luohe's UVI (as analyzed in Section 4.1.4) and the spatial distribution of LSF (from the evaluation in Section 4.2.3 and MST network community analysis in Section 4.3.1) exhibit characteristics of single-center expansion, with high values concentrated in the old city. This monocentric structure limits vitality growth in peripheral areas. In contrast, a polycentric distribution model similar to LEF is more aligned with the city's long-term development needs.

Therefore, cultivating multiple urban centers and distributing vitality across various regions will contribute to the sustained enhancement of overall urban vitality (J. Li et al., 2016).

The global trend toward polycentric cities has been widely recognized. As Peter Hall et al. demonstrated in their study of Northwestern European metropolitan areas, a polycentric structure effectively promotes balanced urban and regional development (Hall, 2006). Empirical research in China also shows that polycentric structures not only enhance urban vitality but also drive economic growth and social development (Lv et al., 2021; X. Wang et al., 2022). Among them, Shenzhen has achieved remarkable results in polycentric development, which is considered to be effective in relieving overcrowding in the central urban area and forming a number of functional district vitality centers (Xie et al., 2018). Research based on Baidu heat maps indicates that polycentric structures, by dispersing traffic and resources, play a vital role in promoting urban vitality and sustainable development (J. Li et al., 2016). Luohe should draw on these experiences to build a polycentric structure, optimize land and vitality distribution, and enhance the city's overall competitiveness.

6.2.2 Mixed social-ecological functions

In Luohe, LSF is primarily concentrated in the urban core, while high LEF areas form a ring around the developed zones, reflecting a "high-edge, low-center" distribution pattern (Cen et al., 2024). The differing clustering characteristics of LSF and LEF suggest that their spatial distribution is not synchronized. Mixed land use, as an active urban public policy, has been shown to produce positive externalities for cities in various aspects (Gu et al., 2019).

In urban renewal and sustainable development practices in Western countries, mixed land use has gradually become an important tool in urban planning. Scholars such as Rowley (1996) and Hoppenbrower (2005) categorized mixed-use development into four scales: urban, district, neighborhood, and building. The Urban Land Institute (ULI) in the United States categorizes mixed-use patterns into three scales: mixed-use sites at the urban scale, mixed-use walkable areas at the community scale, and vertical mixed-use buildings at the building scale (Mandelker, 2023). This study does not address the building scale of mixed-use development; instead, it focuses on three scales: urban scale (Built-up and Unbuilt-up Areas), functional clusters (within developed areas), and neighborhood (grid) scales.

6.2.2.1 Multi-scale relationships for vitality-land coupling

At the city scale, Moran's I analysis shows that high UVI areas (primarily the urban core) remain consistent across different scenarios, indicating that the developed area as a whole can meet residents' demand for land multifunctionality. However, UVI significantly decreases around the edges of the developed area, suggesting that the functional mix needs optimization. Based on the functional identification results (4.3.2.2), more social functions need to be introduced. In this study, the gap between urban and rural land functions and vitality is significant, with the developed area holding an advantage in terms of social-ecological functions and UV indicators. To reduce the urban-rural development imbalance, spatially balanced development strategies should be implemented.

At the district scale, the phenomenon of "vitality migration" is revealed: the peninsula area attracts large crowds on weekends, but due to insufficient LSF functions, the population significantly decreases on workdays. Functional imbalances lead to periodic migration of residents in terms of foot traffic and functional needs, increasing the commuting burden. In Luohe's old city, although UV values are high, the area falls under the "HL" (high LSF, low LEF) category due to insufficient LEF functions. Therefore, the solution is to improve vitality by optimizing social and ecological functions.

At the neighborhood scale, Jacobs (Jacobs, 1961) and Hoppenbrower (Hoppenbrouwer & Louw, 2005) both emphasized that the neighborhood is a core unit for studying land use mix and urban vitality. Through compact city development, land resources can be utilized more efficiently (Sulis et al., 2018; Xia et al., 2022) . However, the paradox of compact cities is that high-density areas may lack sufficient social and ecological services(De Roo, 2000; Neuman, 2005). Therefore, in addition to the aforementioned polycentric approach, it is recommended to improve vegetation quality and increase street greenery to balance human-land functions, leveraging the negative influence of LEF sub-factors (GLSI/VQ) on UVI to regulate vitality distribution (Martinez-Fernandez et al., 2012).

6.2.2.2 Coupling planning based on functional dependencies

Multi-scale spatial dependency analysis reveals that LSF has a significant impact on UV, while the role of LEF is relatively minor. Human activities show a certain dependency on greenery and

vegetation, which can enhance UV, but their effectiveness must be grounded in a robust social function foundation.

(1) Improvements in the planning of the urban core, especially the HM and HL areas identified in the analysis in Section 4.4.3, are recommended. It is suggested to enhance LEF in three aspects: quantity, quality, and structure. In terms of quantity, increasing green infrastructure, such as street parks and rooftop gardens, will enhance the physical capacity for ecological functions. In terms of quality, improving vegetation coverage, diversity, and carbon storage (e.g., converting grass to shrubs, shrubs to trees) will further boost ecological functions. Structurally, it is important to refine the texture of functional zones to ensure the organic integration of social and ecological functions, avoiding overly rigid separations.

(2) For areas surrounding the developed zones, it is recommended, based on the functional identification results, to focus on regions with a CCD rating of [6.7], which have a high potential for redevelopment and are typically dominated by ecological functions. More LSF should be introduced in these areas, with the goal of raising the CCD level above 8, surpassing the critical UVI threshold. Under the current "stock optimization" guiding principle, priority should be given to improving road network accessibility and infrastructure (e.g., supermarkets, functional buildings), promoting pedestrian traffic, and ensuring the implementation of mixed land use. Jacobs emphasized that to achieve urban diversity, streets should be designed to be short and easy to navigate, avoiding a sense of isolation and monotony. Additionally, LEF structure optimization could break down large functional nodes into smaller ones. Although the total functional capacity would remain unchanged, this would enhance accessibility and functional integration, meeting residents' needs and promoting mixed land use.

When exploring the ratio of LSF to LEF, it is important to note that the optimal proportion still requires further investigation. Although LEF and LSF were equally weighted at 0.5:0.5 in CCD calculations, this study found through correlation analysis that the optimal ratio of UVI to LSF/LEF is 0.72:0.28. Therefore, it is recommended that LEF constitute around 30% of the total. This proportion is supported by other studies, such as the "3-30-300" rule proposed in Spain, which suggests that residents should be able to see at least three trees from their homes, each neighborhood should have 30% tree canopy coverage, and the nearest park or green space should be within 300 meters of any residence (Konijnendijk, 2023) . According to Chinese standards,

the green space area in new developments should not be less than 30% of the total area, while in old city renovations, it should not be less than 25%, and for plazas, the minimum green coverage should be 35% (CJJ/T85-2017).

These comparisons suggest that although equal weighting is commonly used in CCD analysis, the proportion of LEF can be adjusted based on the specific characteristics and vitality needs of different regions to promote sustainable urban development and vitality enhancement.

6.2.3 Factor-based vitality creation and risk

This study primarily analyzed UVI under autonomous human activity conditions and differentiated the influence of global, semi-global, and local factors based on bandwidth. Global factors should serve as macro-level guidelines for policy-making, while semi-global and local factors should guide specific development needs based on their spatial variations (X. Wang, Yao, et al., 2023). Human activity is more sensitive to changes in land function on weekends compared to workdays, indicating that the driving effect of land factors is more crucial during this time.

6.2.3.1 Drive force & bandwidth

On weekends, the global factors and their driving forces are ranked as follows: RSEI (+) > POP (-) > GLSI (-) > WI (-) > GIR (+) = VQ (-). The significant positive impact of RSEI on UV suggests that a balanced mix of vegetation, warmth, and humidity is conducive to vitality growth (Z. Fan et al., 2021). In contrast, the VQ indicator shows a negative influence on UV, indicating that pure vegetation cover and carbon storage often do not align with the direct requirements of urban vitality. High vegetation quality alone (potentially creating confined spaces or other limitations) does not necessarily enhance vitality. Studies on the relationship between urban vitality and green spaces suggest that intrinsic factors related to vegetation alone may not effectively foster vitality. This is a recurring observation: despite thoughtful design, many urban spaces remain underutilized, leading to reduced vitality (F. Li et al., 2017; Yue et al., 2019). Moreover, although urban spaces are influenced by various factors due to their multifaceted nature, our understanding of how different urban "goals" and "characteristics" interact remains limited (Ding & Wang, 2024). Similarly, the study by Guo et al. in Beijing focused on internal factors such as land and park reputation, but it found that these internal factors had little to no

impact on park service areas (S. Guo et al., 2019). Overall, internal factors seem to have a minor, if not negative, impact on spatial vitality. In contrast, recent studies have begun exploring the impact of external factors on public space vitality, such as accessibility(Dogan & Lee, 2024; J. Zhang et al., 2022) , land use (Y. Chen et al., 2016), and economic output (Sander & Zhao, 2015).

Regarding accessibility (measured by WI in this study), our findings support Jacobs' view that shorter street segments promote greater diversity in community vitality. Building on this, other scholars have further pointed out that the ideal block size varies depending on the plot and street dimensions. Rather than designing all blocks and street segments uniformly small, creating communities with varying street lengths is more beneficial to urban vitality (Dogan & Lee, 2024) . In some studies, transportation accessibility has been identified as a key factor in controlling regional vitality (S. Guo et al., 2019; Sugiyama et al., 2010) . However, the direction of its influence, whether positive or negative, has been inconsistent (Ding & Wang, 2024) . This inconsistency may be related to the inherent complexity of cities, indirectly supporting the importance of examining multifactor relationships and spatial heterogeneity of variables.

Semi-global factors mainly affect UVI on workdays, with an average bandwidth of 366 and an area of 42.651 km², which is close to the average township area of 31.74 km² in the study area. The bandwidth of local factors is 57, with an area of 6.636 km², approximating the neighborhood scale. Among the local factors, LERNCI (+) > ASR (+) > ALSI (+), indicating that the quality of development and the complexity of patch structure texture have a greater impact on UV than quantity. It also demonstrates how the core urban location influences UVI, with land use, functions, and morphology in developed areas playing a significant role in this process.

MGWR bandwidth calculations show that factors like POP (-), WI (-), VQ (-), RSEI (+), and GLSI (-) remain consistent across different UVI scenarios on a global scale. Factors such as population density, accessibility, vegetation quality, and green patch complexity have a suppressive effect on UV, while areas with high ecological benefits positively promote UV.

6.2.3.2 Factor interactions & risk warnings

Jacobs argued that (Jacobs, 1961) the influence of population density on individual activity cannot be viewed in isolation, as it is significantly affected by other factors. She stated, "No

matter how high the residential density of a neighborhood is, if other factors are not in place to support or promote diversity, high density alone will not be effective. Moreover……without this condition (high density), other factors promoting diversity will not have much effect either." Thus, a proper interaction of factors is essential for better fostering urban vitality.

The factor interaction analysis revealed varying intensities of factor combinations between workdays and weekends. On workdays, the factor interaction intensities are ranked as LERNCI (+) ∩ ASR (+) > LERNCI (+) ∩ VQ (-) > LERNCI (+) ∩ POP (-). On weekends, LERNCI (+) ∩ VQ (-) > LERNCI (+) ∩ GLSI (-) > LERNCI (+) ∩ ASR (+). The core interaction factor is LERNCI (urbanization level), and the combination with other LEF/LSF factors results in better vitality outcomes.

An in-depth analysis of these factor combinations revealed their complex interrelationships. Although vegetation quality has the strongest negative influence on UVI, it is necessary to consider LEF's dependence on LSF to ensure its effectiveness. Further analysis is needed to determine whether high-LSI green infrastructure fail to effectively enhance overall UV due to a lack of social function support or because they are located on the urban periphery with insufficient infrastructure (Yang et al., 2022). The continuous advancement of single factors, especially internal site factors, is quickly constrained by diminishing marginal returns. In the context of urban open green infrastructure, Cohen et al. found through comparative experiments that despite significant financial investment in improving park facilities, park usage rates did not increase, which was disappointing (Cohen et al., 2009). Similarly, Li et al. found that internal factors such as park attributes, including park service areas and landscape shape index (LSI), had a negative impact on park usage (F. Li et al., 2020).

Under the positive influence of LERNCI, the combination of these factors may alleviate the negative effects of high 3D vegetation density through infrastructure improvements. Currently, the complexity, vegetation, and scale of green patches attract foot traffic, but their low usage frequency leads to negative driving effects, a problem that city managers need to address (Hiller, 2007; Sulis et al., 2018). At the same time, this suggests the risk of single-factor development, with boundary effects such that any single-factor drive does not permanently affect the UV in a linear fashion. If these factors are not matched with an appropriate level of LERNCI, they may exert a reverse driving effect on UV.

Using this feature, reasonable combinations of LERNCI (+) ∩ VQ (-) and LERNCI (+) ∩ GLSI (-) in old city areas can be employed to curb excessive vitality clustering or promote vitality growth in other areas. At the same time, this type of conversion, which does not involve the amount of green infrastructure, has better practicability in the core urban areas where land is tight. In areas surrounding the developed zones, the combination of LERNCI (+) ∩ ASR (+) provides a clear direction for vitality creation.

6.2.4 Practical guide for planners

Based on the findings of this study, the following key recommendations are provided to assist urban and regional planners in integrating land functions to enhance urban vitality effectively:

(1) Develop Multi-Center, High-Vitality Zones. Establish multiple localized high-vitality centers rather than relying on a single-core model. Encourage incremental expansion to ensure flexible future urban growth.

(2) Prioritize Weekend Activity Patterns in Land Planning. Weekend activities respond more strongly to land functions than weekday patterns. Designate green spaces, recreational zones, and mixed-use areas based on peak weekend usage to support urban vitality.

(3) Focus on Social Functions First, then Strengthen Ecological Functions. Initial priority: Develop social functions (community spaces, commercial areas, public services) to enhance human interactions and economic activity. Subsequent step: Integrate ecological functions (parks, green spaces) to improve environmental quality and attract long-term engagement.

(4) Promote Mixed-Use Land Development. Encourage multifunctional land use to avoid mono-functional areas. Combine social (commercial, residential, cultural) and ecological (green spaces, water bodies) functions at different urban scales.

(5) Optimize Functional Density in Limited Space. Where land is scarce, increase functional layering: Vertical expansion (multi-level buildings, green roofs). Efficient road networks (multi-modal transit integration). Diverse land use within the same area (e.g., mixed-use complexes).

(6) Address Vitality and Land Function Across Different Scales. Neighborhood scale: Enhance walkability, ensure balanced facility distribution. City scale: Establish green corridors and public

service hubs to connect high-vitality zones.

6.3 Study limitations and future directions

This study employs the "Pattern-Mechanism-Response" framework to analyze the spatial relationships between UV and land functions. By incorporating MGWR and OPGD models, the study captures spatial heterogeneity alongside nonlinear geographic processes and factor interactions. The findings rely on Baidu human activity data and current land classification datasets, which enhance temporal precision and result credibility. However, limitations in demographic segmentation (e.g., gender, age) may restrict generalizability, making the results more applicable to Luohe's specific population structure and behavioral patterns.

To improve accuracy and detail, future research should integrate additional data sources, such as POI and WorldPop data, allowing behavior patterns to be segmented by demographic attributes and refining insights into different groups' contributions to UV. Although MGWR explored key UV drivers, its limited capacity to account for temporal stability may affect long-term policy implications; thus, Geographic Weighted Time Regression (GTWR) is suggested for more precise tracking of these dynamic factors.

Due to limited historical data, this study cannot fully examine the temporal evolution of UV and land functions. Future work should incorporate long-term human activity data and multi-scale analysis methods to enhance model applicability. Current simulation results also require extended observation and field validation to assess the model's effectiveness and robustness.

REFERENCES

Alexander, C. (1965). A city is not a tree. *Ekistics*, *139*, 344–348.

Alexander, C. (1975). *The oregon experiment* (Vol. 3). Center for Environmental Struc.

Anselin, L. (1995). Local indicators of spatial association—LISA. *Geographical Analysis*, *27*(2), 93–115.

Artmann, M., Inostroza, L., & Fan, P. (2019). Urban sprawl, compact urban development and green cities. How much do we know, how much do we agree? *Ecological Indicators*, *96*, 3–9. https://doi.org/10.1016/j.ecolind.2018.10.059

Arts, J., Hanekamp, T., Linssen, R., & Snippe, J. (2016). Benchmarking integrated infrastructure planning across Europe–Moving forward to vital infrastructure networks and urban regions. *Transportation Research Procedia*, *14*, 303–312.

Avram, F., & Bertsimas, D. (1992). The minimum spanning tree constant in geometrical probability and under the independent model: A unified approach. *The Annals of Applied Probability*, 113–130.

Bai, X., Shi, P., & Liu, Y. (2014). Society: Realizing China's urban dream. *Nature*, *509*(7499), 158–160.

Baret, F., & Guyot, G. (1991). Potentials and limits of vegetation indices for LAI and APAR assessment. *Remote Sensing of Environment*, *35*(2–3), 161–173.

Barthélemy, D., & Nieddu, M. (2007). Non-trade concerns in agricultural and environmental economics: How JR Commons and Karl Polanyi can help us. *Journal of Economic Issues*, *41*(2), 519–527.

Batty, M. (2002). Thinking about cities as spatial events. In *Environment and Planning B: Planning and Design* (Vol. 29, Issue 1, pp. 1–2). SAGE Publications Sage UK: London, England.

Batty, M. (2018). *Inventing future cities*. MIT press.

Bertrand, N., Jones, L., Hasler, B., Omodei-Zorini, L., Petit, S., & Contini, C. (2008). Limits and targets for a regional sustainability assessment: An interdisciplinary exploration of the threshold concept. *Sustainability Impact Assessment of Land Use Changes*, 405–424.

Biddulph, M. (2012). Radical streets? The impact of innovative street designs on liveability and activity in residential areas. *Urban Design International*, *17*, 178–205.

Boegh, E., Soegaard, H., Broge, N., Hasager, C. B., Jensen, N. O., Schelde, K., & Thomsen, A. (2002). Airborne multispectral data for quantifying leaf area index, nitrogen concentration, and photosynthetic efficiency in agriculture. *Remote Sensing of Environment*, *81*(2), 179–193. https://doi.org/10.1016/S0034-4257(01)00342-X

Bohman, M., Cooper, J., Mullarkey, D., Normile, M. A., Skully, D., Vogel, S., & Young, E. (1999). The use and abuse of multifunctionality. *Economic Research Service/USDA*, 5.

Braun, L. M., & Malizia, E. (2015). Downtown vibrancy influences public health and safety outcomes in urban counties. *Journal of Transport & Health*, *2*(4), 540–548.

Cai, B., Shao, Z., Fang, S., Huang, X., Huq, M. E., Tang, Y., Li, Y., & Zhuang, Q. (2021). Finer-scale spatiotemporal coupling coordination model between socioeconomic activity and eco-environment: A case study of Beijing, China. *Ecological Indicators*, *131*, 108165.

Çalışkan, M., & Anbaroğlu, B. (2020). Geo-MST: A geographical minimum spanning tree plugin for QGIS. *SoftwareX*, *12*, 100553. https://doi.org/10.1016/j.softx.2020.100553

Calthorpe, P. (1993). *The next American metropolis: Ecology, community, and the American dream*. Princeton architectural press.

Caprotti, F., Cowley, R., Datta, A., Broto, V. C., Gao, E., Georgeson, L., Herrick, C., Odendaal, N., & Joss, S. (2017). The New Urban Agenda: Key opportunities and challenges for policy and practice. *Urban Research & Practice*, *10*(3), 367–378.
Cats, O. (2024). Identifying human mobility patterns using smart card data. *Transport Reviews*, *44*(1), 213–243. https://doi.org/10.1080/01441647.2023.2251688
Cen, Q., Zhou, X., & Qiu, H. (2024). Exploration of urban neighborhood blue-green space quality patterns and influencing factors in waterfront cities based on MGWR and OPGD models. *Urban Climate*, *55*, 101942. https://doi.org/10.1016/j.uclim.2024.101942
Chen, L., Fu, B., & Zhao, W. (2008). Source-sink landscape theory and its ecological significance (Chinese). *Frontiers of Biology in China*, *3*, 131–136.
Chen, L., Liu, Y., Lv, Y., Feng, X., & Fu, B. (2008). Landscape pattern analysis in landscape ecology: Current, challenges and future (Chinese). *Acta Ecologica Sinica*, *28*(11), 5521–5531.
Chen, Y., Liu, T., Xie, X., & Marušić, B. G. (2016). What attracts people to visit community open spaces? A case study of the Overseas Chinese Town community in Shenzhen, China. *International Journal of Environmental Research and Public Health*, *13*(7), 644.
Cheng, C., Yang, X., & Cai, H. (2021). Analysis of Spatial and Temporal Changes and Expansion Patterns in Mainland Chinese Urban Land between 1995 and 2015. *Remote Sensing*, *13*(11), 2090.
Cheng, Y., Liu, H., Chen, D., & Liu, H. (2022). Human activity intensity and its spatial-temporal evolution in China's border areas. *Land*, *11*(7), 1089.
Cohen, D. A., Golinelli, D., Williamson, S., Sehgal, A., Marsh, T., & McKenzie, T. L. (2009). Effects of park improvements on park use and physical activity: Policy and programming implications. *American Journal of Preventive Medicine*, *37*(6), 475–480.
Cui, X., Yang, S., Zhang, G., Liang, B., & Li, F. (2020). An exploration of a synthetic construction land use quality evaluation based on economic-social-ecological coupling perspective: A case study in major Chinese cities. *International Journal of Environmental Research and Public Health*, *17*(10), 3663.
De Roo, G. (2000). Environmental conflicts in compact cities: Complexity, decisionmaking, and policy approaches. *Environment and Planning B: Planning and Design*, *27*(1), 151–162.
Delclòs-Alió, X., Gutiérrez, A., & Miralles-Guasch, C. (2019). The urban vitality conditions of Jane Jacobs in Barcelona: Residential and smartphone-based tracking measurements of the built environment in a Mediterranean metropolis. *Cities*, *86*, 220–228.
Desa, U. (2014). World urbanization prospects: The 2014 revision, highlights. *Retrieved from United Nations-Department of Economic and Social Affairs. Available Online: Http://Esa. Un. Org/Unpd/Wup/Highlights/WUP2014-Highlights. Pdf (Accessed on 9 August 2016)*.
Diakoulaki, D., Mavrotas, G., & Papayannakis, L. (1995). Determining objective weights in multiple criteria problems: The critic method. *Computers & Operations Research*, *22*(7), 763–770. https://doi.org/10.1016/0305-0548(94)00059-H
Ding, Z., & Wang, H. (2024). What are the key and catalytic external factors affecting the vitality of urban blue-green space? A case study of Nanjing Main Districts, China. *Ecological Indicators*, *158*, 111478. https://doi.org/10.1016/j.ecolind.2023.111478
Dogan, O., & Lee, S. (2024). Jane Jacobs's urban vitality focusing on three-facet criteria and its confluence with urban physical complexity. *Cities*, *155*, 105446. https://doi.org/10.1016/j.cities.2024.105446
Dong, L., Longwu, L., Zhenbo, W., Liangkan, C., & Faming, Z. (2021). Exploration of coupling effects in the Economy–Society–Environment system in urban areas: Case study of the Yangtze

River Delta Urban Agglomeration. *Ecological Indicators*, *128*, 107858.
Ermida, S. L., Soares, P., Mantas, V., Göttsche, F.-M., & Trigo, I. F. (2020). Google earth engine open-source code for land surface temperature estimation from the landsat series. *Remote Sensing*, *12*(9), 1471.
Fan, D., Qiu, Y., Sun, W., ZHAO, X., MAI, X., & HU, Y. (2021). Evaluating ecological environment based on remote sensing ecological index in Shenfu mining area (Chinese). *Bulletin of Surveying and Mapping*, *7*, 23.
Fan, L., & Zhang, D. (2022). Research on the Influence Mechanism and Spatial Heterogeneity Characteristics of Block Vitality in Beijing: Based on Multi-scale Geographically Weighted Regression (Chinese). *City Plan. Rev*, *46*, 27–37.
Fan, Z., Duan, J., Lu, Y., Zou, W., & Lan, W. (2021). A geographical detector study on factors influencing urban park use in Nanjing, China. *Urban Forestry & Urban Greening*, *59*, 126996.
FENG, Q., FAN, H., YANG, L., CHEN, L., HUANG, Y., LI, B., FAN, Y., & YANG, N. (2024). Theory and application of the Landscape Ecology Toolbox software for landscape pattern analysis based on the Patch-Corridor-Matrix and the Source-Flow-Sink paradigm (Chinese). *Acta Ecologica Sinica*, *44*(11), 4678–4686. https://doi.org/10.20103/j.stxb.202307041436
Fieller, E. C., Hartley, H. O., & Pearson, E. S. (1957). Tests for rank correlation coefficients. I. *Biometrika*, *44*(3/4), 470–481. https://doi.org/10.2307/2332878
Fotheringham, A. S., Brunsdon, C., & Charlton, M. (2009). Geographically weighted regression. *The Sage Handbook of Spatial Analysis*, *1*, 243–254.
Gadjiev, A., Aral, A., & ALİYEV, İ. (2007). On behaviour of the Riesz and generalized Riesz potentials as order tends to zero. *MATHEMATICAL INEQUALITIES & APPLICATIONS*, *10*(4).
GAO, F., WANG, C., & YANG, R. (2023). Research Progress in Urban Vitality:Scale,Measurement and Mechanism (Chinese). *New Architecture*, *6*, 10–14.
Gaodi, X., Lin, Z., Caixia, Z., Xiangzheng, D., Koenig, H. J., Tscherning, K., & Helming, K. (2010). Assessing the multifunctionalities of land use in China. *Journal of Resources and Ecology*, *1*(4), 311–318. https://doi.org/10.3969/j.issn.1674-764x.2010.04.003
Gehl, J., & Architects, G. (2004). Towards a fine city for people: Public spaces and public life-London. *Report for Transport for London. Gehl Architects: Copenhagen*.
Grant, J. (2002). Mixed use in theory and practice: Canadian experience with implementing a planning principle. *Journal of the American Planning Association*, *68*(1), 71–84.
Gu, D., Newman, G., Kim, J.-H., Park, Y., & Lee, J. (2019). Neighborhood decline and mixed land uses: Mitigating housing abandonment in shrinking cities. *Land Use Policy*, *83*, 505–511.
Guo, H., Chen, Y., Shao, Y., & Kou, W. (2020). A study on spatial vitality and mechanism of influence on typical blocks of the Old Town of Harbin (Chinese). *Architectural Journal*, *2*, 114–119.
Guo, R., Diehl, J. A., Zhang, R., & Wang, H. (2024). Spatial equity of urban parks from the perspective of recreational opportunities and recreational environment quality: A case study in Singapore. *Landscape and Urban Planning*, *247*, 105065.
Guo, S., Yang, G., Pei, T., Ma, T., Song, C., Shu, H., Du, Y., & Zhou, C. (2019). Analysis of factors affecting urban park service area in Beijing: Perspectives from multi-source geographic data. *Landscape and Urban Planning*, *181*, 103–117.
Hall, P. (2006). The Polycentric Metropolis: Learning from Mega-City Regions in Europe. *Earthscan, Pub*.
Hami, A., Moula, F. F., & Maulan, S. B. (2018). Public preferences toward shopping mall interior landscape design in Kuala Lumpur, Malaysia. *Urban Forestry & Urban Greening*, *30*,

1–7.
Han-Qiu, X. (2005). A study on information extraction of water body with the modified normalized difference water index (MNDWI). *National Remote Sensing Bulletin*, *5*, 589–595.
Harvey, L. (2001). Defining and measuring employability. *Quality in Higher Education*, *7*(2), 97–109.
He, Q., He, W., Song, Y., Wu, J., Yin, C., & Mou, Y. (2018). The impact of urban growth patterns on urban vitality in newly built-up areas based on an association rules analysis using geographical 'big data.' *Land Use Policy*, *78*, 726–738.
Hediger, W. (2006). Weak and strong sustainability, environmental conservation and economic growth. *Natural Resource Modeling*, *19*(3), 359–394.
Helming, K., Tscherning, K., König, B., Sieber, S., Wiggering, H., Kuhlman, T., Wascher, D., Perez-Soba, M., Smeets, P., & Tabbush, P. (2008). Ex ante impact assessment of land use changes in European regions—The SENSOR approach. *Sustainability Impact Assessment of Land Use Changes*, 77–105.
Hess, G. R., & Fischer, R. A. (2001). Communicating clearly about conservation corridors. *Landscape and Urban Planning*, *55*(3), 195–208.
Hiller, B. (2007). *Space. Space in the Machine*. Press Syndicate, of the University of Cambridge, United Kingdom.
Hoppenbrouwer, E., & Louw, E. (2005). Mixed-use development: Theory and practice in Amsterdam's Eastern Docklands. *European Planning Studies*, *13*(7), 967–983.
Howard, E., Osborn, F. J., & Mumford, L. (2013). *Garden cities of to-morrow*. Routledge.
Huang, M., Li, Y., Xia, C., Zeng, C., & Zhang, B. (2022). Coupling responses of landscape pattern to human activity and their drivers in the hinterland of Three Gorges Reservoir Area. *Global Ecology and Conservation*, *33*, e01992. https://doi.org/10.1016/j.gecco.2021.e01992
Huang, S., Wong, J., & Chen, T. (1998). A framework of indicator system for measuring Taipei's urban sustainability. *Landscape and Urban Planning*, *42*(1), 15–27.
Huang, Y. (2008). *A Study of Urban Mixed-use Development in Theory and Practice—The Case of Shanghai (Chinese)* [PhD Thesis, Tongji University]. https://chn.oversea.cnki.net/KCMS/detail/detail.aspx?dbcode=CDFD&dbname=CDFD0911&filename=2009024807.nh&uniplatform=OVERSEA&v=UusXD-XPdViatCPQ4-PaNkOUvYC2EyP5FQRNLLX5VPqc0x9ofsbMmsVK121fqQix
HUANG, Y., & YANG, Z. (2008). Land quality evaluation in China: Present status and prospect. *Geological Bulletin of China*, *27*(2), 207–211.
Jacobs, J. (1961). The death and life of great american cities. Randoms house, New York. *Book Unpublished Resources*.
Jalaladdini, S., & Oktay, D. (2012). Urban public spaces and vitality: A socio-spatial analysis in the streets of Cypriot towns. *Procedia-Social and Behavioral Sciences*, *35*, 664–674.
Ji, Q., Feng, X., Sun, S., Zhang, J., Li, S., & Fu, B. (2024). Cross-scale coupling of ecosystem service flows and socio-ecological interactions in the Yellow River Basin. *Journal of Environmental Management*, *367*, 122071. https://doi.org/10.1016/j.jenvman.2024.122071
Jiang, D. (2007). *The theory of city form vitality (Chinese)*. Southeast University Press. https://books.google.hu/books?id=ITCMHwAACAAJ
Jing, Z., & Wang, J. (2020). Sustainable development evaluation of the society–economy–environment in a resource-based city of China:A complex network approach. *Journal of Cleaner Production*, *263*, 121510. https://doi.org/10.1016/j.jclepro.2020.121510
Kang, C., Fan, D., & Jiao, H. (2021). Validating activity, time, and space diversity as essential

components of urban vitality. *Environment and Planning B: Urban Analytics and City Science*, *48*(5), 1180–1197.
Katz, P. (1994). *The New Urbanism. Toward an architecture of community*.
Konijnendijk, C. C. (2023). Evidence-based guidelines for greener, healthier, more resilient neighbourhoods: Introducing the 3–30–300 rule. *Journal of Forestry Research*, *34*(3), 821–830.
Kuang, W., Liu, J., Dong, J., Chi, W., & Zhang, C. (2016). The rapid and massive urban and industrial land expansions in China between 1990 and 2010: A CLUD-based analysis of their trajectories, patterns, and drivers. *Landscape and Urban Planning*, *145*, 21–33.
Levin, S., Xepapadeas, T., Crépin, A.-S., Norberg, J., De Zeeuw, A., Folke, C., Hughes, T., Arrow, K., Barrett, S., & Daily, G. (2013). Social-ecological systems as complex adaptive systems: Modeling and policy implications. *Environment and Development Economics*, *18*(2), 111–132.
Li, F., Li, F., Li, S., & Long, Y. (2020). Deciphering the recreational use of urban parks: Experiments using multi-source big data for all Chinese cities. *Science of the Total Environment*, *701*, 134896.
Li, F., Zhang, F., Li, X., Wang, P., Liang, J., Mei, Y., Cheng, W., & Qian, Y. (2017). Spatiotemporal patterns of the use of urban green spaces and external factors contributing to their use in central Beijing. *International Journal of Environmental Research and Public Health*, *14*(3), 237.
Li, J., Li, M.-Y., Long, Y., & Dang, A. (2016). China polycentric cities based on Baidu heatmap. *Shanghai Urban Planning Review*, *3*, 30–36.
Li, L., Fan, Z., Feng, W., Yuxin, C., & Keyu, Q. (2022). Coupling coordination degree spatial analysis and driving factor between socio-economic and eco-environment in northern China. *Ecological Indicators*, *135*, 108555. https://doi.org/10.1016/j.ecolind.2022.108555
Li, T. (2019). 70 Years of Urban Economic Development in China:Historical Trajectory and Characteristic Facts (Chinese). *Economist*, *1*(10), 5–16.
Li YuRui, L. Y., Long HuaLou, L. H., & Liu YanSui, L. Y. (2015). *Spatio-temporal pattern of China's rural development: A rurality index perspective.*
Liao, Z., & Liang, S. (2024). Spatiotemporal differences and influencing factors of urban vitality and urban expansion coupling coordination in the Pearl River Delta. *Heliyon*, *10*(4), e25682. https://doi.org/10.1016/j.heliyon.2024.e25682
Lin, Y., Peng, C., Chen, P., & Zhang, M. (2022). Conflict or synergy? Analysis of economic-social- infrastructure-ecological resilience and their coupling coordination in the Yangtze River economic Belt, China. *Ecological Indicators*, *142*, 109194. https://doi.org/10.1016/j.ecolind.2022.109194
Liu, C. G., Gao, G. P., & Zhuang, J. (2005). An empirical analysis of urban economic development and land use efficiency in Shandong Province. *China Economist*, *8*, 257–259.
Liu, C., He, X., Chen, W., Zhao, G., & Xue, W. (2008). Simulation of three-dimensional green biomass of urban forests in Shenyang City and the factors affecting the biomass. *Ying Yong Sheng Tai Xue Bao= The Journal of Applied Ecology*, *19*(6), 1173–1178.
Liu, H., Fang, C., & Li, Y. (2019). The coupled human and natural cube: A conceptual framework for analyzing urbanization and eco-environment interactions (Chinese). *Acta Geogr. Sin*, *74*(8), 1489–1507.
Liu, J., Jin, X., Xu, W., Gu, Z., Yang, X., Ren, J., Fan, Y., & Zhou, Y. (2020). A new framework of land use efficiency for the coordination among food, economy and ecology in regional development. *Science of the Total Environment*, *710*, 135670.

Liu, S., Zhang, L., Long, Y., Yao, L., & Xu, M. (2020). A new urban vitality analysis and evaluation framework based on human activity modeling using multi-source big data. *ISPRS International Journal of Geo-Information*, *9*(11), 617.
Liu, X., Huang, Y., Xu, X., Li, X., Li, X., Ciais, P., Lin, P., Gong, K., Ziegler, A. D., & Chen, A. (2020). High-spatiotemporal-resolution mapping of global urban change from 1985 to 2015. *Nature Sustainability*, *3*(7), 564–570.
Liu, Y., Hu, Z., & Li, Y. (2014). Process and cause of urban-rural development transformation in the Bohai Rim Region, China. *Journal of Geographical Sciences*, *24*, 1147–1160.
Liu, Y., Xu, W., Hong, Z., Wang, L., Ou, G., Lu, N., & Dai, Q. (2023). Integrating three-dimensional greenness into RSEI improved the scientificity of ecological environment quality assessment for forest. *Ecological Indicators*, *156*, 111092. https://doi.org/10.1016/j.ecolind.2023.111092
Liu, Y., Yang, Y., Jing, W., Yao, L., Yue, X., & Zhao, X. (2017). A New Urban Index for Expressing Inner-City Patterns Based on MODIS LST and EVI Regulated DMSP/OLS NTL. *Remote Sensing*, *9*(8). https://doi.org/10.3390/rs9080777
Long, H. (2012). Land use transition and rural transformation development (Chinese). *Progress in Geography*, *31*(2), 131–138. https://doi.org/DOI: 10.11820/dlkxjz.2012.02.001
Long, Y., & Huang, C. (2019). Does block size matter? The impact of urban design on economic vitality for Chinese cities. *Environment and Planning B: Urban Analytics and City Science*, *46*(3), 406–422.
Long, Y., & Wu, K. (2016). *Several emerging issues of China's urbanization: Spatial expansion, population shrinkage, low-density human activities and city boundary delimitation (Chinese)*. *2*, 72–77.
Long, Y., Zhang, E., Long, Y., & Zhang, E. (2021). Data augmented design (DAD): Definitions, dimensions, performance, and applications. *Data Augmented Design: Embracing New Data for Sustainable Urban Planning and Design*, 15–33.
Long, Y., & Zhou, Y. (2016). Quantitative evaluation on street vibrancy and its impact factors: A case study of Chengdu (Chinese). *New Architecture*, *1*(1), 52–57.
Luo, K., Hu, X., He, Q., Wu, Z., Cheng, H., Hu, Z., & Mazumder, A. (2018). Impacts of rapid urbanization on the water quality and macroinvertebrate communities of streams: A case study in Liangjiang New Area, China. *Science of the Total Environment*, *621*, 1601–1614.
Lv, Y., Zhou, L., Yao, G., & Zheng, X. (2021). Detecting the true urban polycentric pattern of Chinese cities in morphological dimensions: A multiscale analysis based on geospatial big data. *Cities*, *116*, 103298. https://doi.org/10.1016/j.cities.2021.103298
Lynch, K. (1984). *Good city form*. MIT press.
Ma, L., Bo, J., Li, X., Fang, F., & Cheng, W. (2019). Identifying key landscape pattern indices influencing the ecological security of inland river basin: The middle and lower reaches of Shule River Basin as an example. *Science of The Total Environment*, *674*, 424–438. https://doi.org/10.1016/j.scitotenv.2019.04.107
Maas, P. R. (1984). *Towards a theory of urban vitality*.
Manchun LI, Y. C., Mengru YAO, Xia WANG, Xiaoqiang LIU. (2019). A review of studies on the "pole-axis system" theory based on citation analysis. *PROGRESS IN GEOGRAPHY*, *38*(2), 164. https://doi.org/10.18306/dlkxjz.2019.02.002
Mandelker, D. R. (2023). *Zoning for mixed-use development*. HeinOnline.
MAO, W., & ZHONG, Y. (2020). Spatial pattern and influencing factors of urban vitality in the middle reaches of the Yangtze River (Chines). *World Regional Studies*, *29*(1), 86.

Martinez-Fernandez, C., Audirac, I., Fol, S., & Cunningham-Sabot, E. (2012). Shrinking cities: Urban challenges of globalization. *International Journal of Urban and Regional Research*, *36*(2), 213–225.
McGarigal, K., Cushman, S. A., & Ene, E. (2012). FRAGSTATS v4: Spatial pattern analysis program for categorical and continuous maps. *Computer Software Program Produced by the Authors at the University of Massachusetts, Amherst*, *15*, 153–162.
McGarigal, K., Cushman, S. A., Neel, M. C., & Ene, E. (2002). FRAGSTATS: spatial pattern analysis program for categorical maps. *Computer Software Program Produced by the Authors at the University of Massachusetts, Amherst. Available at the Following Web Site: Www. Umass. Edu/Landeco/Research/Fragstats/Fragstats. Html*, *6*.
Meng, Y., & Xing, H. (2019). Exploring the relationship between landscape characteristics and urban vibrancy: A case study using morphology and review data. *Cities*, *95*, 102389.
Montgomery, J. (1995). Editorial urban vitality and the culture of cities. *Planning Practice & Research*, *10*(2), 101–110.
Montgomery, J. (1998). Making a city: Urbanity, vitality and urban design. *Journal of Urban Design*, *3*(1), 93–116.
Montgomery, J. (2017). *The new wealth of cities: City dynamics and the fifth wave*. Routledge.
Moran, E. F., Ojima, D., McConnell, W., Stafford Smith, M., Laumann, G., Morais, J., & Young, B. (2005). Global land project: Science plan and implementation strategy. *IGBP Report*, *53*.
Moran, P. A. (1948). The interpretation of statistical maps. *Journal of the Royal Statistical Society. Series B (Methodological)*, *10*(2), 243–251.
Morzillo, A. T., de Beurs, K. M., & Martin-Mikle, C. J. (2014). A conceptual framework to evaluate human-wildlife interactions within coupled human and natural systems. *Ecology and Society*, *19*(3).
Mulligan, G. F. (2006). Logistic population growth in the world's largest cities. *Geographical Analysis*, *38*(4), 344–370.
Nambuge, G. S., Peiris, M. T. O. V., & Kalugalla, K. G. P. (2020). Assessment of urban public spaces within shopping malls: Youth perspective in the city of colombo. *International Journal of Real Estate Studies*, *14*(2), 28–38.
Neuhaus, F., & Neuhaus, F. (2015). Urban rhythms. *Emergent Spatio-Temporal Dimensions of the City: Habitus and Urban Rhythms*, 1–11.
Neuman, M. (2005). The compact city fallacy. *Journal of Planning Education and Research*, *25*(1), 11–26.
Nguyen, L. H., Joshi, D. R., Clay, D. E., & Henebry, G. M. (2020). Characterizing land cover/land use from multiple years of Landsat and MODIS time series: A novel approach using land surface phenology modeling and random forest classifier. *Remote Sensing of Environment*, *238*, 111017.
Nie, X., Zhang, Y., Zhou, W., Su, H., Yang, T., Li, X., & Lan, S. (2021). Research Status and Trend of Urban Space Vitality——Comparative Analysis of Chinese and English Literature (Chinese). *Journal of Southwest University(Natural Science Edition)*, *43*(3), 147–155.
Northam, R. M. (1979). Urban geography. *(No Title)*.
Paköz, M. Z., & Işık, M. (2022). Rethinking urban density, vitality and healthy environment in the post-pandemic city: The case of Istanbul. *Cities*, *124*, 103598.
Pendall, R. (2003). The limitless city: A primer on the urban sprawl debate. *American Planning Association. Journal of the American Planning Association*, *69*(1), 99.
Peng, W., Wang, G., Zhou, J., Xu, X., Luo, H., Zhao, J., & Yang, C. (2016). Dynamic

monitoring of fractional vegetation cover along Minjiang River from Wenchuan County to Dujiangyan City using multi-temporal landsat 5 and 8 images (Chinese). *Acta Ecol. Sin*, *36*, 1975–1988. https://doi.org/10.5846/stxb201409051756

Penn, B. S. (2005). Using self-organizing maps to visualize high-dimensional data. *Computers & Geosciences*, *31*(5), 531–544.

Pérez-Soba, M., Petit, S., Jones, L., Bertrand, N., Briquel, V., Omodei-Zorini, L., Contini, C., Helming, K., Farrington, J. H., & Mossello, M. T. (2008). Land use functions—A multifunctionality approach to assess the impact of land use changes on land use sustainability. *Sustainability Impact Assessment of Land Use Changes*, 375–404. https://doi.org/10.1007/978-3-540-78648-1_19

Port, A. (2004). *Application of selected new urbanist principles to residential infill developments in mature suburbs of Greater Boston*.

Portugali, J. (2016). What makes cities complex? In *Complexity, cognition, urban planning and design* (pp. 3–19). Springer.

Qi, J., Chen, J., Wan, S., & Ai, L. (2012). Understanding the coupled natural and human systems in Dryland East Asia. *Environmental Research Letters*, *7*(1), 015202.

Qiao, W., & Huang, X. (2024). Assessment the urbanization sustainability and its driving factors in Chinese urban agglomerations: An urban land expansion—Urban population dynamics perspective. *Journal of Cleaner Production*, *449*, 141562. https://doi.org/10.1016/j.jclepro.2024.141562

Raux, C., Ma, T.-Y., & Cornelis, E. (2016). Variability in daily activity-travel patterns: The case of a one-week travel diary. *European Transport Research Review*, *8*, 1–14.

Ravenscroft, N. (2000). The vitality and viability of town centres. *Urban Studies*, *37*(13), 2533–2549.

Rowley, A. (1996). Mixed-use development: Ambiguous concept, simplistic analysis and wishful thinking? *Planning Practice & Research*, *11*(1), 85–98.

Rowley, A. (1998). *Planning Mixed Use Development: Issues and Practice: A Report on Research Funded by the Education Trust of the Royal Institution of Chartered Surveyors and Carried Out by the Department of Land Management of the University of Reading*. Royal Institution of Chartered Surveyors.

Saaty, R. W. (1987). The analytic hierarchy process—What it is and how it is used. *Mathematical Modelling*, *9*(3), 161–176. https://doi.org/10.1016/0270-0255(87)90473-8

Sander, H. A., & Zhao, C. (2015). Urban green and blue: Who values what and where? *Land Use Policy*, *42*, 194–209.

SHENG, Q., YANG, T., & HOU, J. (2015). Continuous Movement and Hyper-link Spatial Mechanisms——A Large-scale Space Syntax Analysis on Chongqing's Vehicle and Metro Flow Data. *Journal of Human Settlements in West China*, *30*(05), 16–21. https://doi.org/10.13791/j.cnki.hsfwest.20150503

Smith, L. I. (2002). *A tutorial on principal components analysis*.

Song, X., & LI, X. (2019). Theoretical explanation and case study of regional cultivated land use function transition (Chinese). *Acta Geographica Sinica*, *74*(5), 992–1010. https://doi.org/10.11821/dlxb201905012

Song, Y., Wang, J., Ge, Y., & Xu, C. (2020). An optimal parameters-based geographical detector model enhances geographic characteristics of explanatory variables for spatial heterogeneity analysis: Cases with different types of spatial data. *GIScience & Remote Sensing*, *57*(5), 593–610. https://doi.org/10.1080/15481603.2020.1760434

Steffen, W., Crutzen, P. J., & McNeill, J. R. (2007). The Anthropocene: Are humans now overwhelming the great forces of nature. *Ambio-Journal of Human Environment Research and Management*, *36*(8), 614–621.
Sugiyama, T., Francis, J., Middleton, N. J., Owen, N., & Giles-Corti, B. (2010). Associations between recreational walking and attractiveness, size, and proximity of neighborhood open spaces. *American Journal of Public Health*, *100*(9), 1752–1757.
Sulis, P., Manley, E., Zhong, C., & Batty, M. (2018). Using mobility data as proxy for measuring urban vitality. *Journal of Spatial Information Science*, *2018*(16), 137–162.
Sung, H., Lee, S., & Cheon, S. (2015). Operationalizing jane jacobs's urban design theory: Empirical verification from the great city of seoul, korea. *Journal of Planning Education and Research*, *35*(2), 117–130.
Tang, L., Xu, H., & Ding, Y. (2022). Comprehensive Vitality Evaluation of Urban Blocks based on Multi-source Geo-graphic Big Data (Chinese). *J. Geo Inf. Sci*, *24*, 1575–1588.
Tang, S., & Ta, N. (2022). How the built environment affects the spatiotemporal pattern of urban vitality: A comparison among different urban functional areas. *Computational Urban Science*, *2*(1), 39.
Wang, D., Zhenxuan Yan, & Yu, X. (2019). International experience of mixed land use: Models, measures and effects (Chinese). *Urban Planning Internationa*, *6*, 79–85.
Wang, H., Yan, S., Liang, Z., Jiao, K., Li, D., Wei, F., & Li, S. (2021). Strength of association between vegetation greenness and its drivers across China between 1982 and 2015: Regional differences and temporal variations. *Ecological Indicators*, *128*, 107831.
Wang, J., & Xu, C. D. (2017). Geodetector: Principle and prospective. *Acta Geographica Sinica*, *72*(1), 116–134.
Wang, J.-F., & Hu, Y. (2012). Environmental health risk detection with GeogDetector. *Environmental Modelling & Software*, *33*, 114–115.
Wang, X., Li, X., & Zhang, S. (2022). Has the polycentric spatial structure promoted high-quality urban development. *China Popul. Resour. Environ*, *32*, 57–67.
Wang, X., Shi, Z., Kollányi, L., Yang, Y., Liu, M., & Zhang, X. (2023). Exploration of Urban Subsystem Coupling Coordination Based on Resilience in Luohe City. *4D Tájépítészeti És Kertművészeti Folyóirat*, 22–29. https://doi.org/10.36249/4d.67.3700
Wang, X., Yao, X., Shao, H., Bai, T., Xu, Y., Tian, G., Fekete, A., & Kollányi, L. (2023). Land Use Quality Assessment and Exploration of the Driving Forces Based on Location: A Case Study in Luohe City, China. *Land*, *12*(1), 1–17.
Wang, X., Zhong, X., Liu, S., Liu, J., Wang, Z., & Li, M. (2008). Regional assessment of environmental vulnerability in the Tibetan Plateau: Development and application of a new method. *Journal of Arid Environments*, *72*(10), 1929–1939.
WANG, Y., CHENG, R., ZENG, P., & CHE, Y. (2019). Spatial Differentiation of Water Quality in River Networks in Shanghai and Its Response to Land Use in Riparian Zones (Chinese). *Journal of Ecology and Rural Environment*, *35*(7), 925–932. https://doi.org/DOI: 10.19741/j.issn.1673-4831.2018.0549
Wang, Z., Liu, Y., Luo, X., Tong, Z., & An, R. (2023). Nonlinear relationship between urban vitality and the built environment based on multi-source data: A case study of the main urban area of Wuhan City at the weekend (Chinese). *Progress in Geography*, *42*, 716–729. https://doi.org/10.18306/dlkxjz.2023.04.008
Wang, Z., Wang, X., Liu, Y., & Zhu, L. (2024). Identification of 71 factors influencing urban vitality and examination of their spatial dependence: A comprehensive validation applying

multiple machine-learning models. *Sustainable Cities and Society*, *108*, 105491. https://doi.org/10.1016/j.scs.2024.105491
Weng, Q., Lian, H., & Qin, Q. (2022). Spatial disparities of the coupling coordinated development among the economy, environment and society across China's regions. *Ecological Indicators*, *143*, 109364.
Wiggering, H., Dalchow, C., Glemnitz, M., Helming, K., Müller, K., Schultz, A., Stachow, U., & Zander, P. (2006). Indicators for multifunctional land use—Linking socio-economic requirements with landscape potentials. *Ecological Indicators*, *6*(1), 238–249. https://doi.org/10.1016/j.ecolind.2005.08.014
Witherspoon, R., Abbett, J. P., & Gladstone, R. M. (1976). Mixed-use developments: New ways of land use. *(No Title)*.
World Health Organization. (2005). *Ecosystems and human well-being: Health synthesis: A report of the Millennium Ecosystem Assessment*. World Health Organization.
Wu, C., Ye, X., Ren, F., & Du, Q. (2018). Check-in behaviour and spatio-temporal vibrancy: An exploratory analysis in Shenzhen, China. *Cities*, *77*, 104–116.
Wu, C., Zhao, M., & Ye, Y. (2023). Measuring urban nighttime vitality and its relationship with urban spatial structure: A data-driven approach. *Environment and Planning B: Urban Analytics and City Science*, *50*(1), 130–145.
Wu, J. (2000). *Landscape ecology: Pattern, process, scale and hierarchy*.
Wu, J., Ta, N., Song, Y., Lin, J., & Chai, Y. (2018). Urban form breeds neighborhood vibrancy: A case study using a GPS-based activity survey in suburban Beijing. *Cities*, *74*, 100–108.
Xia, C., Zhang, A., & Yeh, A. G. (2022). The varying relationships between multidimensional urban form and urban vitality in Chinese megacities: Insights from a comparative analysis. *Annals of the American Association of Geographers*, *112*(1), 141–166.
Xie, X., Hou, W., & Herold, H. (2018). Ex post impact assessment of master plans—The case of Shenzhen in shaping a polycentric urban structure. *ISPRS International Journal of Geo-Information*, *7*(7), 252.
Xu, H. (2008). A new index for delineating built-up land features in satellite imagery. *International Journal of Remote Sensing*, *29*(14), 4269–4276.
XU, H. (2013). A remote sensing urban ecological index and its application (Chinese). *Acta Ecologica Sinica*, *33*(24), 7853. https://doi.org/10.5846/stxb201208301223
Yang, Y., He, R., Tian, G., Shi, Z., Wang, X., & Fekete, A. (2022). Equity Study on Urban Park Accessibility Based on Improved 2SFCA Method in Zhengzhou, China. *Land*, *11*(11). https://doi.org/10.3390/land11112045
Ye, Y., Li, D., & Liu, X. (2018). How block density and typology affect urban vitality: An exploratory analysis in Shenzhen, China. *Urban Geography*, *39*(4), 631–652.
Yue, W., Chen, Y., Zhang, Q., & Liu, Y. (2019). Spatial explicit assessment of urban vitality using multi-source data: A case of Shanghai, China. *Sustainability*, *11*(3), 638.
Zeng, P., Wei, M., & Liu, X. (2020). Investigating the spatiotemporal dynamics of urban vitality using bicycle-sharing data. *Sustainability*, *12*(5), 1714.
Zhang, A., Li, W., Wu, J., Lin, J., Chu, J., & Xia, C. (2021). How can the urban landscape affect urban vitality at the street block level? A case study of 15 metropolises in China. *Environment and Planning B: Urban Analytics and City Science*, *48*(5), 1245–1262.
Zhang, J., Chen, Y., Yao, Y., & Shi, S. (2008). Study on land use regionalization based on land-use function: Case study of Jilin Province (Chinese). *Journal of China Agricultural University*, *3*, 29–35. https://doi.org/Journal of China Agricultural University

Zhang, J., Liu, Y., Zhou, S., Cheng, Y., & Zhao, B. (2022). Do various dimensions of exposure metrics affect biopsychosocial pathways linking green spaces to mental health? A cross-sectional study in Nanjing, China. *Landscape and Urban Planning*, *226*, 104494.
Zhang, Y., Ding, X., Dong, L., & Yu, S. (2024). Research on spatiotemporal patterns and influencing factors of county-level urban shrinkage in urbanizing China. *Sustainable Cities and Society*, *109*, 105544. https://doi.org/10.1016/j.scs.2024.105544
Zhang, Z., Tong, Z., Zhang, L., & Liu, Y. (2023). What are the dominant factors and optimal driving threshold for the synergy and tradeoff between ecosystem services, from a nonlinear coupling perspective? *Journal of Cleaner Production*, *422*, 138609. https://doi.org/10.1016/j.jclepro.2023.138609
Zhao, G., & Song, J. (2022). Improving the Measurement of Urban Land-use Mix (Chinese). *Urban Planning Forum*, *1*, 51–58. https://doi.org/10.16361/j.upf.202201007
Zhao, W., & Fang, X. (2014). Landscape sustainability and landscape sustainability science (Chinese). *Acta Ecol. Sin*, *34*, 2453–2459.
Zhen, L., Wei, Y., Xie, G., Helming, K., Cao, S., Yang, L., Pan, Y., & Koenig, H. (2010). Regional analysis of dynamic land use functions in China (Chinese). *Shengtai Xuebao/Acta Ecologica Sinica*, *30*(24), 6749–6761.
Zheng, Y., Tang, L., & Wang, H. (2021). An improved approach for monitoring urban built-up areas by combining NPP-VIIRS nighttime light, NDVI, NDWI, and NDBI. *Journal of Cleaner Production*, *328*, 129488.
Zheng, Z., & Chen, Y. (2019). Review and prospect of application of nighttime light remote sensing data. In *PROGRESS IN GEOGRAPHY* (Vol. 38, Issue 2, pp. 205–223).
Zhongping, W., Changliang, S., Qiang, L., & Gang, W. (2011). Coupling trending analysis about urbanization and urban resource in Beijing. *Energy Procedia*, *5*, 1589–1596.
Zhou, L., Dang, X., Sun, Q., & Wang, S. (2020). Multi-scenario simulation of urban land change in Shanghai by random forest and CA-Markov model. *Sustainable Cities and Society*, *55*, 102045.
Zhu, S., Kong, X., & Jiang, P. (2020). Identification of the human-land relationship involved in the urbanization of rural settlements in Wuhan city circle, China. *Journal of Rural Studies*, *77*, 75–83. https://doi.org/10.1016/j.jrurstud.2020.05.004
Zhuo, L., Zhang, X., Zheng, J., Tao, H., & Guo, Y. (2015). An EVI-based method to reduce saturation of DMSP/OLS nighttime light data. *Acta Geographica Sinica*, *70*(8), 1339–1350.

ACKNOWLEDGEMENTS

As I near the end of my doctoral studies, I look back on a journey filled with both challenges and rewards. These past four years have been a mix of tough climbs and joyful breakthroughs. I am deeply thankful to everyone who helped me along the way. Your support lifted me over many hurdles and guided me to this point.

I want to begin by expressing my sincere gratitude to my supervisor, Dr. László Kollányi. His deep knowledge and clear insights have been a true guiding light in my research. He offered practical advice and steady encouragement that always kept me on track. I am also very grateful to Professor Jombach Sandor. His rigorous approach and many thoughtful discussions helped me deepen my work. Their willingness to share their expertise and care for international students will always be a cherished part of my journey.

I must also thank my mentors from China, Professor Tian Guohang and Mr. Ge Shidong. During my time studying by the Budapest, their warm support and guidance made a big difference. I also appreciate the friendship of classmates like Shizhen, Liu Manshu, Zhang Xiaoyan, and Du Chenyu, as well as other international friends. Our lively exchanges and shared experiences brought color and energy to my daily work.

I am grateful to the faculty at the College, including Prof. Fekete Albert and Dr. Sallay Agnes, for their strong support and expert advice. I also value the constructive feedback from reviewers such as Dr. András Jung and Dr. Li Huawi, and the patient guidance from my defense committee.

Finally, I want to thank all the friends I made in Budapest. Your company turned my time abroad into a memorable adventure. Above all, I must thank my family, especially my parents, whose unconditional love and support have given me the strength to keep going. I am also thankful for the joint sponsorship from the China Scholarship Council and the Stipendium Hungaricum Programme, which made this cross-cultural academic journey possible. I will always treasure these experiences and the wisdom shared by everyone who believed in me. Truly grateful.